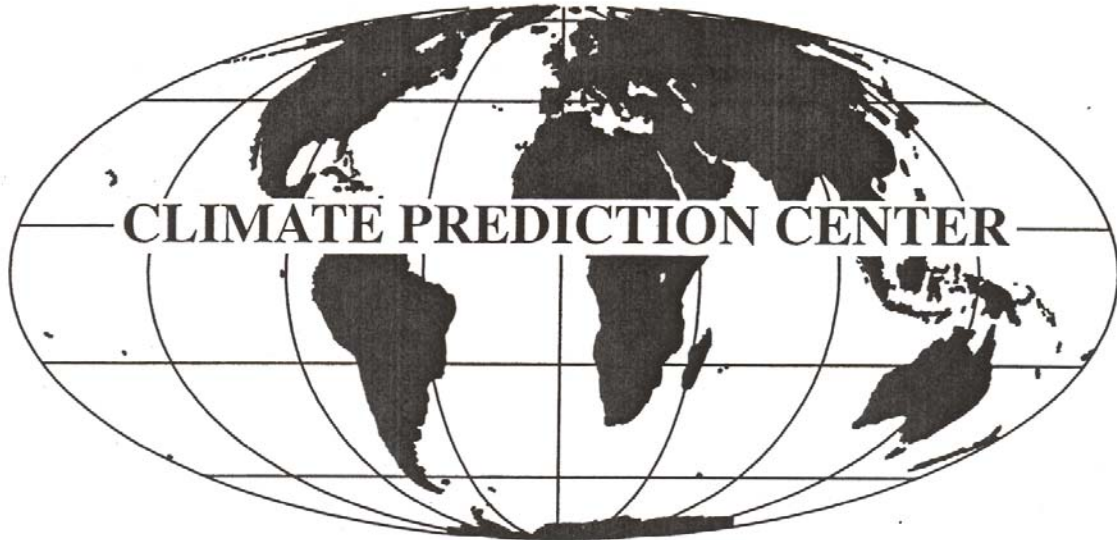


# CLIMATE DIAGNOSTICS BULLETIN



**SEPTEMBER 2016**

**NEAR REAL-TIME OCEAN / ATMOSPHERE**

**Monitoring, Assessments, and Prediction**

**U.S. DEPARTMENT OF COMMERCE  
National Oceanic and Atmospheric Administration  
National Weather Service  
National Centers for Environmental Prediction**

## CLIMATE DIAGNOSTICS BULLETIN



### CLIMATE PREDICTION CENTER Attn: Climate Diagnostics Bulletin W/NP52, Room 605, WWBG Camp Springs, MD 20746-4304

**Chief Editor:** Gerald D. Bell

**Editors:** Wei Shi, Michelle L'Heureux, and Michael Halpert

**Bulletin Production:** Wei Shi

**External Collaborators:**

Center for Ocean-Atmospheric Prediction Studies (COAPS)

Cooperative Institute for Research in the Atmosphere (CIRA)

Earth & Space Research

International Research Institute for Climate and Society (IRI)

Joint Institute for the Study of the Atmosphere and Ocean (JISAO)

Lamont-Doherty Earth Observatory (LDEO)

NOAA-CIRES, Climate Diagnostics Center

NOAA-AOML, Atlantic Oceanographic and Meteorological Laboratory

NOAA-NESDIS-STAR, Center for Satellite Applications and Research

NOAA-NDBC, National Data Buoy Center

Scripps Institution of Oceanography

**Software:** Most of the bulletin figures generated at CPC are created using the Grid Analysis and Display System (GrADS).

**- Climate Diagnostics Bulletin available on the World Wide Web**

The CDB is available on the World Wide Web. The address of the online version of the CDB is:

**<http://www.cpc.ncep.noaa.gov/products/CDB>**

If you have any problems accessing the bulletin, contact Dr. Wei Shi by E-mail:

*Wei.Shi@noaa.gov*

# Table of Contents

## TROPICS

Highlights . . . . . page 6  
 Table of Atmospheric Indices . . . . . page 7  
 Table of Oceanic Indices . . . . . page 8

## FIGURE

Time Series	
Southern Oscillation Index (SOI)	T1
Tahiti and Darwin SLP Anomalies	T1
OLR Anomalies	T1
CDAS/Reanalysis SOI & Equatorial SOI	T2
200-hPa Zonal Wind Anomalies	T3
500-hPa Temperature Anomalies	T3
30-hPa and 50-hPa Zonal Wind Anomalies	T3
850-hPa Zonal Wind Anomalies	T4
Equatorial Pacific SST Anomalies	T5
Time-Longitude Sections	
Mean and Anomalous Sea Level Pressure	T6
Mean and Anomalous 850-hPa Zonal Wind	T7
Mean and Anomalous OLR	T8
Mean and Anomalous SST	T9
Pentad SLP Anomalies	T10
Pentad OLR Anomalies	T11
Pentad 200-hPa Velocity Potential Anomalies	T12
Pentad 850-hPa Zonal Wind Anomalies	T13
Anomalous Equatorial Zonal Wind	T14
Mean and Anomalous Depth of the 20°C Isotherm	T15
Mean & Anomaly Fields	
Depth of the 20°C Isotherm	T16
Subsurface Equatorial Pacific Temperatures	T17
SST	T18
SLP	T19
850-hPa Vector Wind	T20
200-hPa Vector Wind	T21
200-hPa Streamfunction	T22
200-hPa Divergence	T23
200-hPa Velocity Potential and Divergent Wind	T24
OLR	T25
SSM/I Tropical Precipitation Estimates	T26
Cloud Liquid Water	T27
Precipitable Water	T28
Divergence & E-W Divergent Circulation	T29 - T30
Pacific Zonal Wind & N-S Divergent Circulation	T31 - T32
Appendix 1: Outside Contributions	
Tropical Drifting Buoys	A1.1

## FIGURE

Pacific Wind Stress and Anomalies	A1.2
Satellite-Derived Surface Currents	A1.3 - A1.4
<b>FORECAST FORUM</b>	
Discussion . . . . .	page 49
Canonical Correlation Analysis Forecasts	F1 - F2
NCEP Coupled Model Forecasts	F3 - F4
NCEP Markov Model Forecasts	F5 - F6
LDEO Model Forecasts	F7 - F8
Linear Inverse Modeling Forecasts	F9 - F10
Scripps/MPI Hybrid Coupled Model Forecast	F11
ENSO-CLIPER Model Forecast	F12
Model Forecasts of Niño 3.4	F13
<b>EXTRATROPICS</b>	
Highlights . . . . .	page 64
Table of Teleconnection Indices . . . . .	page 66
Global Surface Temperature	E1
Temperature Anomalies (Land Only)	E2
Global Precipitation	E3
Regional Precipitation Estimates	E4 - E5
U. S. Precipitation	E6
Northern Hemisphere	
Teleconnection Indices	E7
Mean and Anomalous SLP	E8
Mean and Anomalous 500-hPa heights	E9
Mean and Anomalous 300-hPa Wind Vectors	E10
500-hPa Persistence	E11
Time-Longitude Sections of 500-hPa Height Anomalies	E12
700-hPa Storm Track	E13
Southern Hemisphere	
Mean and Anomalous SLP	E14
Mean and Anomalous 500-hPa heights	E15
Mean and Anomalous 300-hPa Wind Vectors	E16
500-hPa Persistence	E17
Time-Longitude Sections of 500-hPa Height Anomalies	E18
Stratosphere	
Height Anomalies	S1 - S2
Temperatures	S3 - S4
Ozone	S5 - S6
Vertical Component of EP Flux	S7
Ozone Hole	S8
Appendix 2: Additional Figures	
Arctic Oscillation and 500-hPa Anomalies	A2.1
Snow Cover	A2.2

## Tropical Highlights - September 2016

Sea surface temperatures (SSTs) were slightly below-average over the east-central equatorial Pacific during September 2016 (Fig. T18, Table T2). The latest monthly Niño indices were  $-0.2^{\circ}\text{C}$  for the Niño 3 region,  $-0.6^{\circ}\text{C}$  for the Niño 3.4 region, and  $+0.5^{\circ}\text{C}$  for the Niño 1+2 region (Table T2, Fig. T5). The depth of the oceanic thermocline (measured by the depth of the  $20^{\circ}\text{C}$  isotherm) remained below-average across the central and eastern equatorial Pacific (Figs. T15, T16), and the corresponding sub-surface temperatures were  $1\text{-}2^{\circ}\text{C}$  below average (Fig. T17).

Also during September, the lower-level winds were near-average across the central and eastern equatorial Pacific, while upper-level westerly anomalies were seen near the Date Line, just south of the equator (Table T1, Figs. T20, T21). Meanwhile, suppressed convection was observed across the eastern and central equatorial Pacific (Figs. T25, E3). Collectively, these oceanic and atmospheric anomalies reflect ENSO-neutral conditions.

For the latest status of the ENSO cycle see the ENSO Diagnostic Discussion at:  
[http://www.cpc.ncep.noaa.gov/products/analysis\\_monitoring/enso\\_advisory/index.html](http://www.cpc.ncep.noaa.gov/products/analysis_monitoring/enso_advisory/index.html)

Month	SLP Anomalies		Tahiti minus Darwin SOI	850-hPa Zonal Wind Index			200-hPa Wind Index	OLR Index
	Tahiti	Darwin		5N-5S 135E-180	5N-5S 175W-140W	5N-5S 135W-120W		
SEP 16	1.0	-1.2	1.2	0.8	0.3	0.0	5N-5S 165W-110W	5N-5S 160E-160W
AUG 16	0.3	-1.0	0.7	0.1	0.3	0.1		0.8
JUL 16	0.5	-0.3	0.4	0.3	-0.2	-0.5		0.5
JUN 16	0.4	-0.7	0.6	0.0	-0.4	-0.6		0.1
MAY 16	0.2	-0.6	0.4	0.7	0.1	-0.4		-0.2
APR 16	-1.3	0.9	-1.2	0.2	-0.2	-0.3		-0.9
MAR 16	0.7	0.9	-0.1	0.1	-0.2	-0.3		-1.6
FEB 16	-1.9	1.8	-2.0	0.1	-0.5	-0.2		-2.4
JAN 16	-0.4	3.5	-2.2	-0.4	-2.2	-1.5		-1.9
DEC 15	-1.4	-0.4	-0.6	-0.1	-1.1	-1.5		-2.5
NOV 15	-0.3	0.6	-0.5	0.0	-1.2	-1.3		-1.3
OCT 15	-0.1	3.0	-1.7	-1.1	-2.3	-2.0		-1.4
SEP 15	-1.3	1.7	-1.6	-1.3	-1.0	-1.0		-1.5

TABLE T1 - Atmospheric index values for the most recent 12 months. Indices are standardized by the mean annual standard deviation, except for the Tahiti and Darwin SLP anomalies which are in units of hPa. Positive (negative) values of 200-hPa zonal wind index imply westerly (easterly) anomalies. Positive (negative) values of 850-hPa zonal wind indices imply easterly (westerly) anomalies. Anomalies are departures from the 1981-2010 base period means.

Month	PACIFIC SST				ATLANTIC SST		GLOBAL				
	Niño 1+2 0-10S 90W-80W	Niño 3 5N-5S 150W-90W	Niño 3.4 5N-5S 170W-120W	Niño 4 5N-5S 160E-150W	N.ATL 5N-20N 60W-30W	S. ATL 0-20S 30W-10E		TROPICS 10N-10S 0-360			
SEP 16	0.5	20.9	24.7	-0.2	28.5	0.4	28.6	0.1	23.1	0.2	27.4
AUG 16	0.4	21.0	24.5	-0.5	28.7	0.4	28.2	0.3	23.4	0.2	27.4
JUL 16	0.2	21.8	25.1	-0.5	29.1	0.4	27.6	0.5	24.3	0.3	27.7
JUN 16	0.3	23.2	26.3	-0.1	29.4	0.4	27.1	0.4	25.4	0.4	28.4
MAY 16	0.3	24.6	27.1	0.3	29.4	0.5	26.8	0.1	26.3	0.5	29.0
APR 16	0.2	25.8	28.3	1.1	29.4	0.3	26.2	0.1	27.2	0.6	29.3
MAR 16	0.9	27.6	28.7	1.7	29.5	0.4	26.0	0.3	27.4	0.8	29.1
FEB 16	0.7	26.8	28.4	2.4	29.6	0.3	25.9	0.5	27.1	0.8	28.6
JAN 16	1.4	25.9	28.2	2.6	29.7	0.3	26.3	0.6	26.2	1.0	28.7
DEC 15	2.2	25.0	28.0	2.8	30.1	0.1	26.9	0.4	25.2	1.0	28.7
NOV 15	2.1	23.7	27.9	3.0	30.3	0.3	28.0	0.1	24.0	0.9	28.6
OCT 15	2.5	23.3	27.6	2.5	29.2	0.7	28.8	-0.1	23.3	0.8	28.2
SEP 15	2.6	22.9	27.5	2.3	29.0	0.5	28.6	-0.3	22.8	0.7	28.0

TABLE T2. Mean and anomalous sea surface temperature (°C) for the most recent 12 months. Anomalies are departures from the 1981–2010 adjusted OI climatology (Smith and Reynolds 1998, *J. Climate*, **11**, 3320–3323).



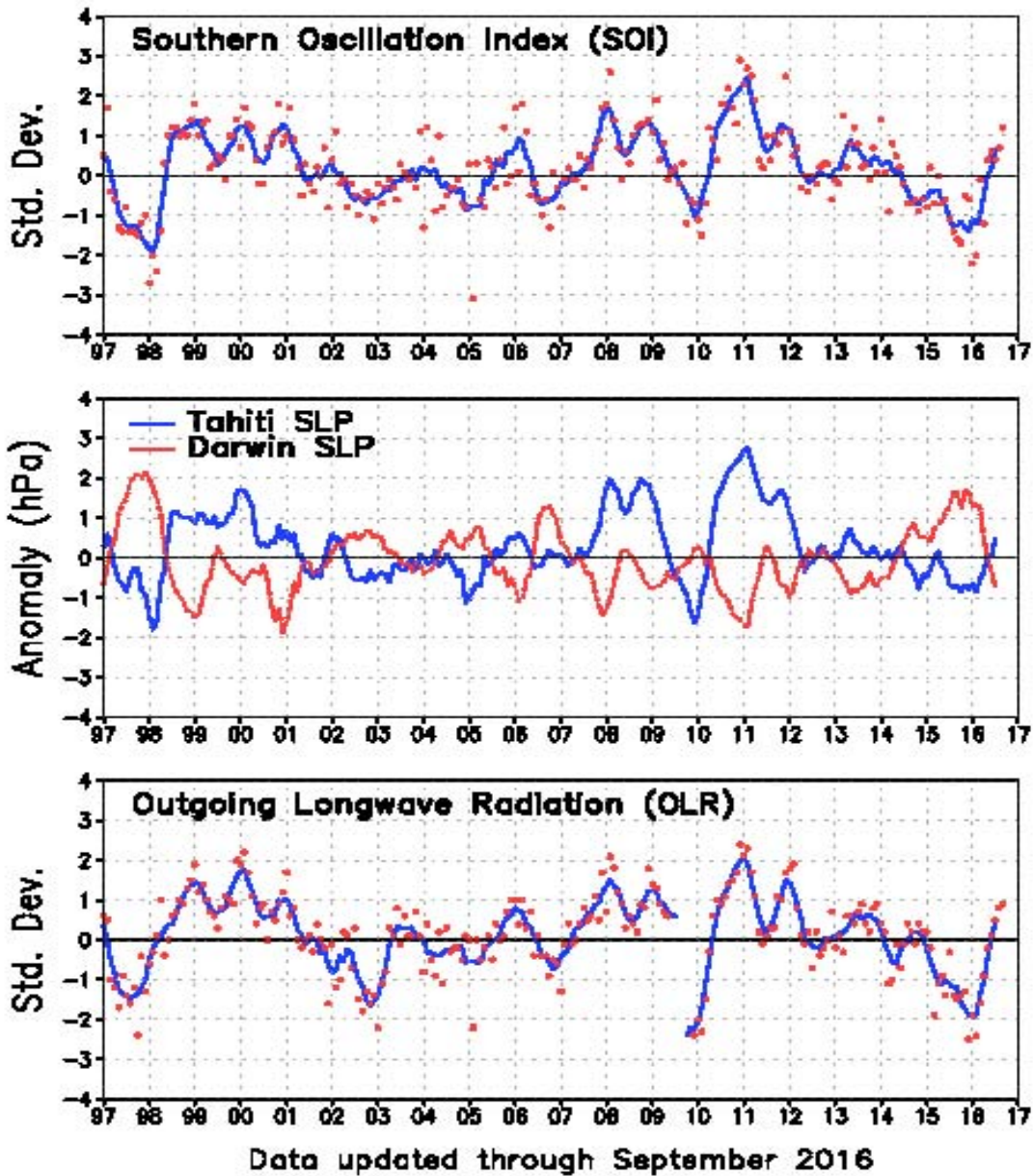


FIGURE T1. Five-month running mean of the Southern Oscillation Index (SOI) (top), sea-level pressure anomaly (hPa) at Darwin and Tahiti (middle), and outgoing longwave radiation anomaly (OLR) averaged over the area 5N-5S, 160E-160W (bottom). Anomalies in the top and middle panels are departures from the 1981-2010 base period means and are normalized by the mean annual standard deviation. Anomalies in the bottom panel are departures from the 1981-2010 base period means. Individual monthly values are indicated by “x”s in the top and bottom panels. The x-axis labels are centered on July.

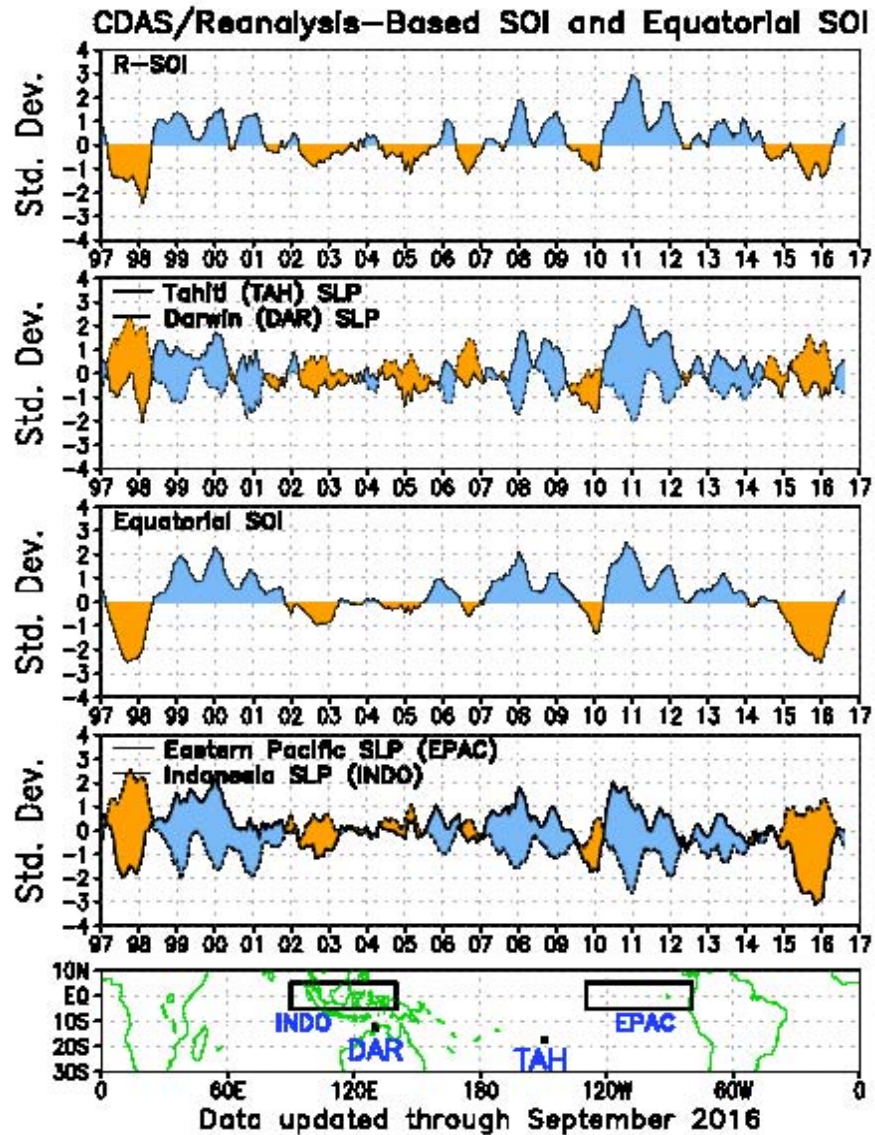


FIGURE T2. Three-month running mean of a CDAS/Reanalysis-derived (a) Southern Oscillation Index (RSOI), (b) standardized pressure anomalies near Tahiti (solid) and Darwin (dashed), (c) an equatorial SOI ([EPAC] - [INDO]), and (d) standardized equatorial pressure anomalies for (EPAC) (solid) and (INDO) (dashed). Anomalies are departures from the 1981-2010 base period means and are normalized by the mean annual standard deviation. The equatorial SOI is calculated as the normalized difference between the standardized anomalies averaged between 5°N–5°S, 80°W–130°W (EPAC) and 5°N–5°S, 90°E–140°E (INDO).

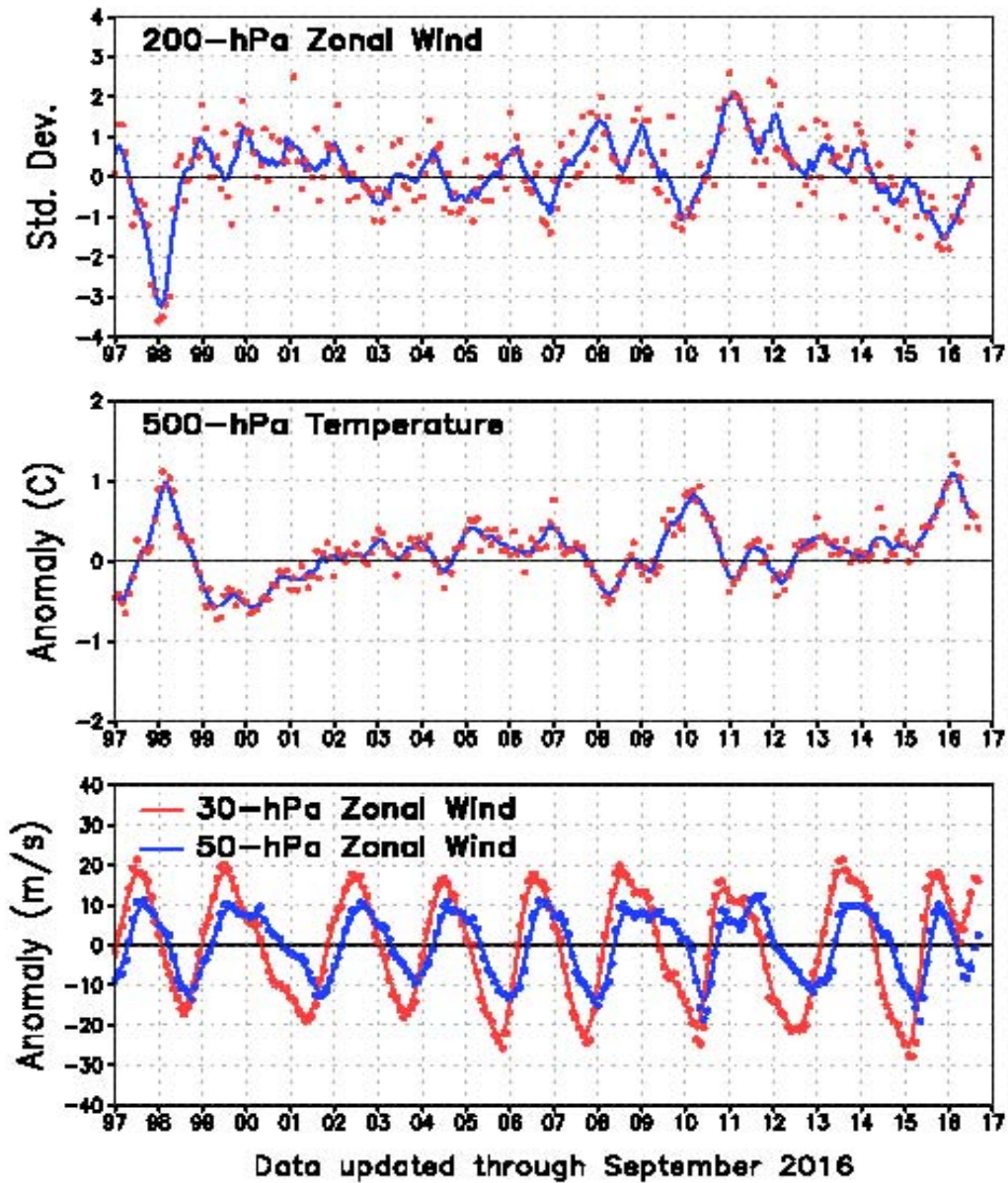


FIGURE T3. Five-month running mean (solid lines) and individual monthly mean (dots) of the 200-hPa zonal wind anomalies averaged over the area 5N-5S, 165W-110W (top), the 500-hPa virtual temperature anomalies averaged over the latitude band 20N-20S (middle), and the equatorial zonally-averaged zonal wind anomalies at 30-hPa (red) and 50-hPa (blue) (bottom). In the top panel, anomalies are normalized by the mean annual standard deviation. Anomalies are departures from the 1981-2010 base period means. The x-axis labels are centered on January.



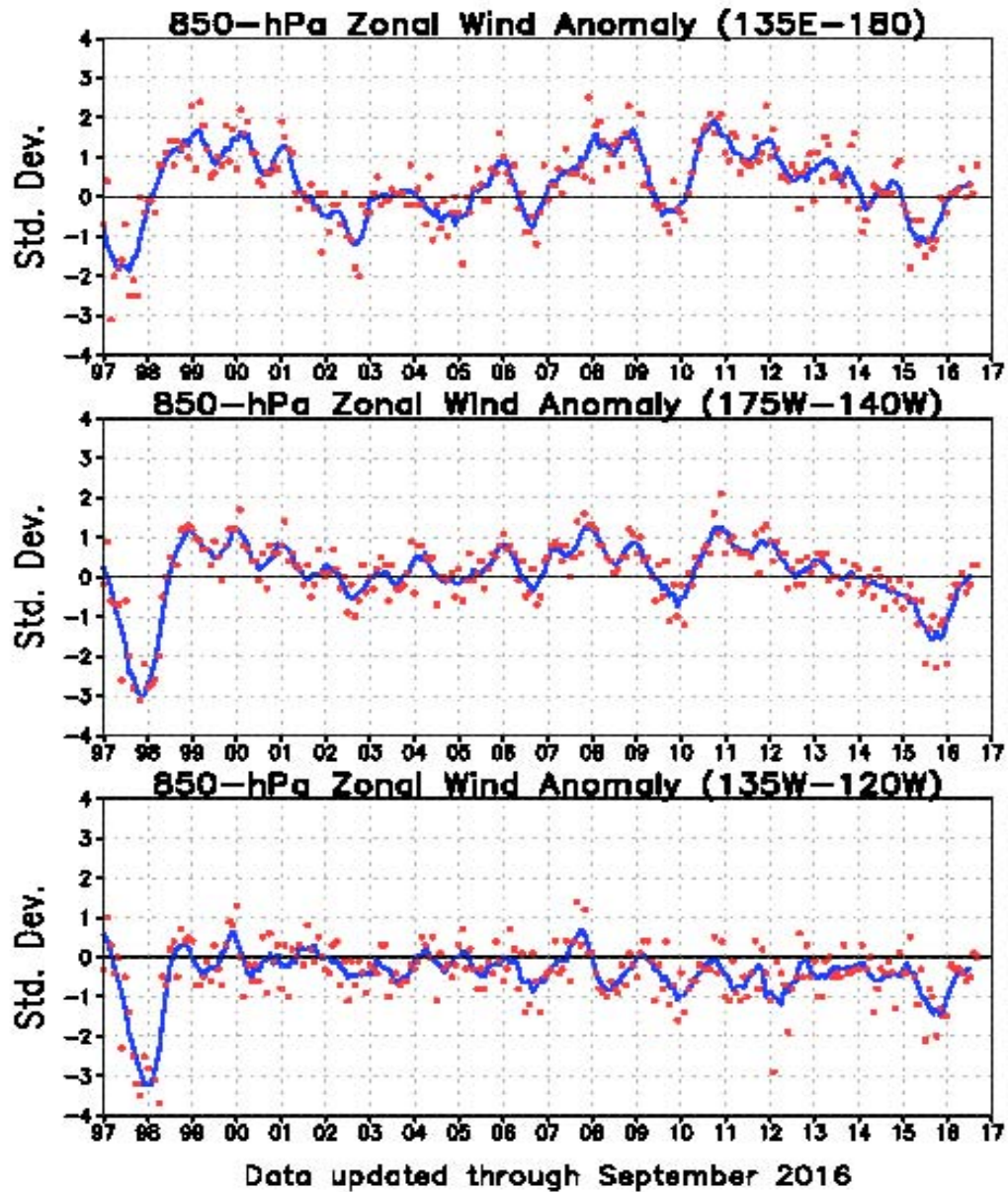


FIGURE T4. Five-month running mean (solid line) and individual monthly mean (dots) of the standardized 850-hPa zonal wind anomaly index in the latitude belt 5N-5S for 135E-180 (top), 175W-140W (middle) and 135W-120W (bottom). Anomalies are departures from the 1981-2010 base period means and are normalized by the mean annual standard deviation. The x-axis labels are centered on January. Positive (negative) values indicate easterly (westerly) anomalies.

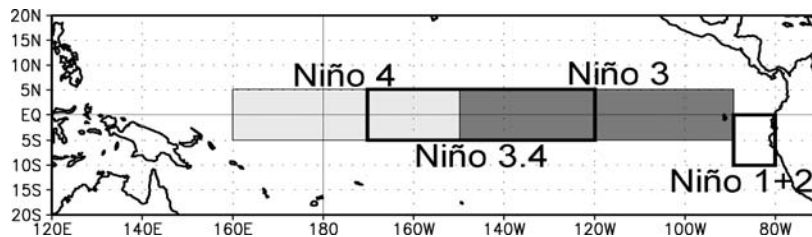
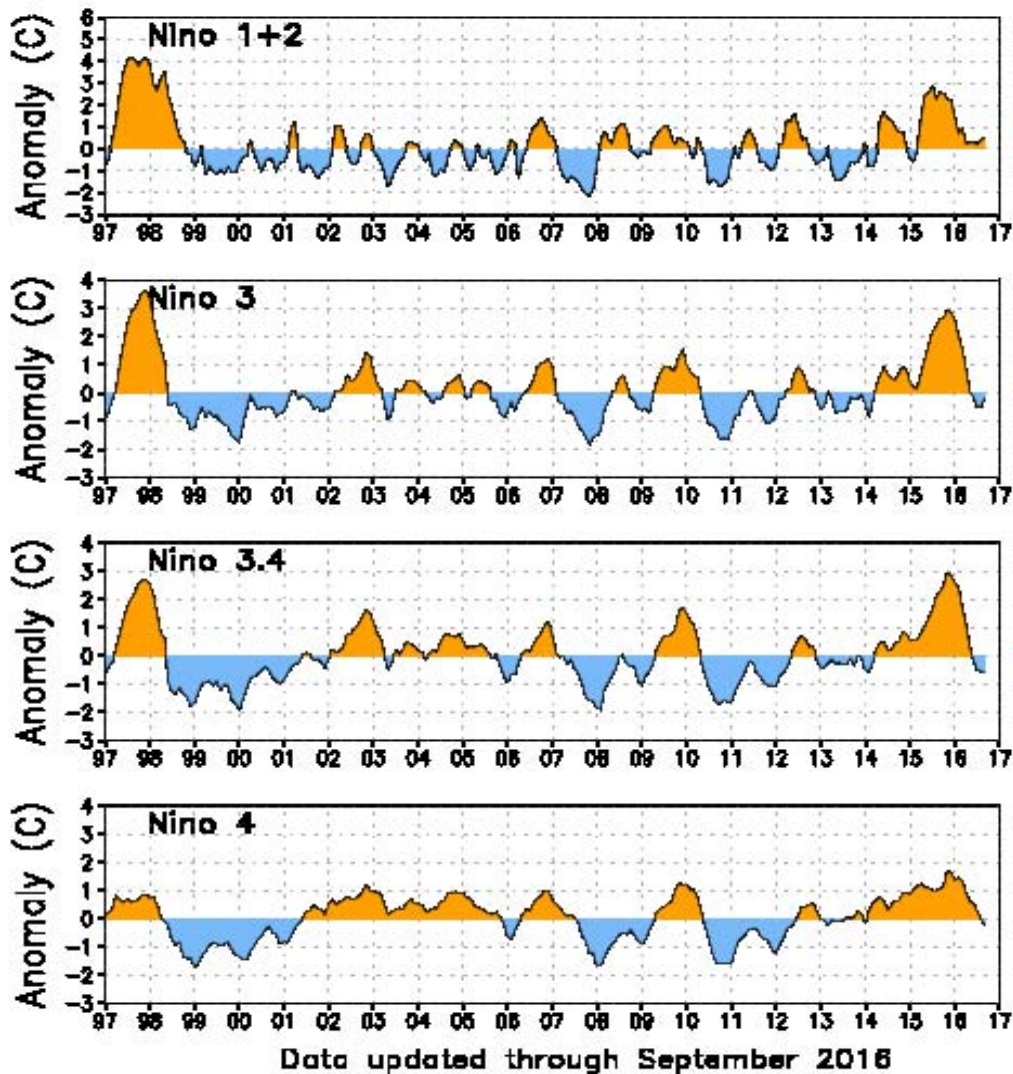


FIGURE T5. Niño region indices, calculated as the area-averaged sea surface temperature anomalies (C) for the specified region. The Niño 1+2 region (top) covers the extreme eastern equatorial Pacific between 0-10S, 90W-80W. The Niño-3 region (2nd from top) spans the eastern equatorial Pacific between 5N-5S, 150W-90W. The Niño 3.4 region (3rd from top) spans the east-central equatorial Pacific between 5N-5S, 170W-120W. The Niño 4 region (bottom) spans the date line and covers the area 5N-5S, 160E-150W. Anomalies are departures from the 1981-2010 base period monthly means (*Smith and Reynolds 1998, J. Climate, 11, 3320-3323*). Monthly values of each index are also displayed in [Table 2](#).

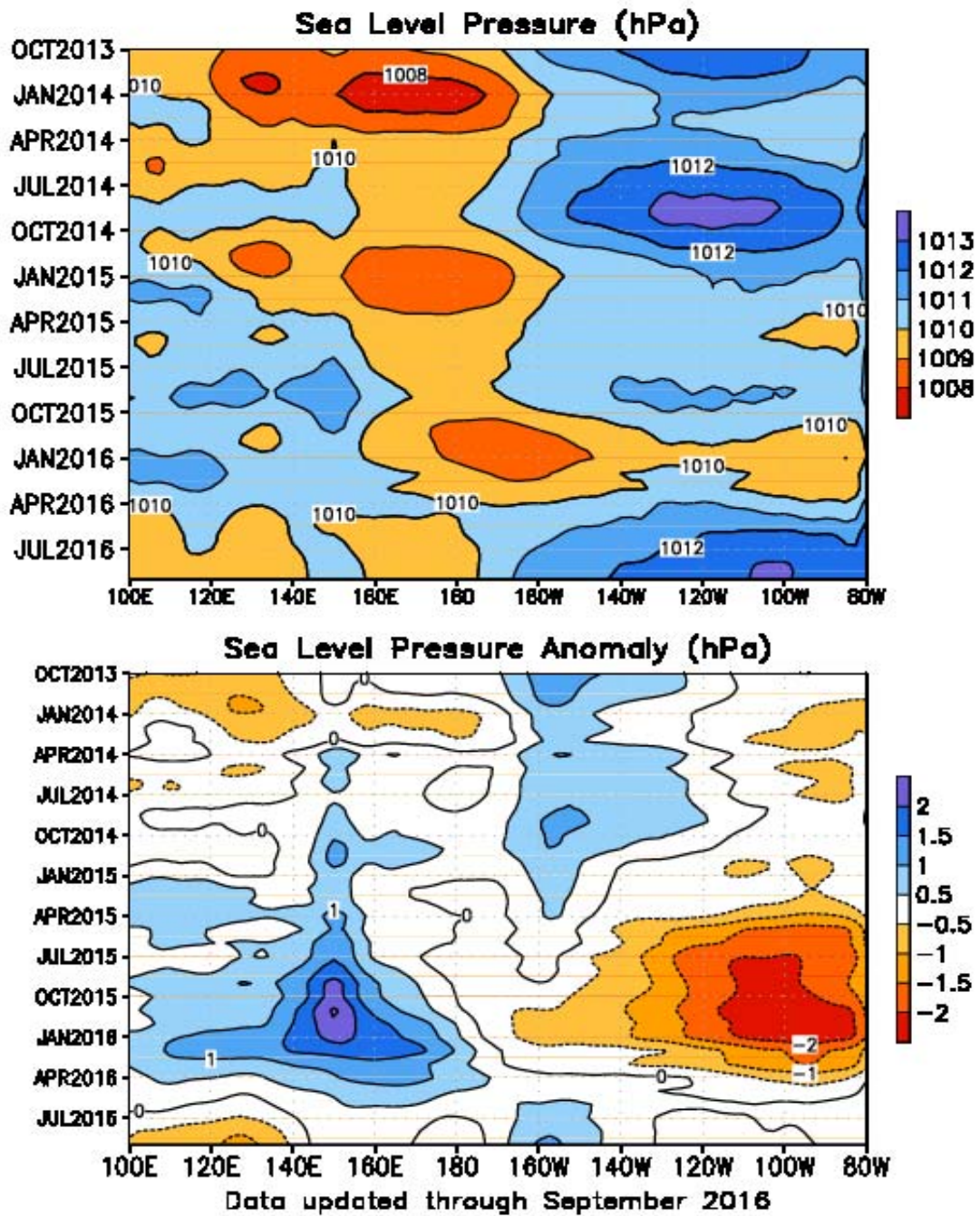


FIGURE T6. Time-longitude section of mean (top) and anomalous (bottom) sea level pressure (SLP) averaged between 5N-5S (CDAS/Reanalysis). Contour interval is 1.0 hPa (top) and 0.5 hPa (bottom). Dashed contours in bottom panel indicate negative anomalies. Anomalies are departures from the 1981-2010 base period monthly means. The data are smoothed temporally using a 3-month running average.



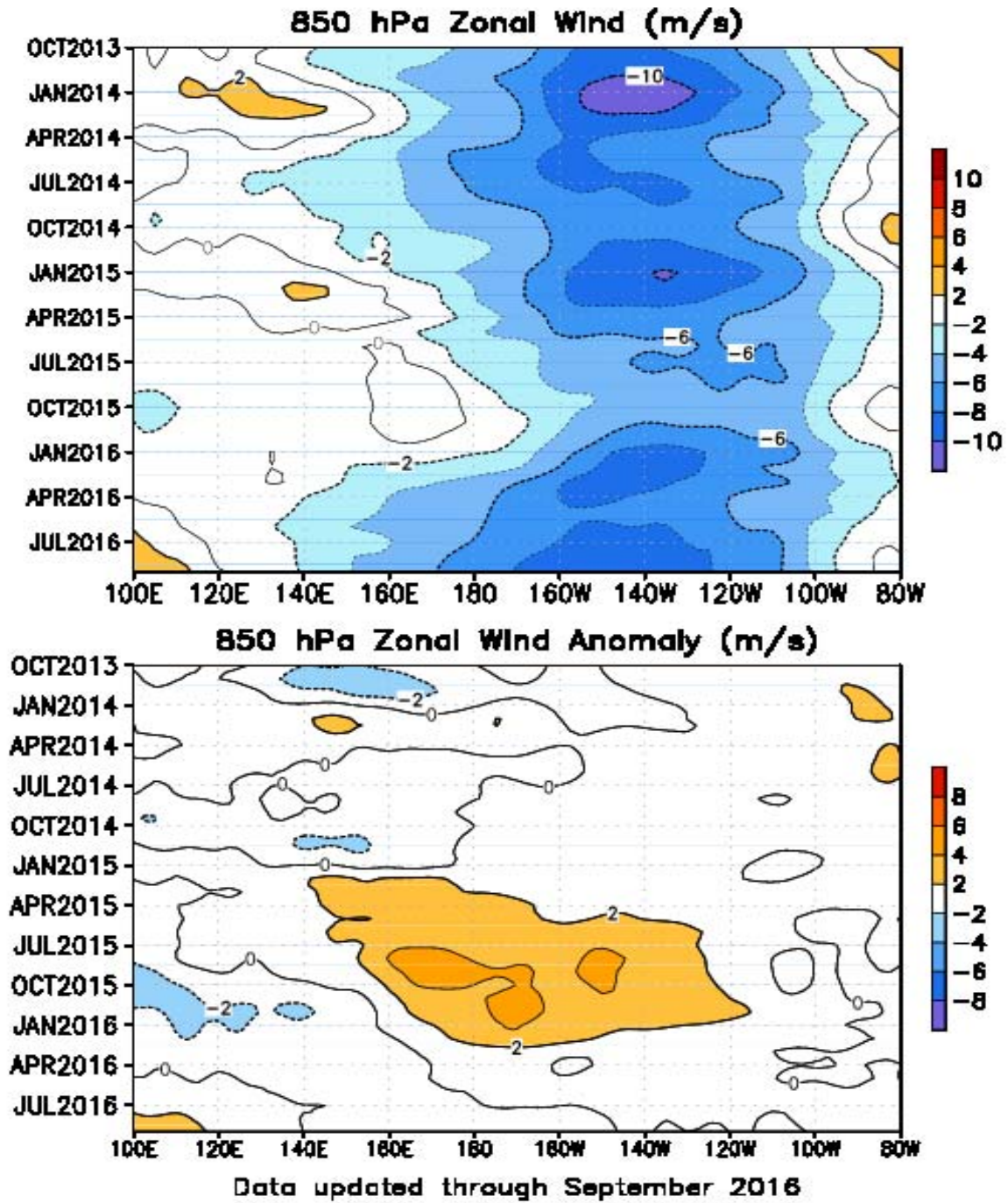


FIGURE T7. Time-longitude section of mean (top) and anomalous (bottom) 850-hPa zonal wind averaged between 5N-5S (CDAS/Reanalysis). Contour interval is  $2 \text{ ms}^{-1}$ . Blue shading and dashed contours indicate easterlies (top) and easterly anomalies (bottom). Anomalies are departures from the 1981-2010 base period monthly means. The data are smoothed temporally using a 3-month running average.

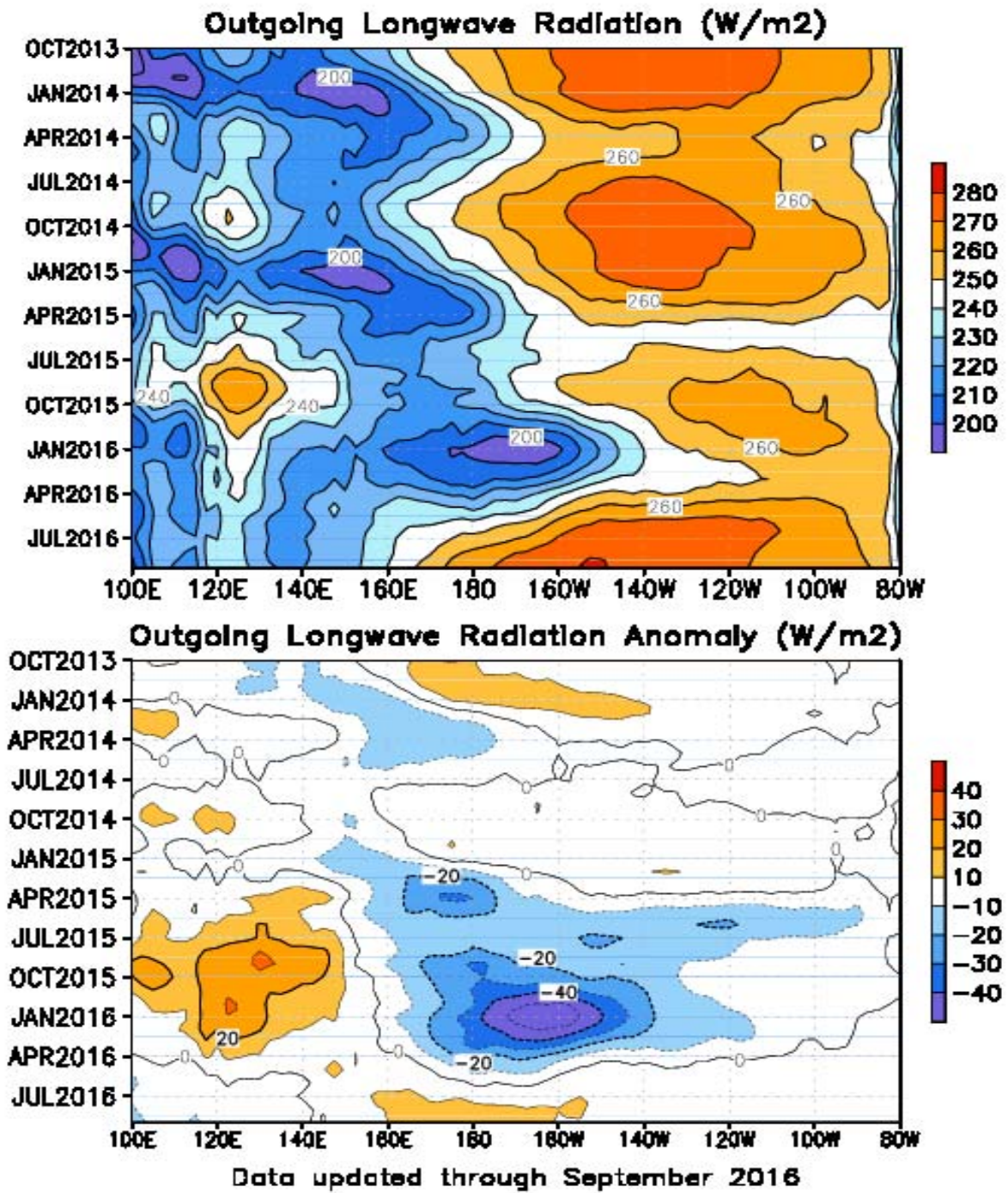


FIGURE T8. Time-longitude section of mean (top) and anomalous (bottom) outgoing longwave radiation (OLR) averaged between 5N-5S. Contour interval is 10 Wm<sup>-2</sup>. Dashed contours in bottom panel indicate negative OLR anomalies. Anomalies are departures from the 1981-2010 base period monthly means. The data are smoothed temporally using a 3-month running average.



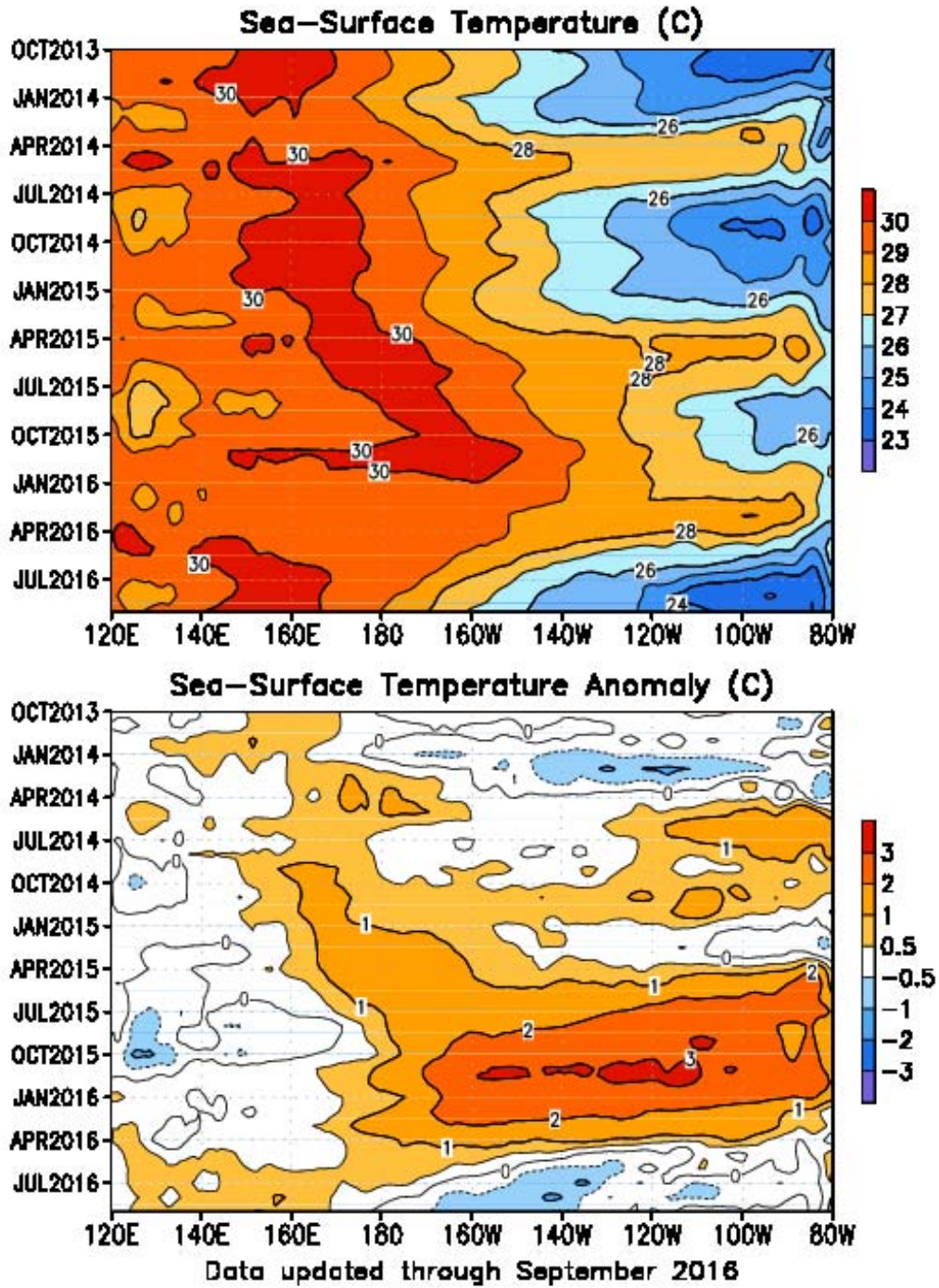


FIGURE T9. Time-longitude section of monthly mean (top) and anomalous (bottom) sea surface temperature (SST) averaged between 5N-5S. Contour interval is 1C (top) and 0.5C (bottom). Dashed contours in bottom panel indicate negative anomalies. Anomalies are departures from the 1981-2010 base period means (Smith and Reynolds 1998, *J. Climate*, **11**, 3320-3323).

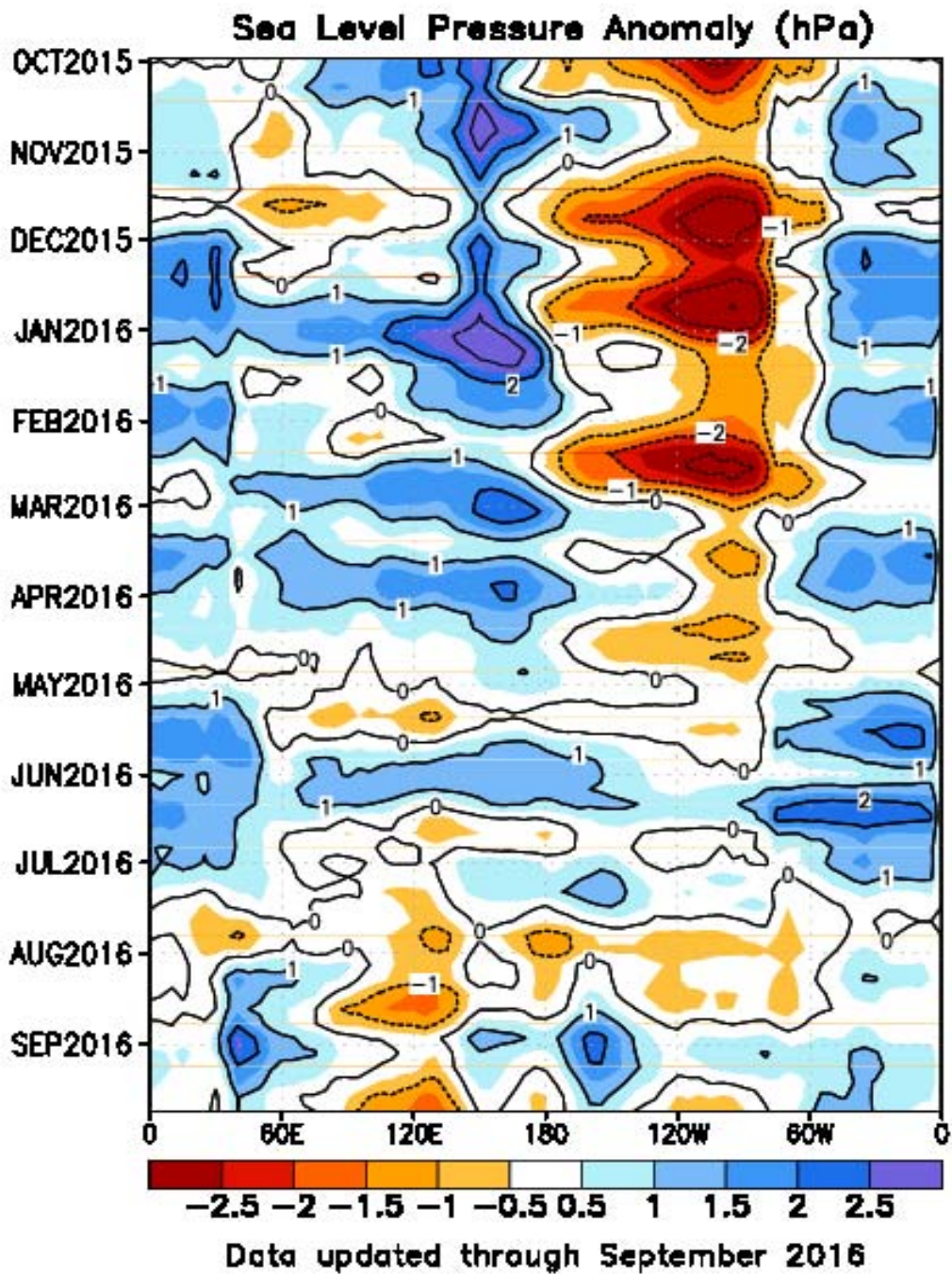


FIGURE T10. Time-longitude section of anomalous sea level pressure (hPa) averaged between 5N-5S (CDAS/Re-analysis). Contour interval is 1 hPa. Dashed contours indicate negative anomalies. Anomalies are departures from the 1981-2010 base period pentad means. The data are smoothed temporally using a 3-point running average.



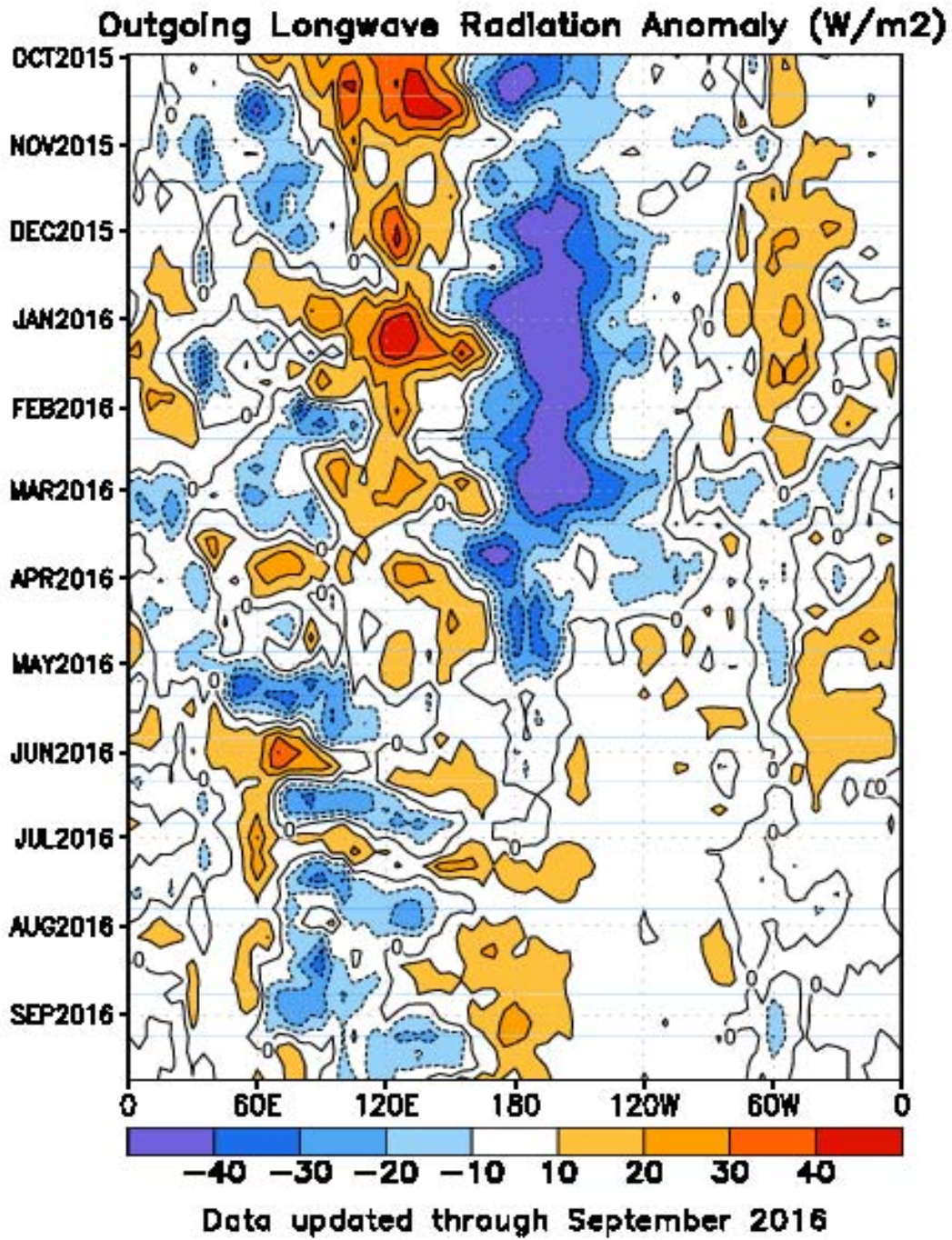


FIGURE T11. Time-longitude section of anomalous outgoing longwave radiation averaged between 5N-5S. Contour interval is 15 Wm<sup>-2</sup>. Dashed contours indicate negative anomalies. Anomalies are departures from the 1981-2010 base period pentad means. The data are smoothed temporally using a 3-point running average.

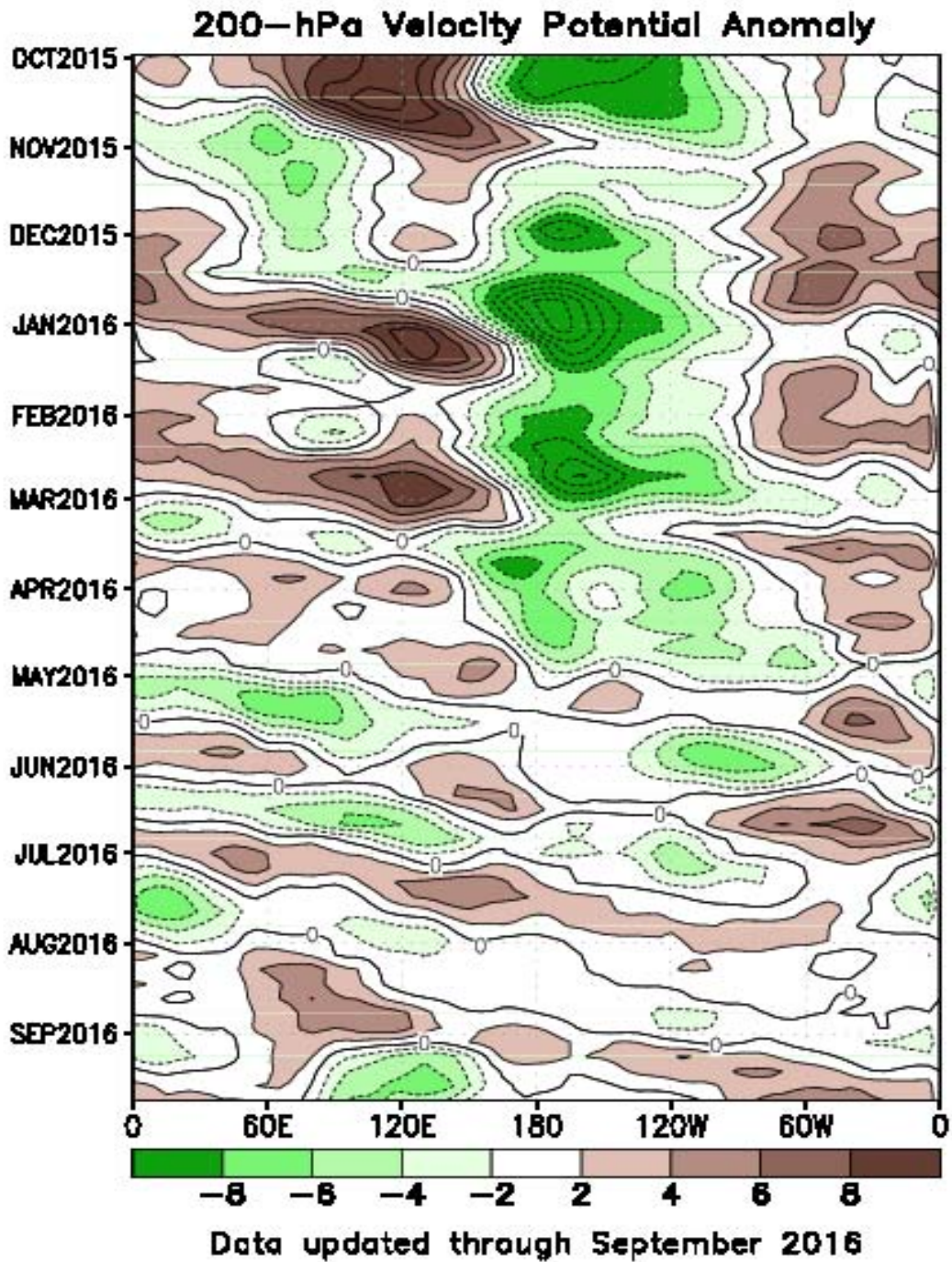
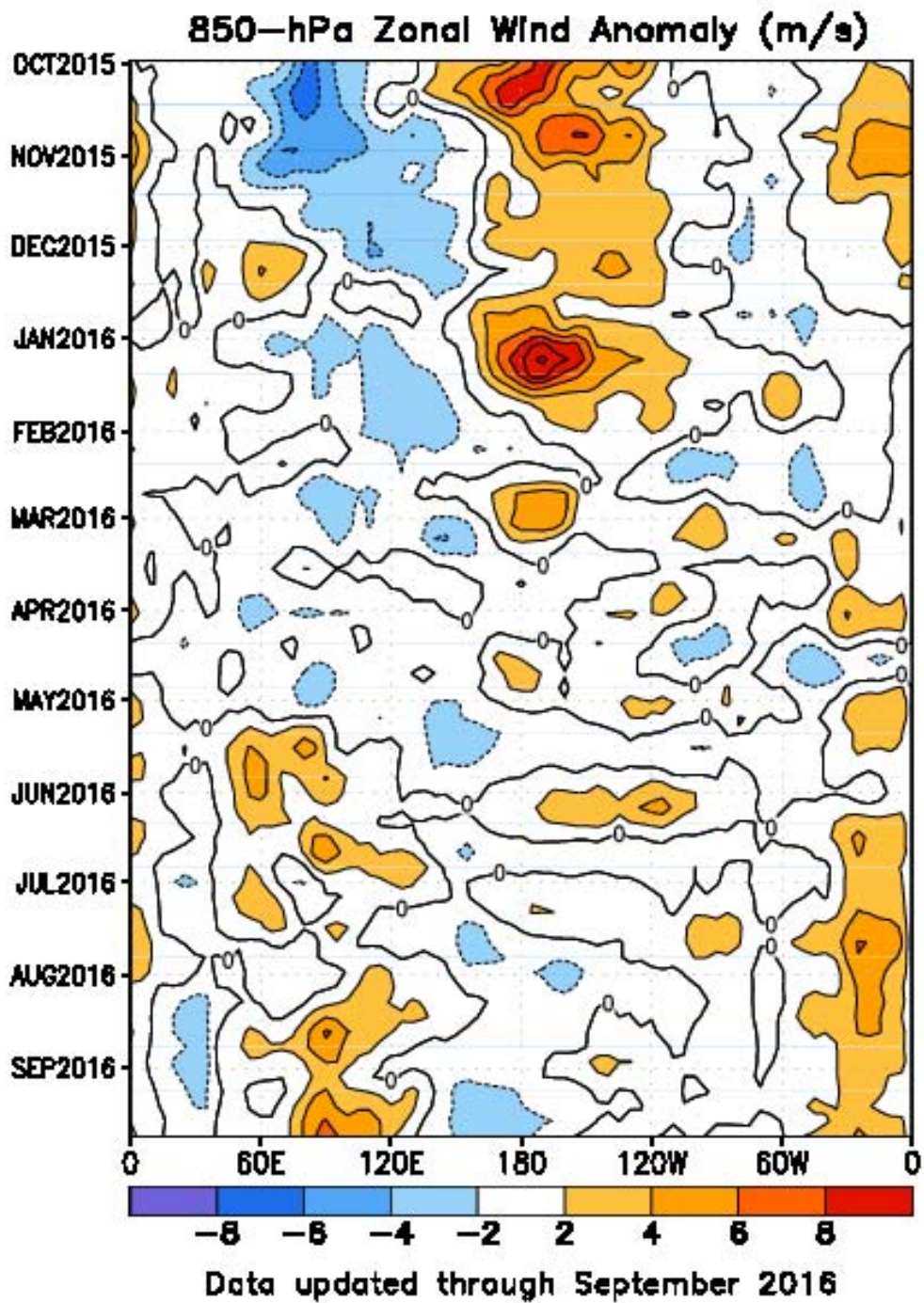


FIGURE T12. Time-longitude section of anomalous 200-hPa velocity potential averaged between 5N-5S (CDAS/Re-analysis). Contour interval is  $3 \times 10^6 \text{ m}^2\text{s}^{-1}$ . Dashed contours indicate negative anomalies. Anomalies are departures from the 1981-2010 base period pentad means. The data are smoothed temporally using a 3-point running average.





Contour interval is  $2 \text{ m/s}^{-1}$ . Dashed contours indicate negative anomalies. Anomalies are departures from the 1981-2010 base period pentad means. The data are smoothed temporally by using a 3-point running average.

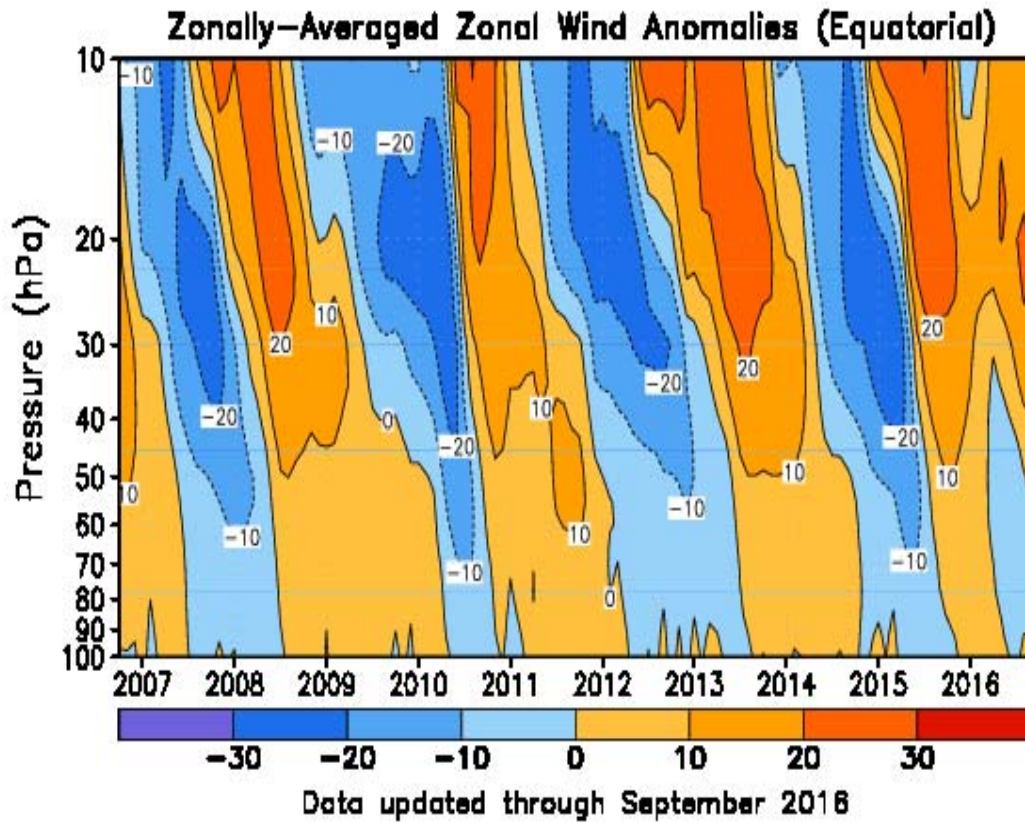


FIGURE T14. Equatorial time-height section of anomalous zonally-averaged zonal wind ( $\text{m s}^{-1}$ ) (CDAS/Reanalysis). Contour interval is  $10 \text{ m s}^{-1}$ . Anomalies are departures from the 1981-2010 base period monthly means.



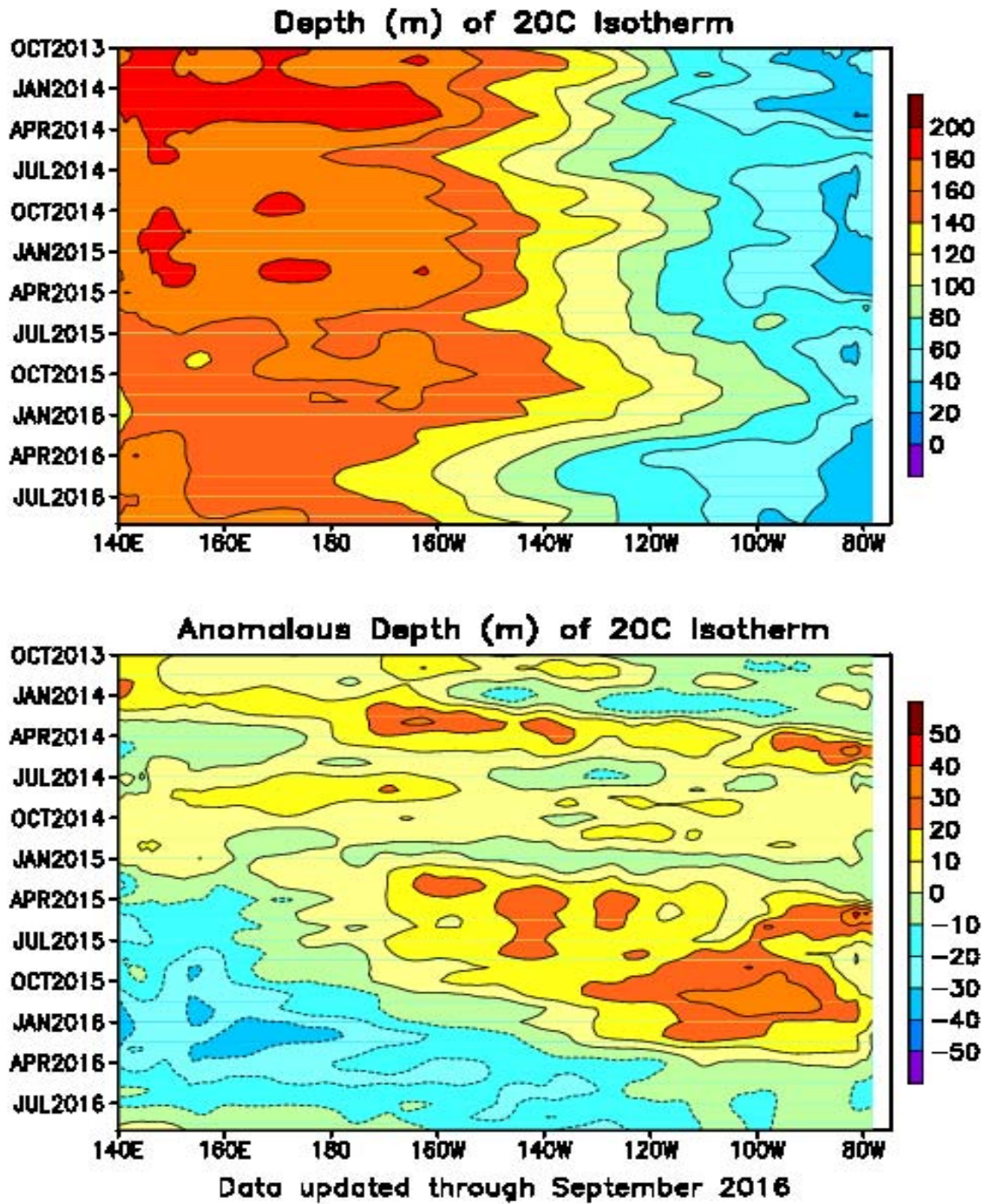


FIGURE T15. Mean (top) and anomalous (bottom) depth of the 20C isotherm averaged between 5N-5S in the Pacific Ocean. Data are derived from the NCEP's global ocean data assimilation system which assimilates oceanic observations into an oceanic GCM (Behringer, D. W., and Y. Xue, 2004: Evaluation of the global ocean data assimilation system at NCEP: The Pacific Ocean. AMS 84th Annual Meeting, Seattle, Washington, 11-15). The contour interval is 10 m. Dashed contours in bottom panel indicate negative anomalies. Anomalies are departures from the 1981-2010 base period means.

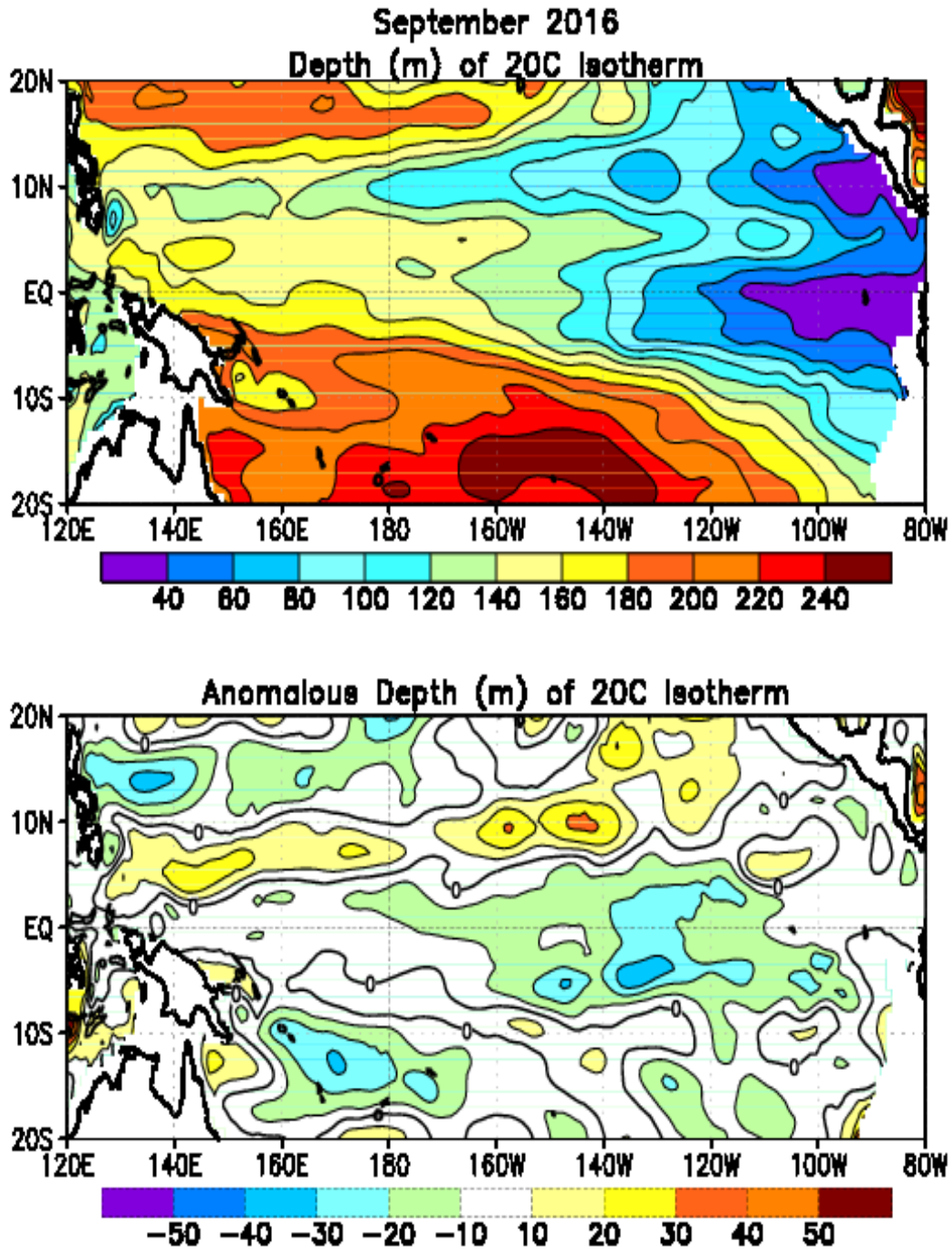
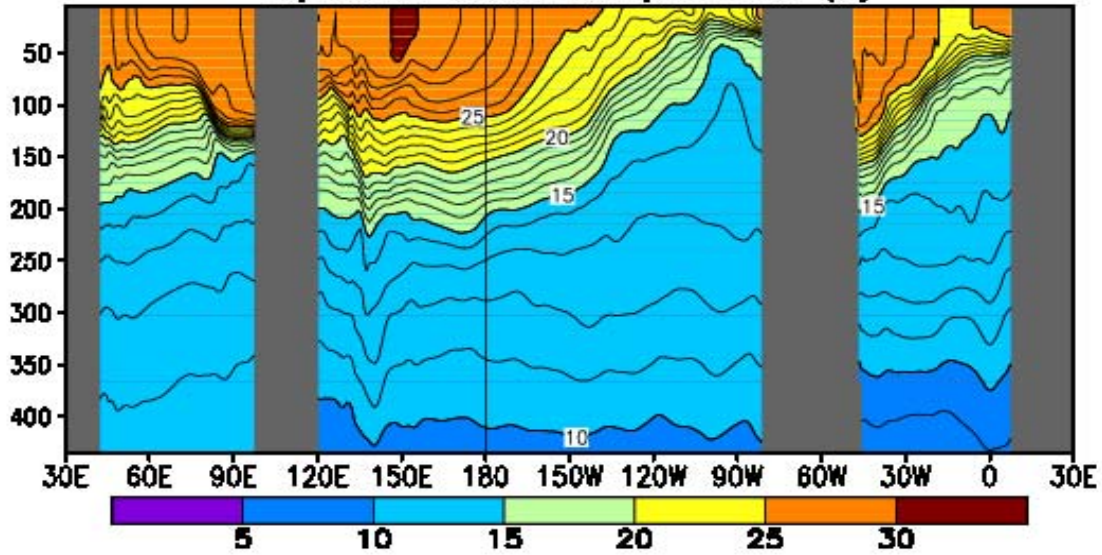


FIGURE T16. Mean (top) and anomalous (bottom) depth of the 20°C isotherm for SEP 2016. Contour interval is 40 m (top) and 10 m (bottom). Dashed contours in bottom panel indicate negative anomalies. Data are derived from the NCEP’s global ocean data assimilation system version 2 which assimilates oceanic observations into an oceanic GCM (Xue, Y. and Behringer, D.W., 2006: Operational global ocean data assimilation system at NCEP, to be submitted to BAMS). Anomalies are departures from the 1981–2010 base period means.



**September 2016: Depth–Longitude Section  
Equatorial Ocean Temperatures (C)**



**Equatorial Ocean Temperature Anomalies (C)**

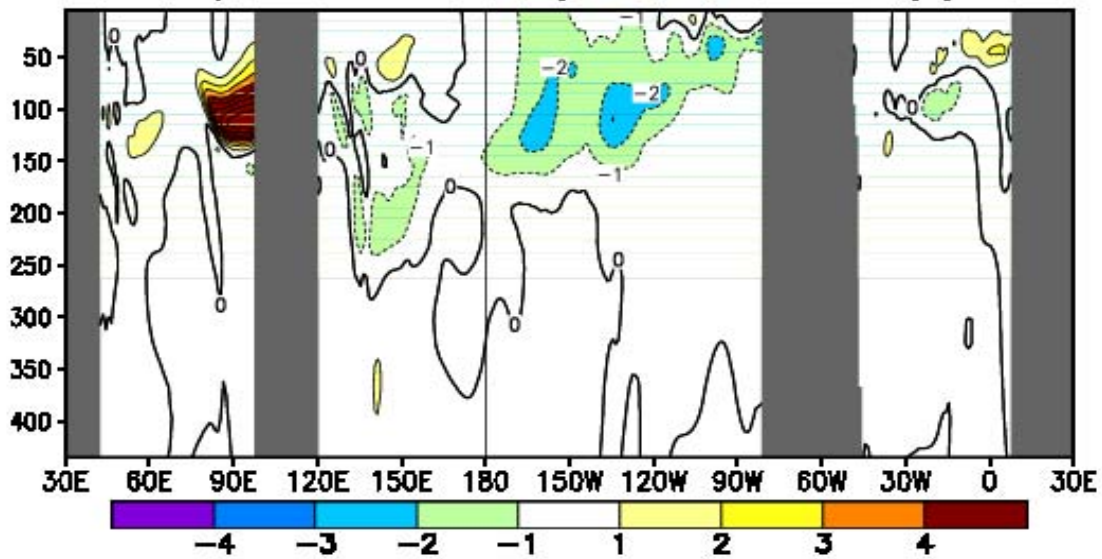


FIGURE T17. Equatorial depth–longitude section of ocean temperature (top) and ocean temperature anomalies (bottom) for SEP 2016. Contour interval is 1°C. Dashed contours in bottom panel indicate negative anomalies. Data are derived from the NCEP’s global ocean data assimilation system version 2 which assimilates oceanic observations into an oceanic GCM (Xue, Y. and Behringer, D.W., 2006: Operational global ocean data assimilation system at NCEP, to be submitted to BAMS). Anomalies are departures from the 1981–2010 base period means.

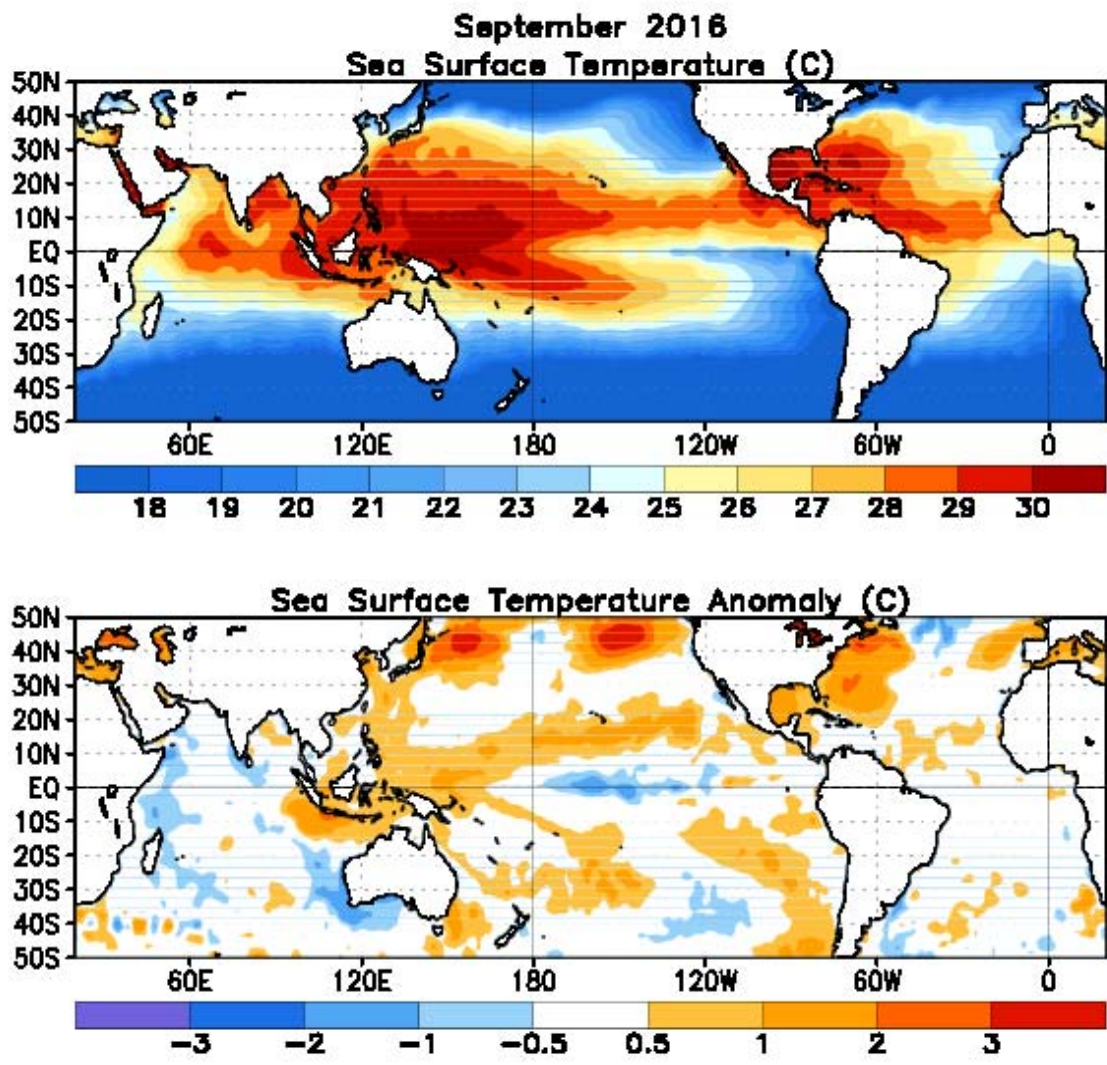


FIGURE T18. Mean (top) and anomalous (bottom) sea surface temperature (SST). Anomalies are departures from the 1981-2010 base period monthly means (Smith and Reynolds 1998, *J. Climate*, **11**, 3320-3323).

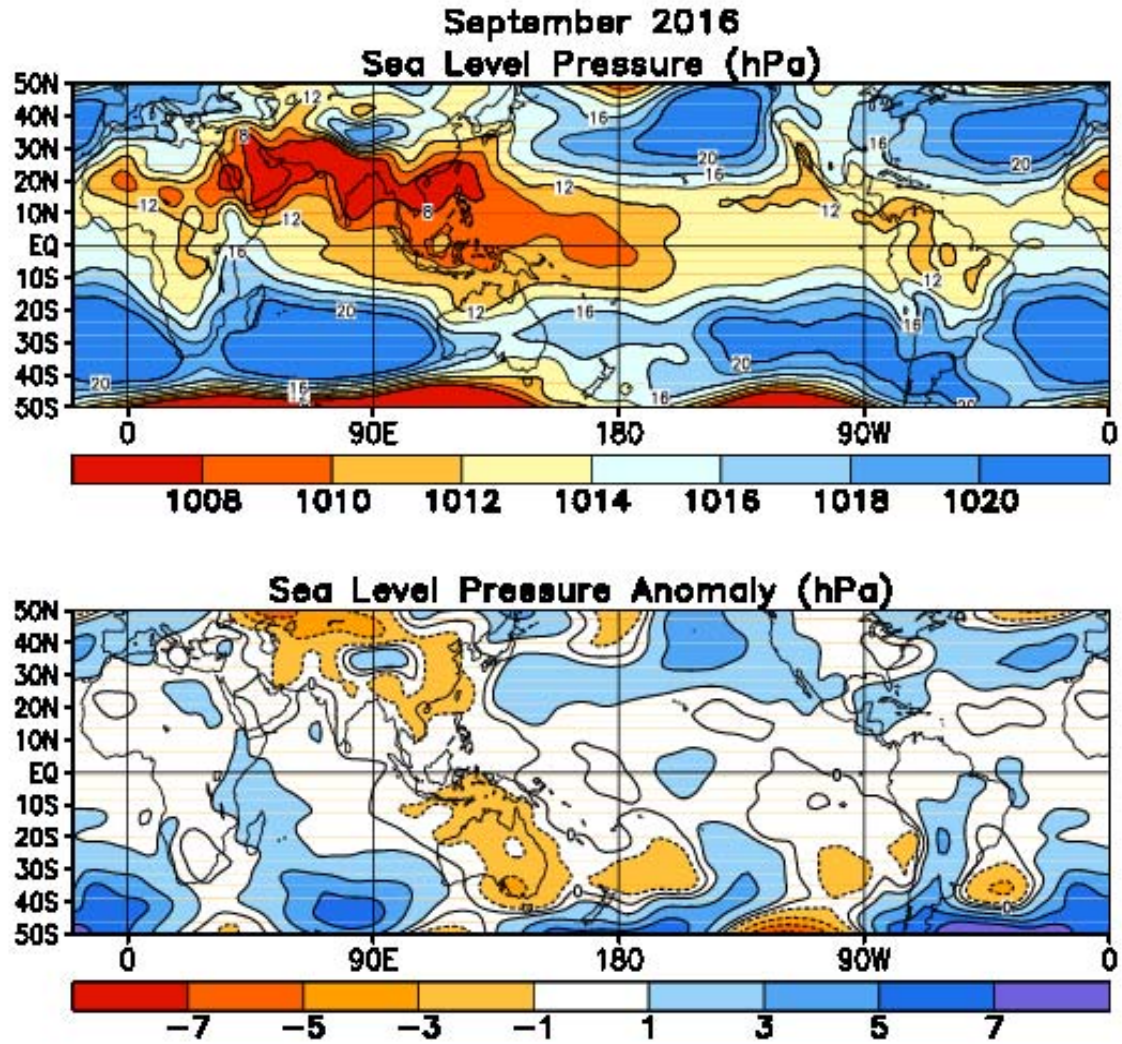


FIGURE T19. Mean (top) and anomalous (bottom) sea level pressure (SLP) (CDAS/Reanalysis). In top panel, 1000 hPa has been subtracted from contour labels, contour interval is 2 hPa, and values below 1000 hPa are indicated by dashed contours. In bottom panel, anomaly contour interval is 1 hPa and negative anomalies are indicated by dashed contours. Anomalies are departures from the 1981-2010 base period monthly means.



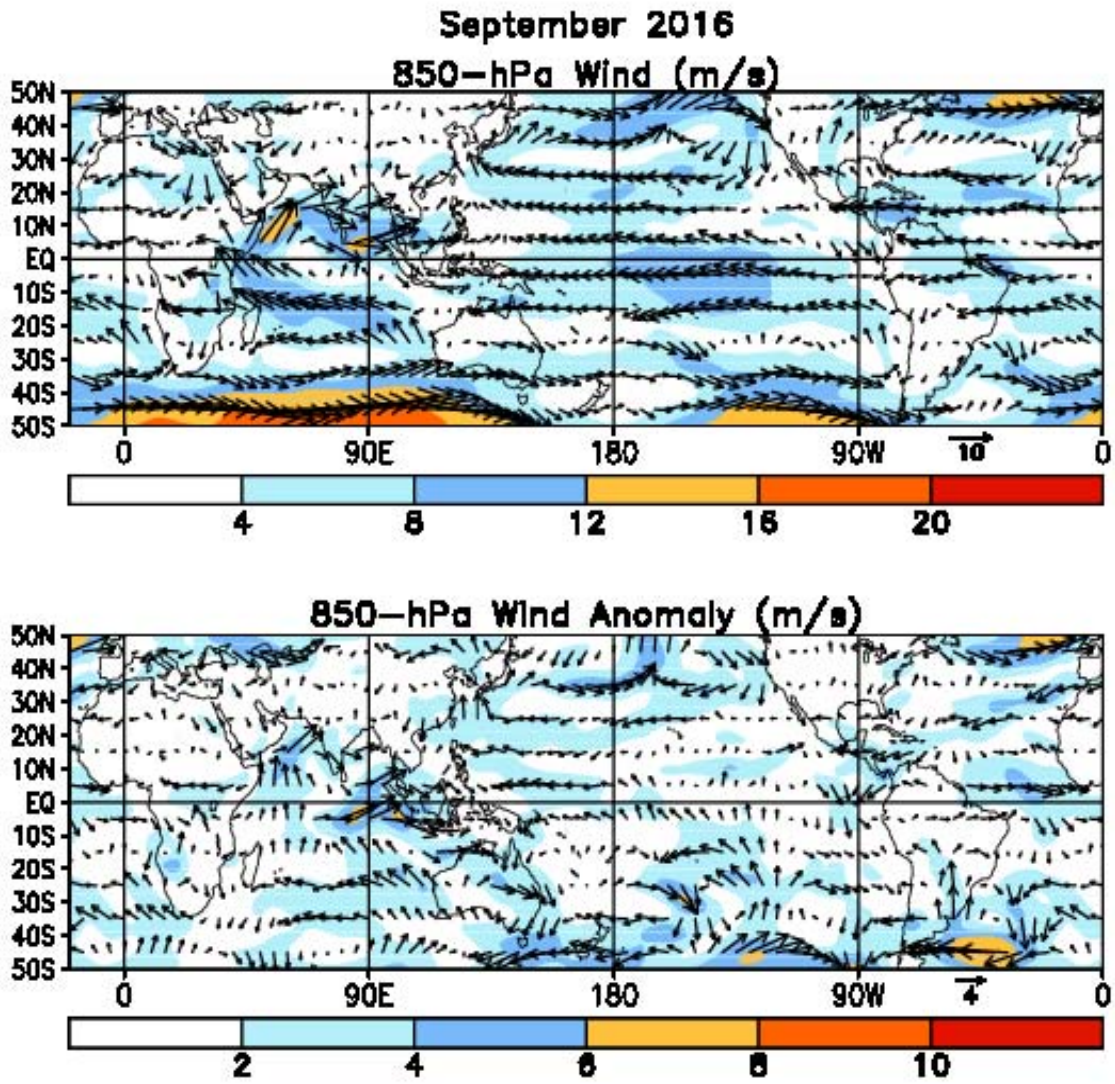


FIGURE T20. Mean (top) and anomalous (bottom) 850-hPa vector wind (CDAS/Reanalysis) for SEP 2016. Contour interval for isotachs is  $4 \text{ ms}^{-1}$  (top) and  $2 \text{ ms}^{-1}$  (bottom). Anomalies are departures from the 1981-2010 base period monthly means.

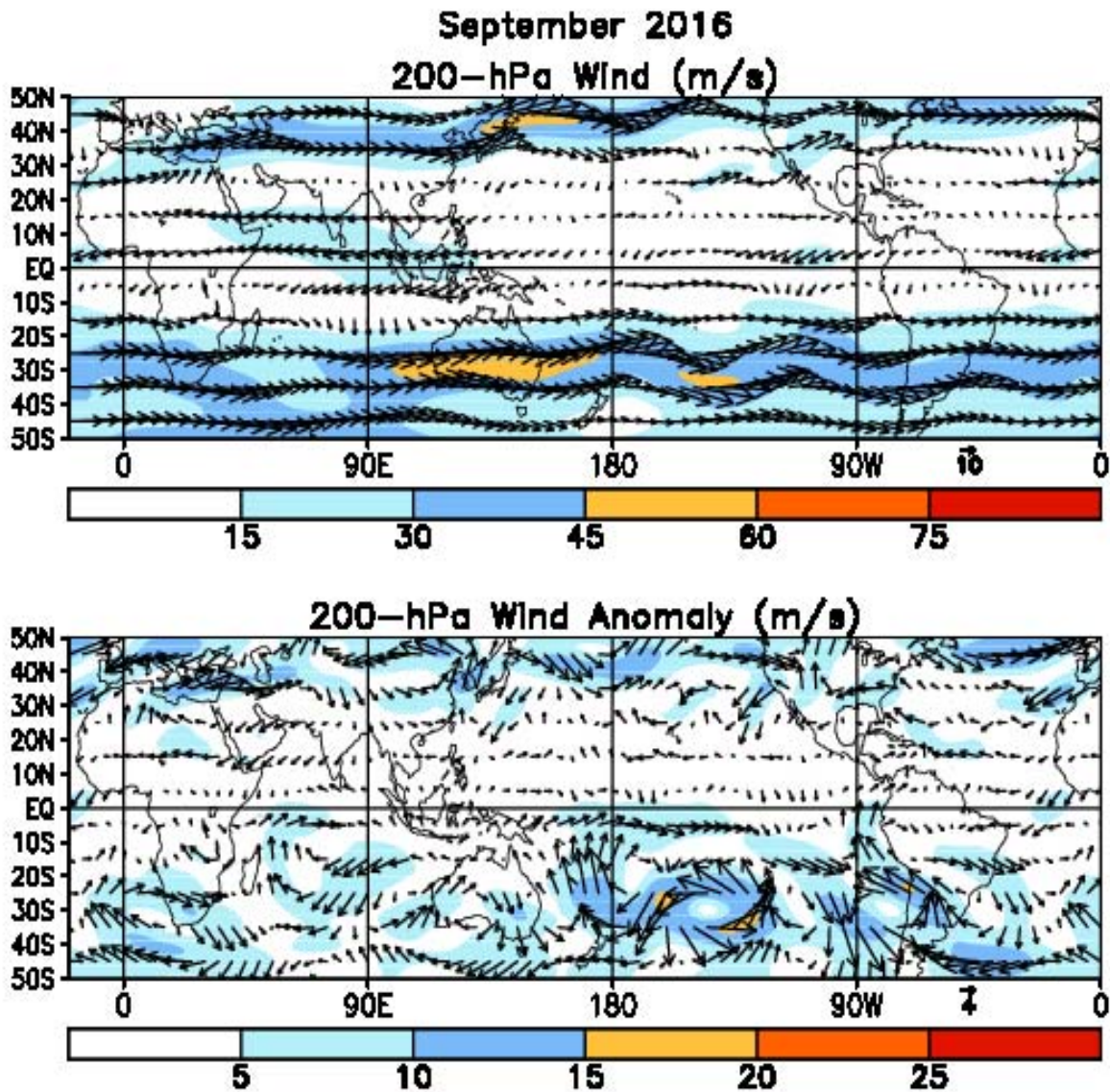


FIGURE T21. Mean (top) and anomalous (bottom) 200-hPa vector wind (CDAS/Reanalysis) for SEP 2016. Contour interval for isotachs is  $15 \text{ ms}^{-1}$  (top) and  $5 \text{ ms}^{-1}$  (bottom). Anomalies are departures from 1981-2010 base period monthly means.



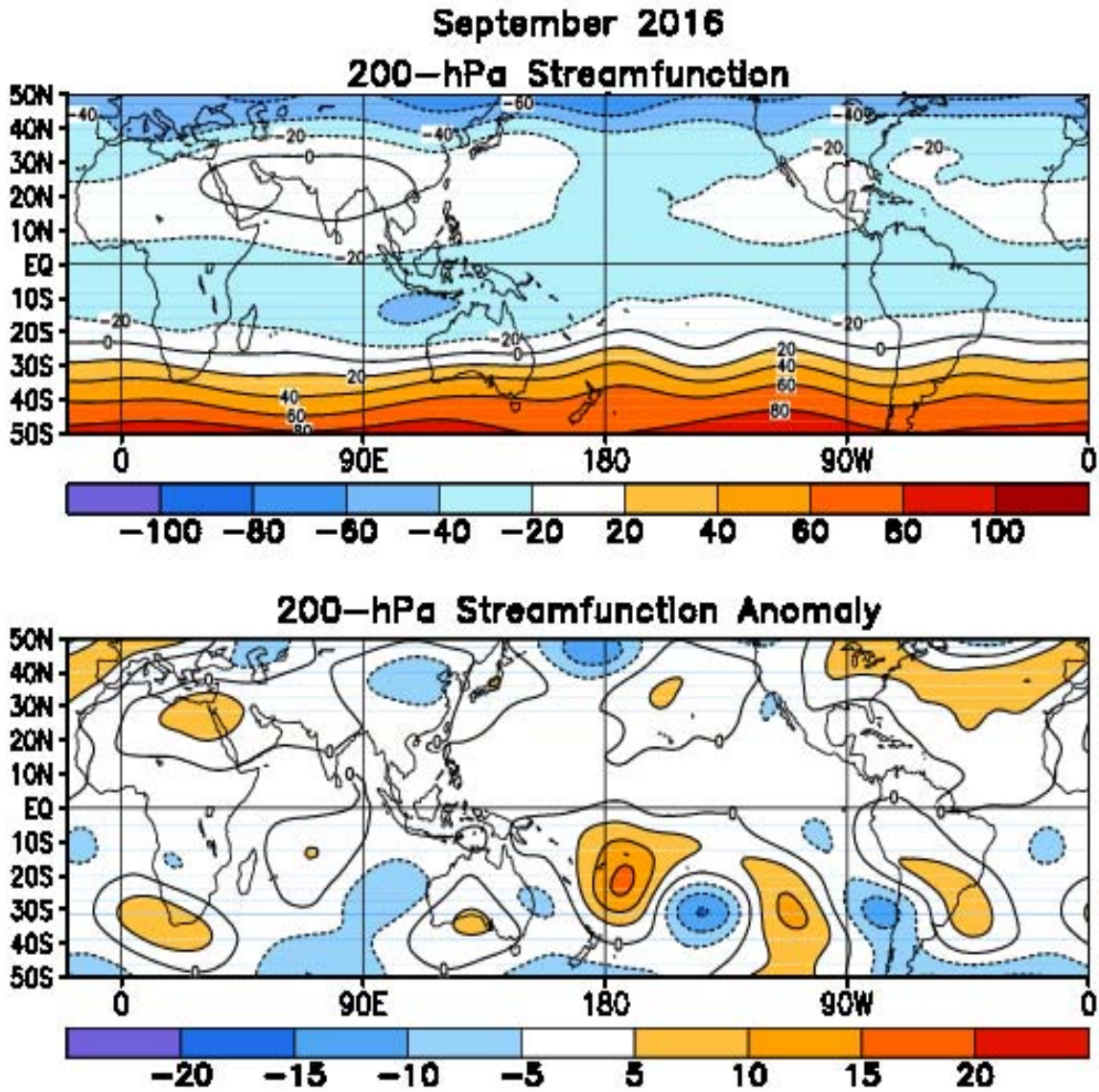


FIGURE T22. Mean (top) and anomalous (bottom) 200-hPa streamfunction (CDAS/Reanalysis). Contour interval is  $20 \times 10^6 \text{ m}^2\text{s}^{-1}$  (top) and  $5 \times 10^6 \text{ m}^2\text{s}^{-1}$  (bottom). Negative (positive) values are indicated by dashed (solid) lines. The non-divergent component of the flow is directed along the contours with speed proportional to the gradient. Thus, high (low) stream function corresponds to high (low) geopotential height in the Northern Hemisphere and to low (high) geopotential height in the Southern Hemisphere. Anomalies are departures from the 1981-2010 base period monthly means.

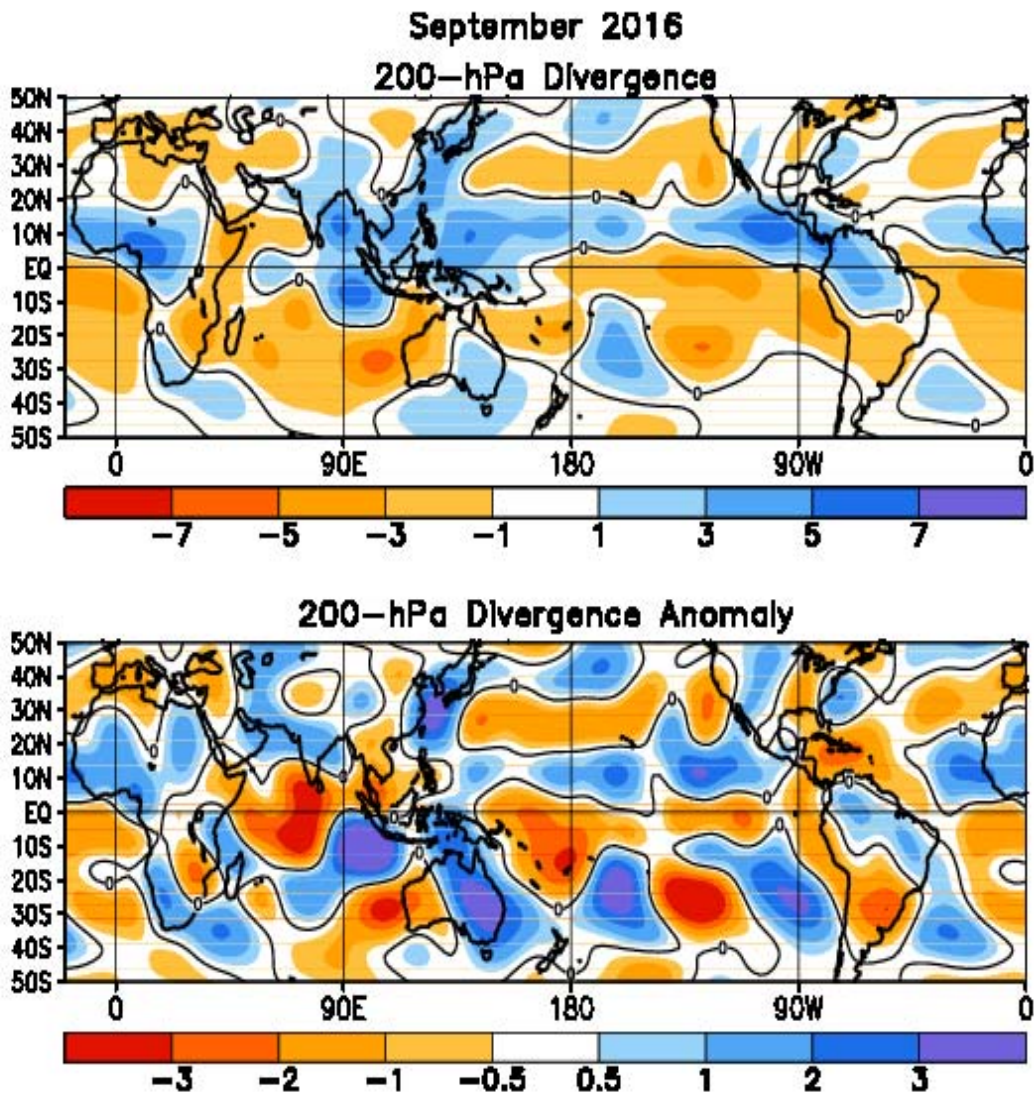


FIGURE T23. Mean (top) and anomalous (bottom) 200-hPa divergence (CDAS/Reanalysis). Divergence and anomalous divergence are shaded blue. Convergence and anomalous convergence are shaded orange. Anomalies are departures from the 1981-2010 base period monthly means.



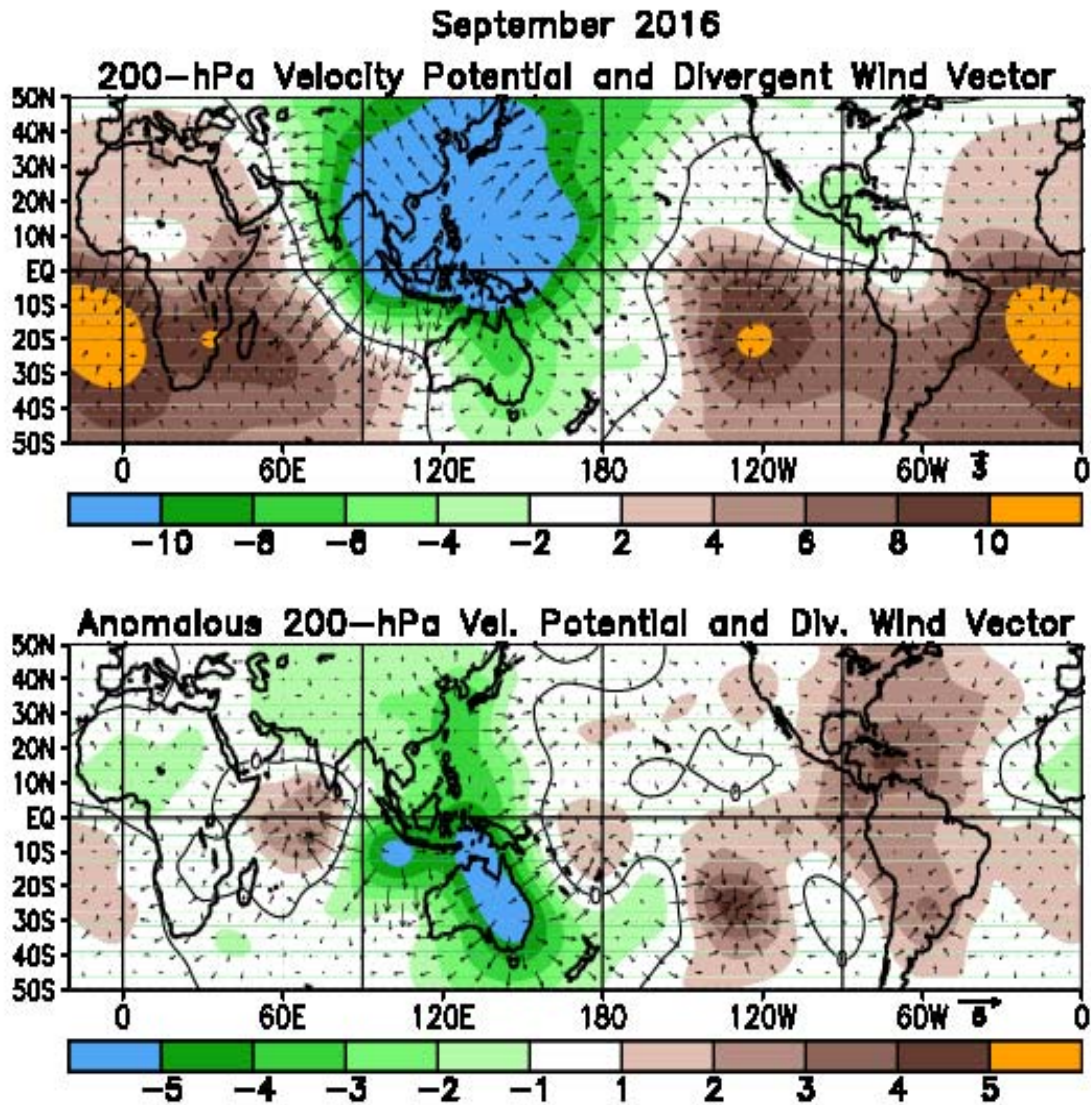


FIGURE T24. Mean (top) and anomalous (bottom) 200-hPa velocity potential ( $10^6\text{m}^2\text{s}$ ) and divergent wind (CDAS/Reanalysis). Anomalies are departures from the 1981-2010 base period monthly means.



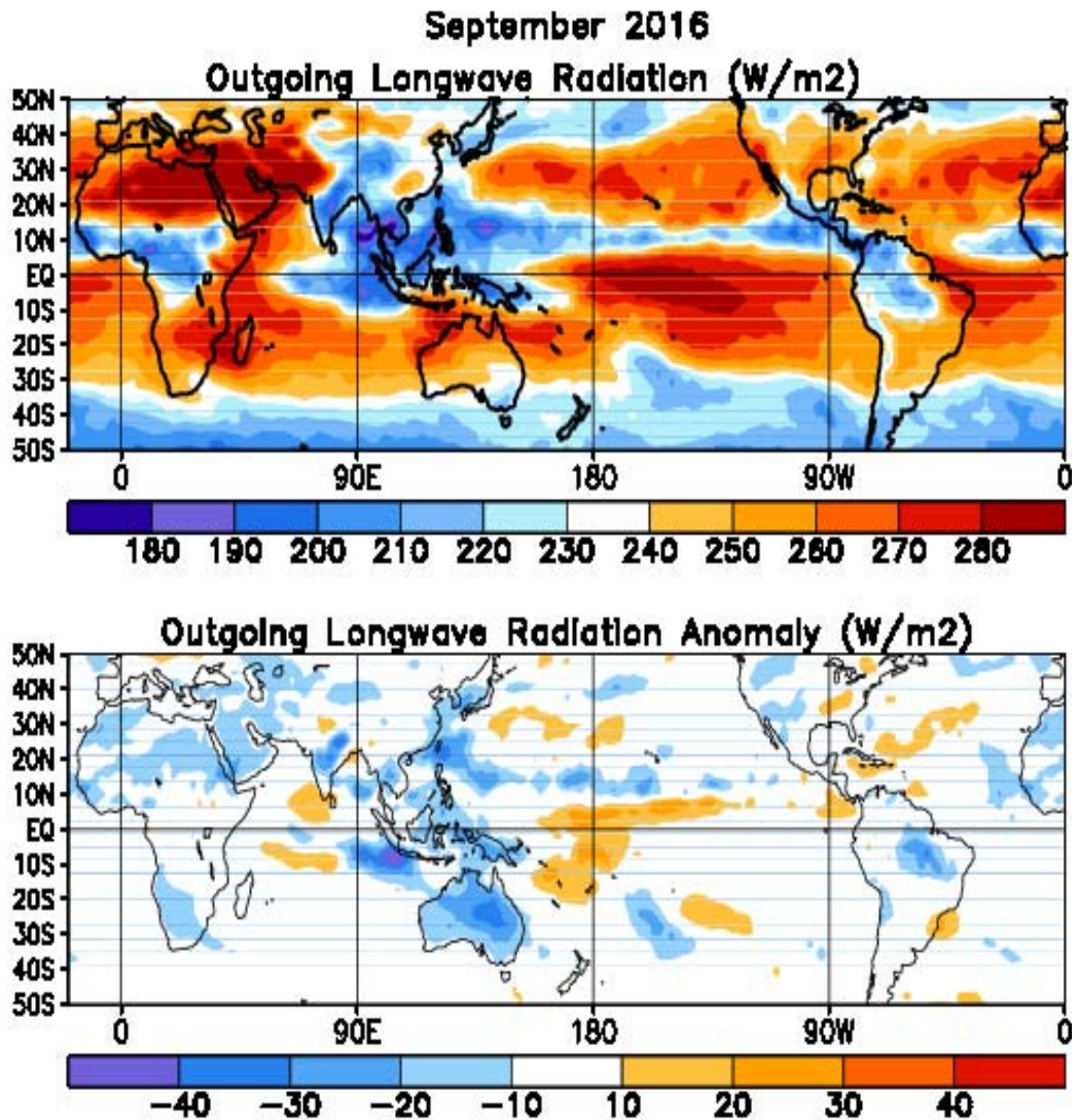


FIGURE T25. Mean (top) and anomalous (bottom) outgoing longwave radiation for SEP 2016 (NOAA 18 AVHRR IR window channel measurements by NESDIS/ORA). OLR contour interval is 20 Wm<sup>-2</sup> with values greater than 280 Wm<sup>-2</sup> indicated by dashed contours. Anomaly contour interval is 15 Wm<sup>-2</sup> with positive values indicated by dashed contours and light shading. Anomalies are departures from the 1981-2010 base period monthly means.

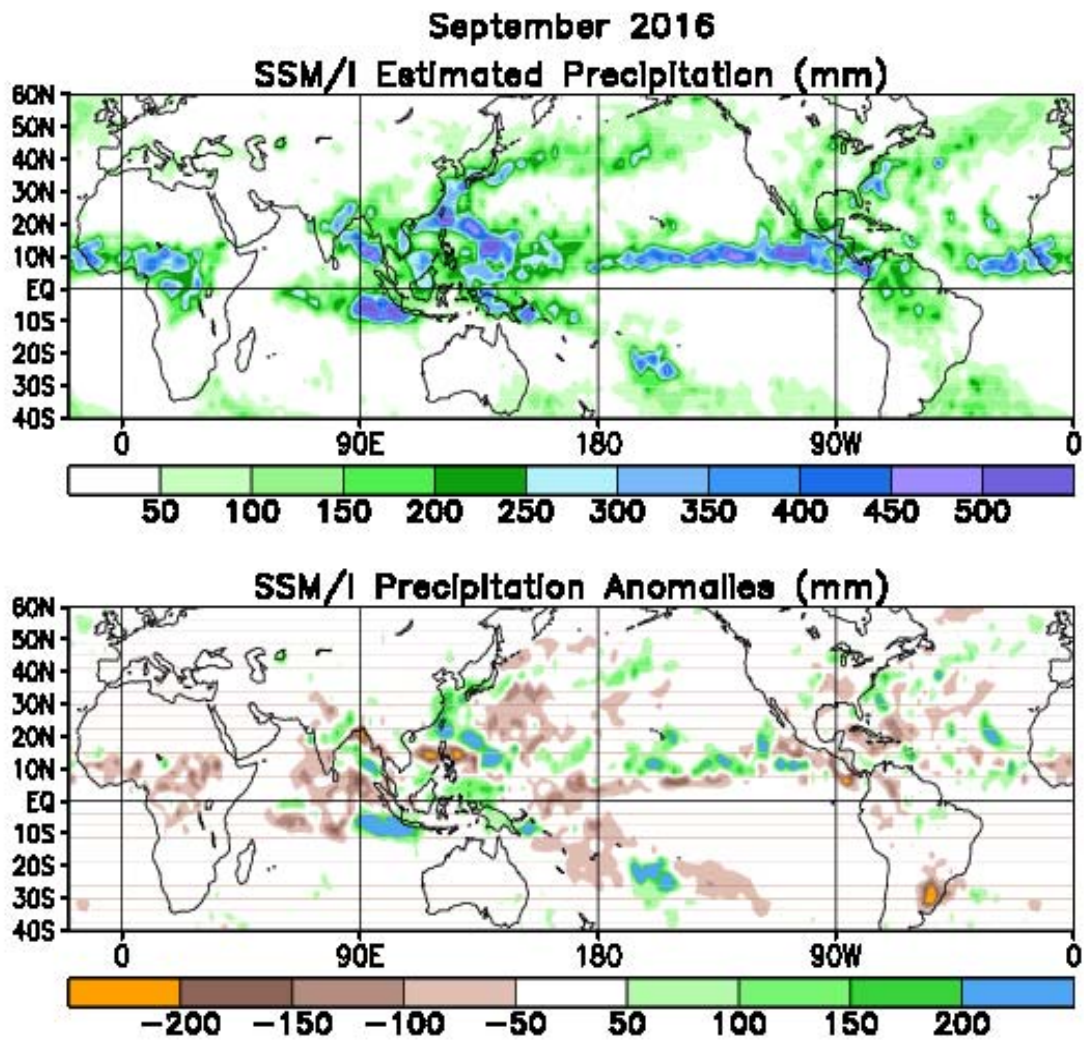


FIGURE T26. Estimated total (top) and anomalous (bottom) rainfall (mm) based on the Special Sensor Microwave/Imager (SSM/S) precipitation index (Ferraro 1997, *J. Geophys. Res.*, **102**, 16715-16735). Anomalies are computed from the SSM/I 1987-2010 base period monthly means. Anomalies have been smoothed for display purposes.

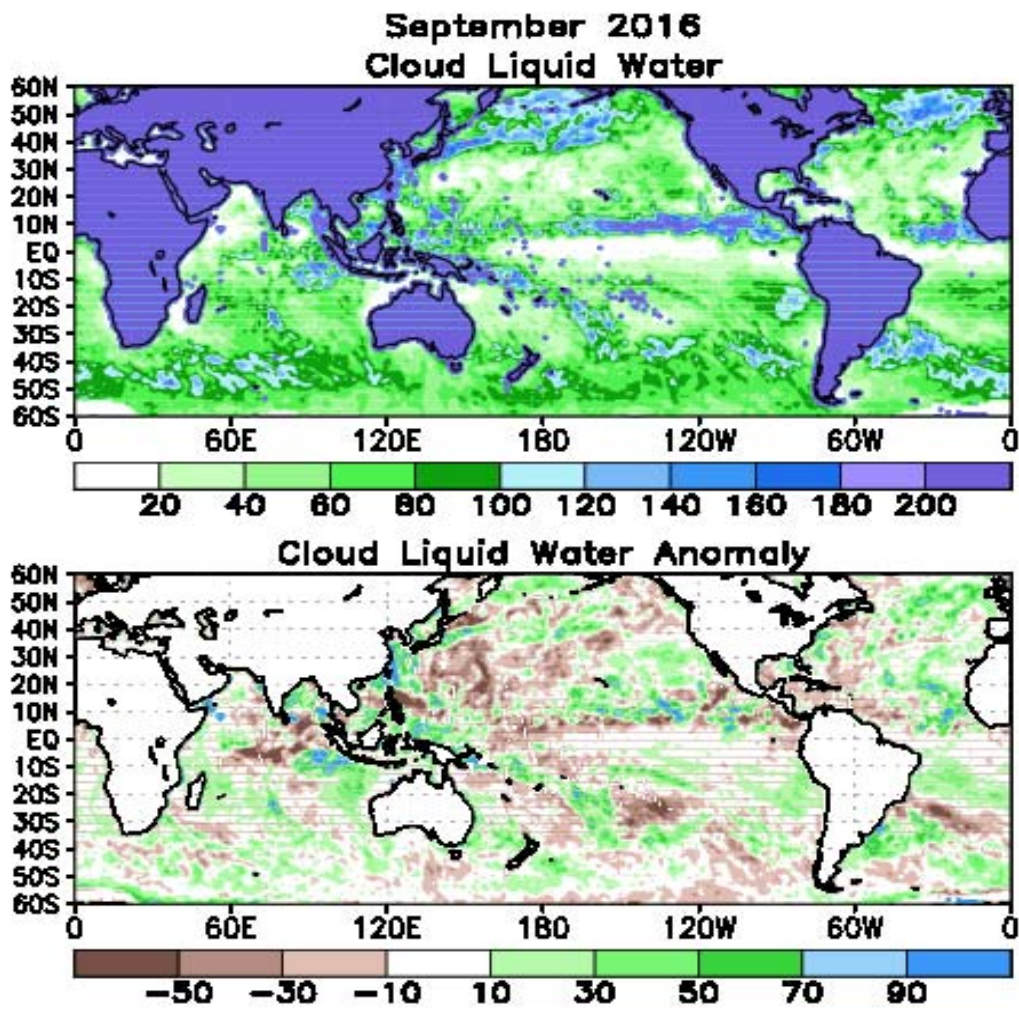


FIGURE T27. Mean (top) and anomalous (bottom) cloud liquid water ( $\text{g m}^{-2}$ ) based on the Special Sensor Microwave/Imager (SSM/I) (Weng et al 1997: *J. Climate*, **10**, 1086-1098). Anomalies are calculated from the 1987-2010 base period means.



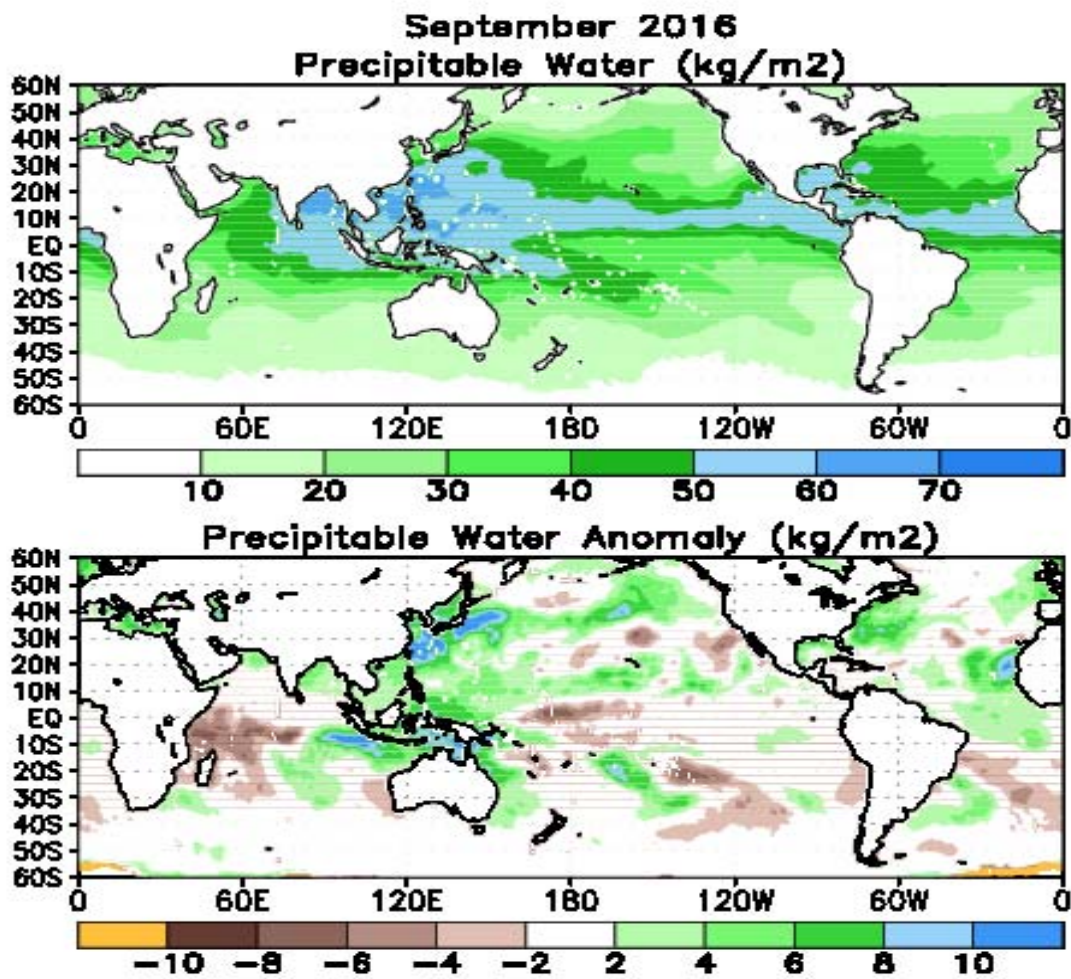


FIGURE T28. Mean (top) and anomalous (bottom) vertically integrated water vapor or precipitable water ( $\text{kg m}^{-2}$ ) based on the Special Sensor Microwave/Imager (SSM/I) (Ferraro et. al, 1996: *Bull. Amer. Meteor. Soc.*, 77, 891-905). Anomalies are calculated from the 1987-2010 base period means.

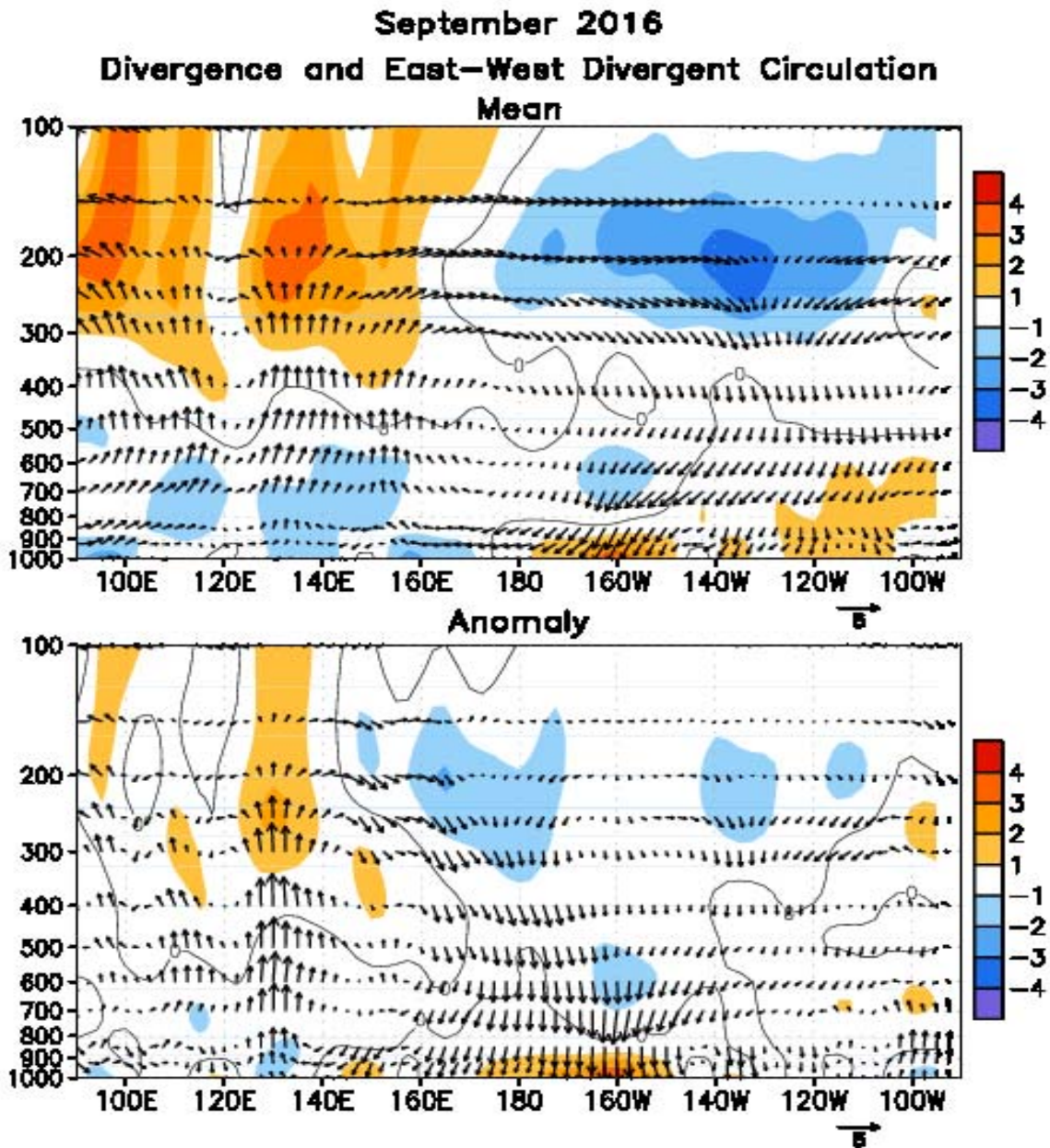


FIGURE T29. Pressure-longitude section (100E–80W) of the mean (top) and anomalous (bottom) divergence (contour interval is  $1 \times 10^{-6} \text{ s}^{-1}$ ) and divergent circulation averaged between 5N–5S. The divergent circulation is represented by vectors of combined pressure vertical velocity and the divergent component of the zonal wind. Red shading and solid contours denote divergence (top) and anomalous divergence (bottom). Blue shading and dashed contours denote convergence (top) and anomalous convergence (bottom). Anomalies are departures from the 1981–2010 base period monthly means.



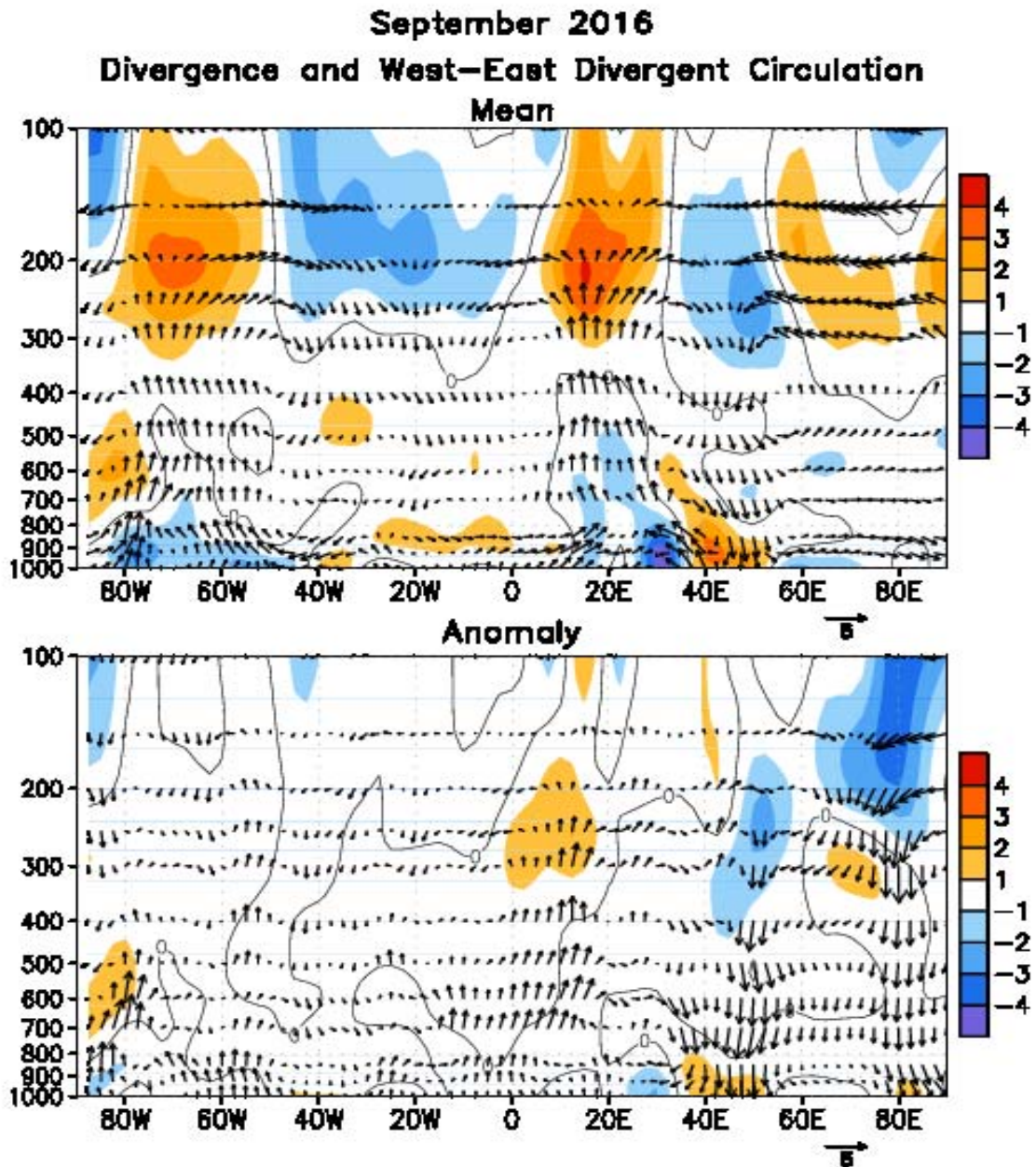


FIGURE T30. Pressure-longitude section (80W-100E) of the mean (top) and anomalous (bottom) divergence (contour interval is  $1 \times 10^{-6} \text{ s}^{-1}$ ) and divergent circulation averaged between 5N-5S. The divergent circulation is represented by vectors of combined pressure vertical velocity and the divergent component of the zonal wind. Red shading and solid contours denote divergence (top) and anomalous divergence (bottom). Blue shading and dashed contours denote convergence (top) and anomalous convergence (bottom). Anomalies are departures from the 1981-2010 base period monthly means.

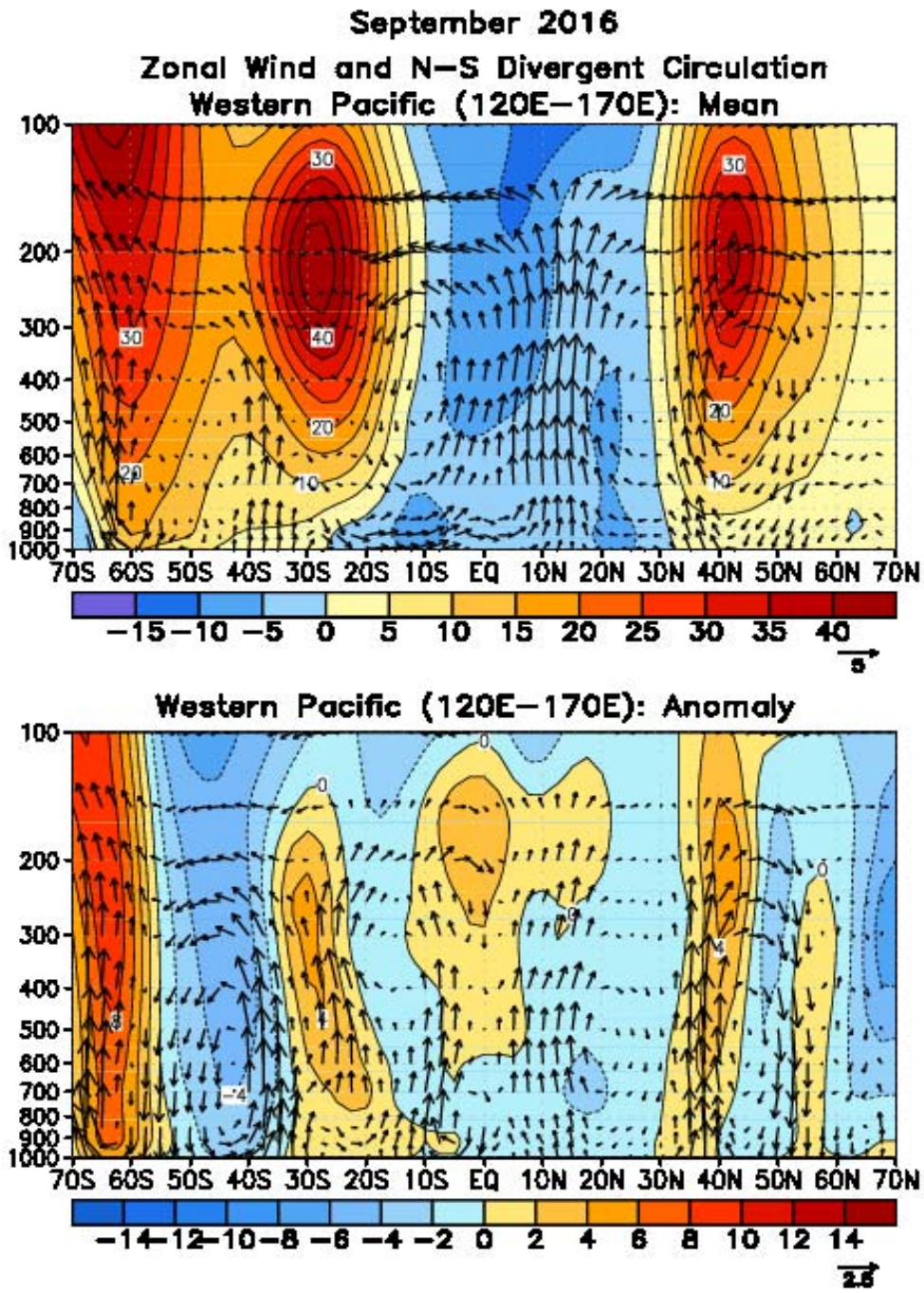


FIGURE T31. Pressure-latitude section of the mean (top) and anomalous (bottom) zonal wind ( $\text{m s}^{-1}$ ) and divergent circulation averaged over the west Pacific sector (120E-170E). The divergent circulation is represented by vectors of combined pressure vertical velocity and the divergent component of the meridional wind. Red shading and solid contours denote a westerly (top) or anomalous westerly (bottom) zonal wind. Blue shading and dashed contours denote an easterly (top) or anomalous easterly (bottom) zonal wind. Anomalies are departures from the 1981-2010 base period monthly means.



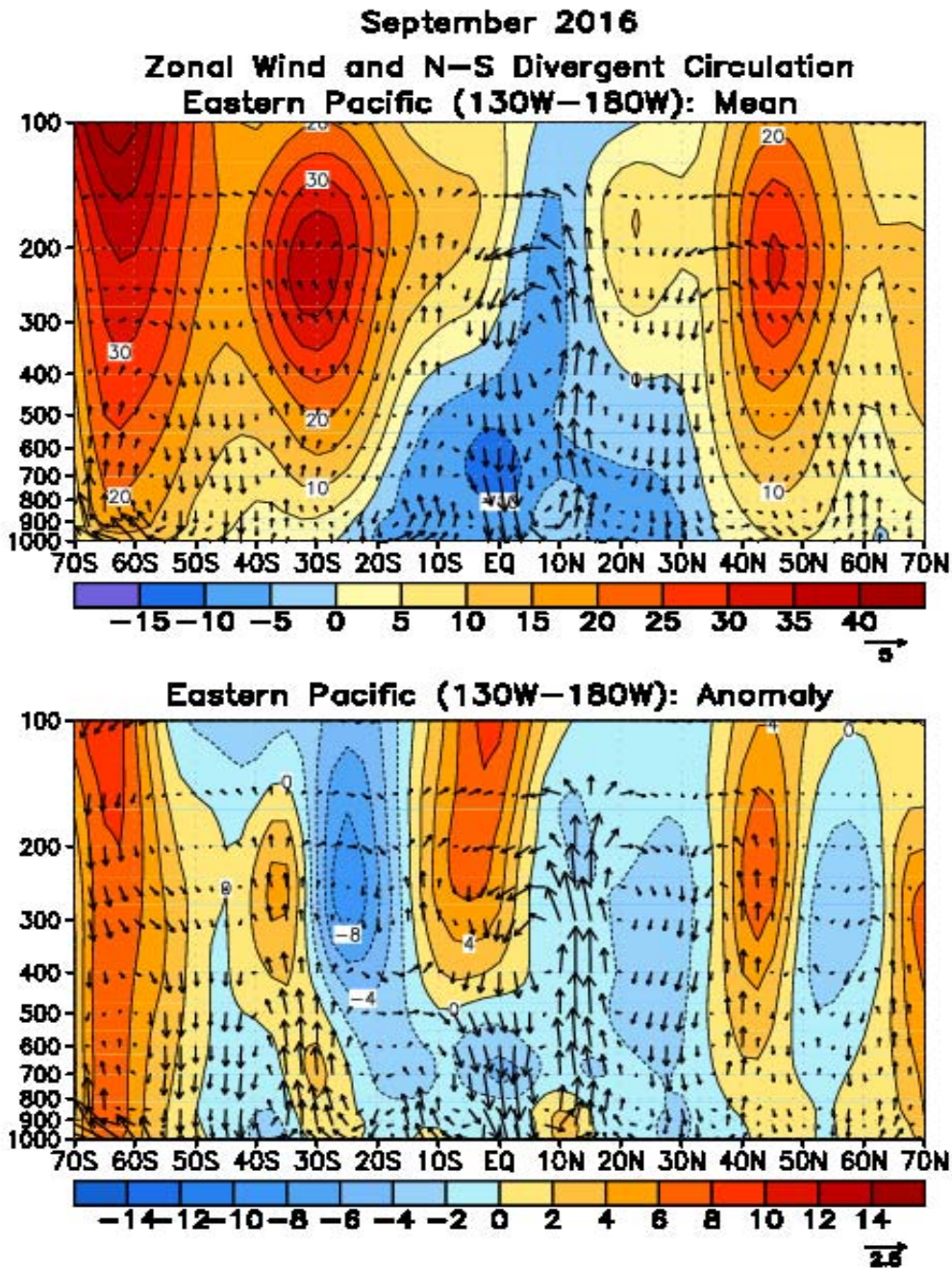
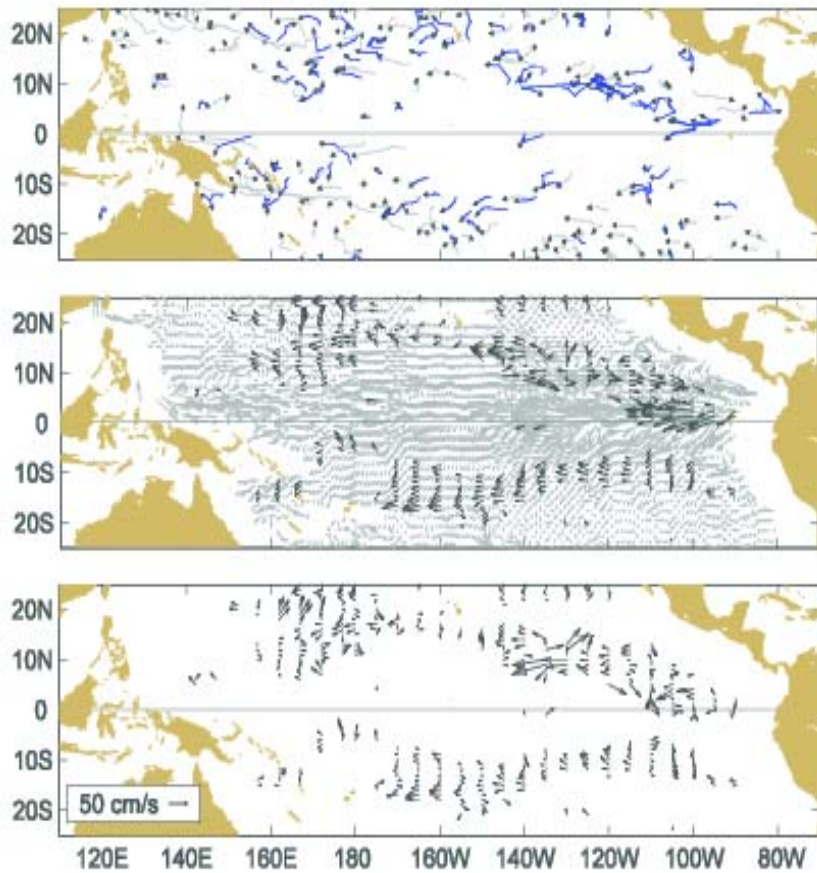


FIGURE T32. Pressure-latitude section of the mean (top) and anomalous (bottom) zonal wind ( $\text{m s}^{-1}$ ) and divergent circulation averaged over the central Pacific sector (130W-180W). The divergent circulation is represented by vectors of combined pressure vertical velocity and the divergent component of the meridional wind. Red shading and solid contours denote a westerly (top) or anomalous westerly (bottom) zonal wind. Blue shading and dashed contours denote an easterly (top) or anomalous easterly (bottom) zonal wind. Anomalies are departures from the 1981-2010 base period monthly means.



Tropical Pacific Drifting Buoys R. Lumpkin/M. Pazos, AOML, Miami

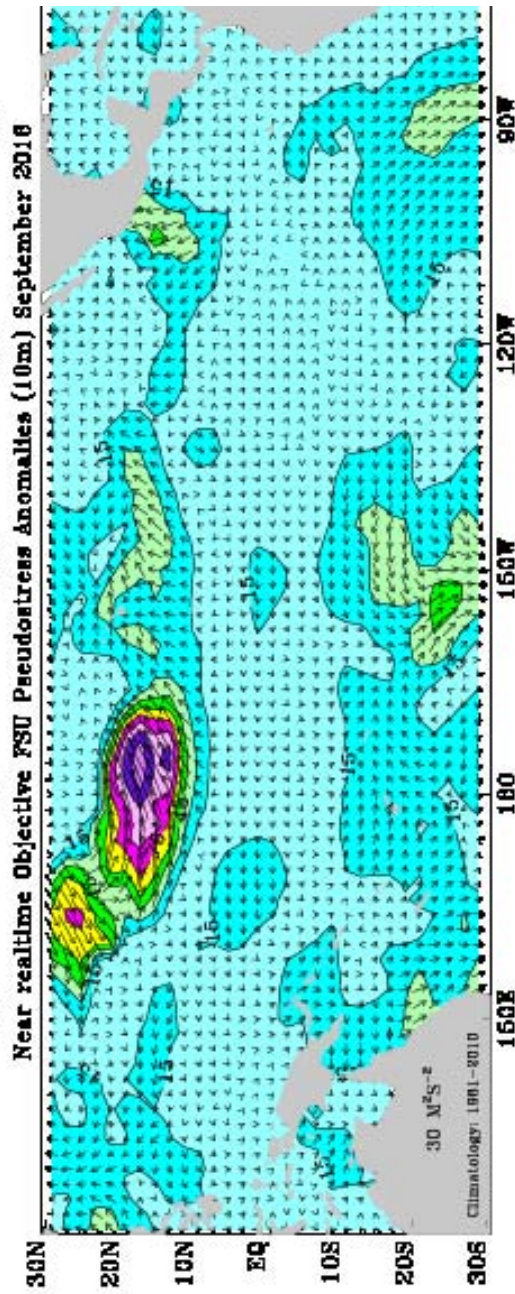
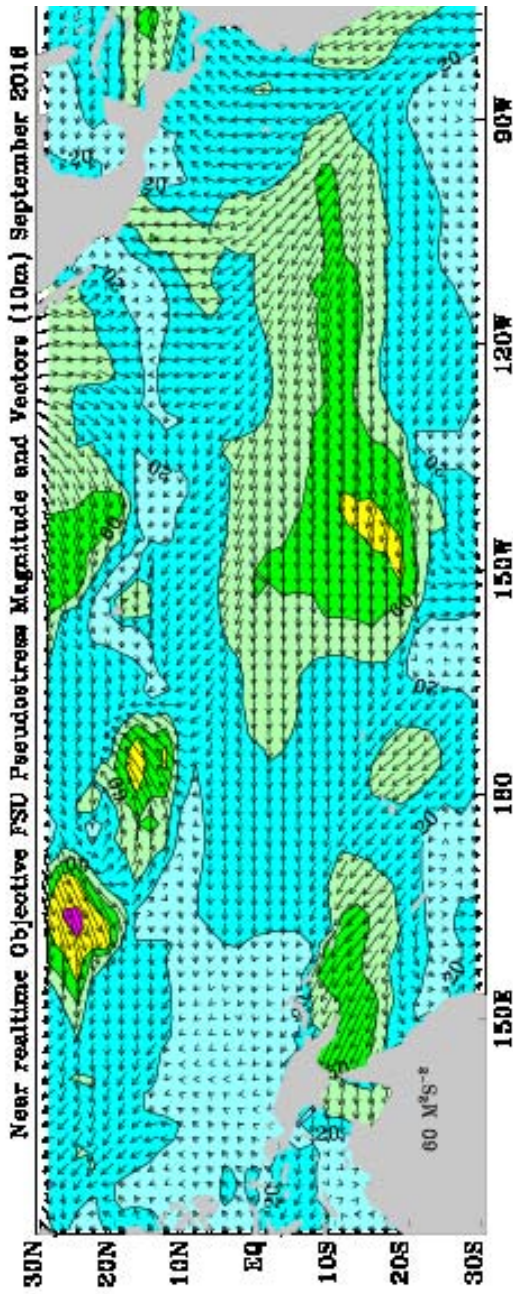
During September 2016, 303 satellite-tracked surface drifting buoys, 41% with subsurface drogues attached for measuring mixed layer currents, were reporting from the tropical Pacific. As in August, the drifter array did not reveal any large-scale current anomalies in the basin during this time.



**Figure A1.1 Top:** Movements of drifting buoys in the tropical Pacific Ocean during September 2016. The linear segments of each trajectory represent a one week displacement. Trajectories of buoys which have lost their subsurface drogues are gray; those with drogues are black.

**Middle:** Monthly mean currents calculated from all buoys 1993-2002 (gray), and currents measured by the drogued buoys this month (black) smoothed by an optimal filter.

**Bottom:** Anomalies from the climatological monthly mean currents for this month.



**FSU SURFACE PSEUDO-STRESS VECTORS AND ANOMALIES: September 2018.** Pseudo-stress vectors (top) are objectively created from ship and buoy winds on a 2° grid. Ship and buoy data are independently weighted and the background field created from the data. Contour interval of the vector magnitudes is  $20 \text{ N}^2\text{S}^{-2}$ . Anomalies (bottom) are departures from 1991-2010 mean. The contour interval is  $10 \text{ N}^2\text{S}^{-2}$ . For more information, please visit our web site at <http://www.coaps.fsu.edu/EVEMDC/html/winds.html>. Produced by Jeremy Kolib, Mark A. Bourassa, and Shawn R. Smith, Center for Ocean-Atmospheric Prediction Studies, Florida State University, Tallahassee, FL 32309-2640, USA.



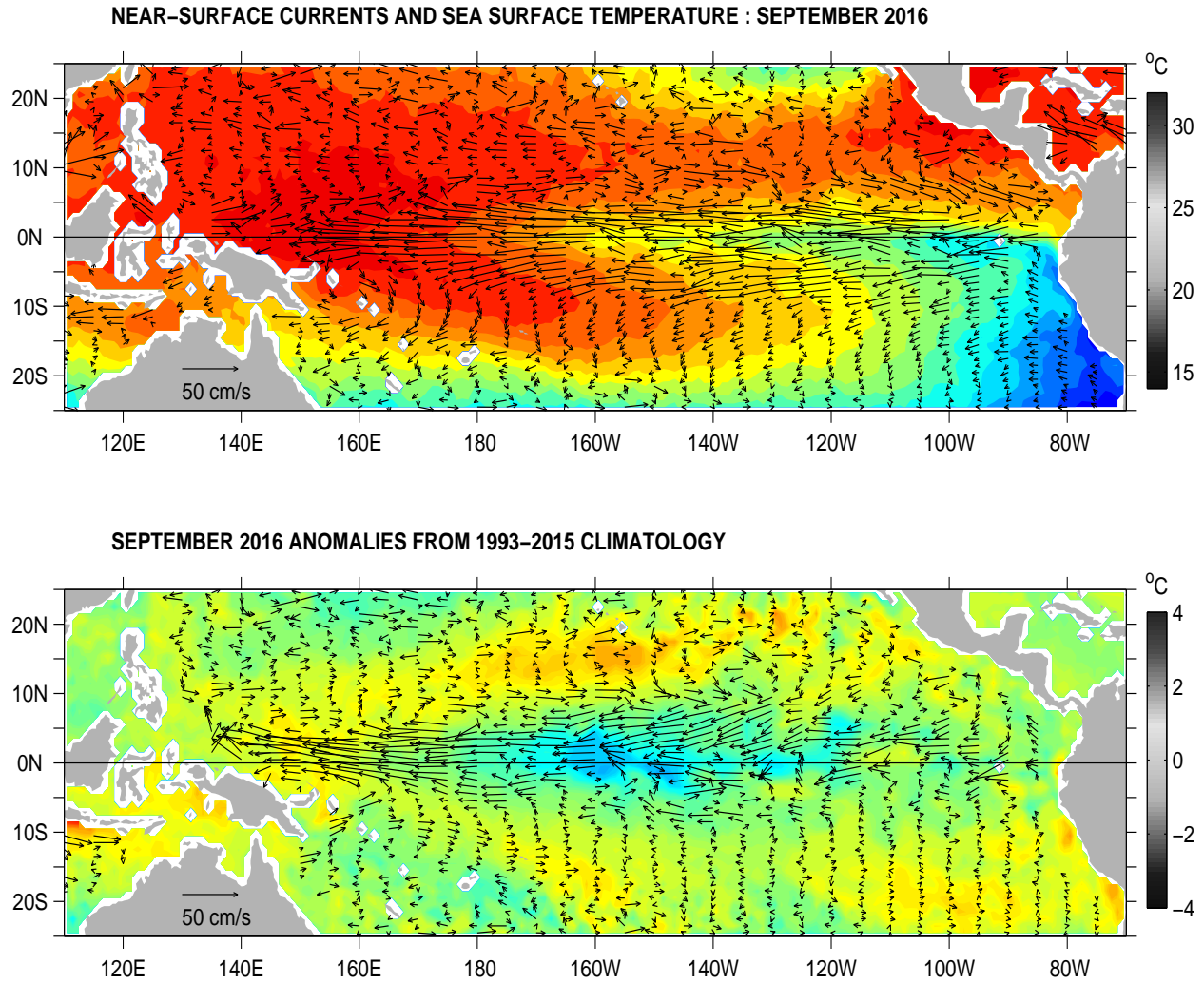


FIGURE A1.3. Ocean Surface Current Analysis-Real-time (OSCAR) for SEP 2016 (Bonjean and Lagerloef 2002, *J. Phys. Oceanogr.*, Vol. 32, No. 10, 2938-2954; Lagerloef et al. 1999, *JGR-Oceans*, 104, 23313-23326). (top) Total velocity. Surface currents are calculated from satellite data including Jason sea level anomalies and NCEP winds. (bottom) Velocity anomalies. The subtracted climatology was based on SSM/I and QuickScat winds and Topex/Poseidon and Jason from 1993-2003. See also <http://www.oscar.noaa.gov>.



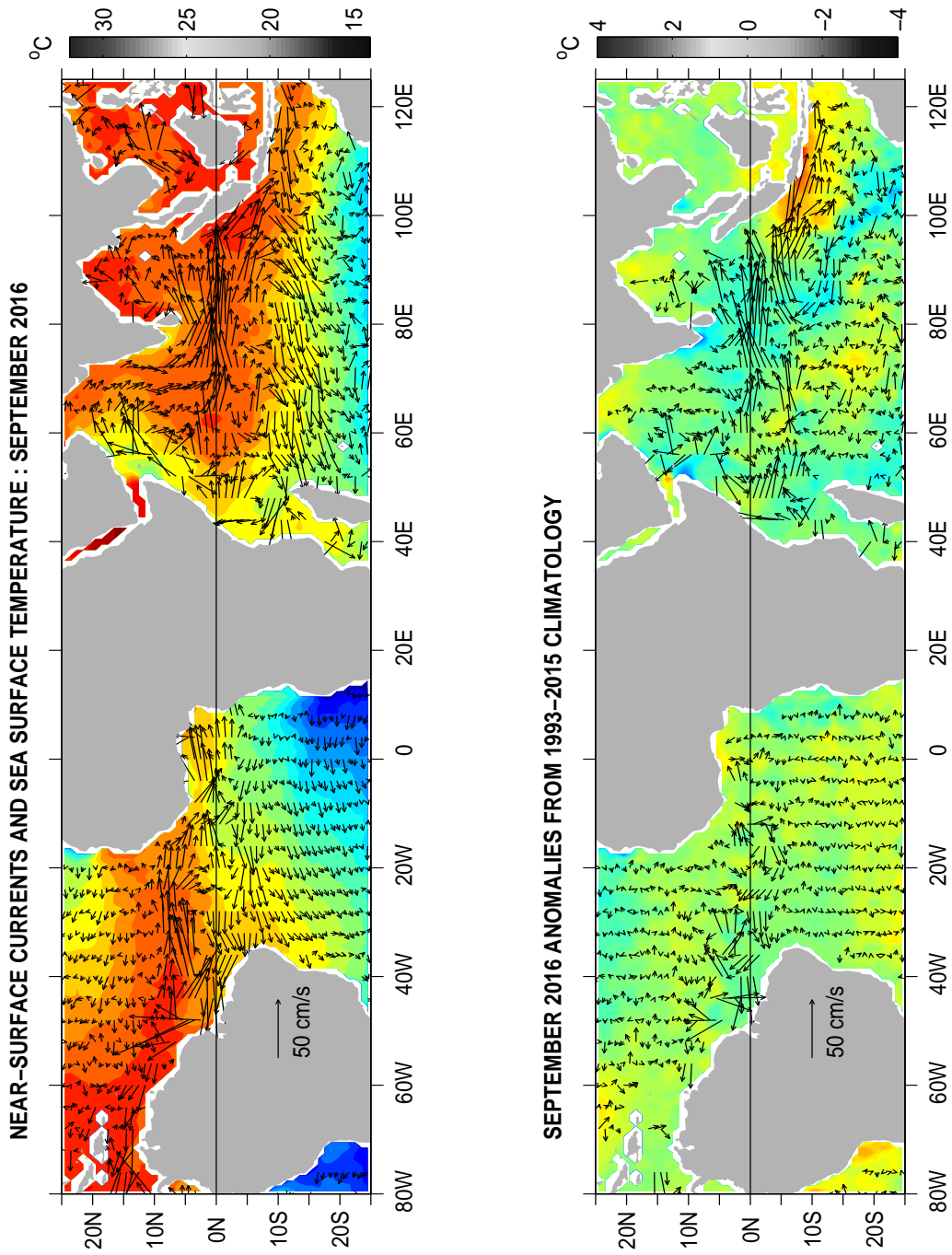


FIGURE A1.4. Ocean Surface Current Analysis-Real-time (OSCAR) for SEP 2016 (Bonjean and Lagerloef 2002, J. Phys. Oceanogr., Vol. 32, No. 10, 2938-2954; Lagerloef et al. 1999, JGR-Oceans, 104, 23313-23326). (top) Total velocity. Surface currents are calculated from satellite data including Jason sea level anomalies and NCEP winds. (bottom) Velocity anomalies. The subtracted climatology was based on SSM/I and QuickScat winds and Topex/Poseidon and Jason from 1993-2003. See also <http://www.oscar.noaa.gov>.

## Forecast Forum

The canonical correlation analysis (CCA) forecast of SST in the central Pacific (Barnett et al. 1988, *Science*, **241**, 192196; Barnston and Ropelewski 1992, *J. Climate*, **5**, 13161345), is shown in **Figs. F1 and F2**. This forecast is produced routinely by the Prediction Branch of the Climate Prediction Center. The predictions from the National Centers for Environmental Prediction (NCEP) Coupled Forecast System Model (CFS03) are presented in **Figs. F3 and F4a, F4b**. Predictions from the Markov model (Xue, et al. 2000: *J. Climate*, **13**, 849871) are shown in **Figs. F5 and F6**. Predictions from the latest version of the LDEO model (Chen et al. 2000: *Geophys. Res. Lett.*, **27**, 25852587) are shown in **Figs. F7 and F8**. Predictions using linear inverse modeling (Penland and Magorian 1993: *J. Climate*, **6**, 10671076) are shown in **Figs. F9 and F10**. Predictions from the Scripps / Max Planck Institute (MPI) hybrid coupled model (Barnett et al. 1993: *J. Climate*, **6**, 15451566) are shown in **Fig. F11**. Predictions from the ENSOCLIPER statistical model (Knaff and Landsea 1997, *Wea. Forecasting*, **12**, 633652) are shown in **Fig. F12**. Niño 3.4 predictions are summarized in **Fig. F13**, provided by the Forecasting and Prediction Research Group of the IRI.

The CPC and the contributors to the **Forecast Forum** caution potential users of this predictive information that they can expect only modest skill.

## ENSO Alert System Status: [La Niña Watch](#)

### Outlook

La Niña is favored to develop (~70% chance) during the Northern Hemisphere fall 2016 and slightly favored to persist (~55% chance) during winter 2016-17.

### Discussion

ENSO-Neutral conditions were observed during September, with negative sea surface temperatures (SSTs) anomalies expanding across the eastern equatorial Pacific Ocean by early October (Fig. T18). For the September monthly average, the Niño-3.4 index was  $-0.6^{\circ}\text{C}$ , though cooled even further by early October (Table T2). Subsurface temperature anomalies also decreased toward the end of the month, reflecting the strengthening of below-average temperatures at depth in the east-central equatorial Pacific (Fig. T17). Atmospheric anomalies across the equatorial Pacific edged toward La Niña during September, with a stronger tendency toward La Niña late in the month. The traditional Southern Oscillation index and the equatorial Southern Oscillation index were positive (Table T1 & Fig. T2). The lower-level winds were near average across most of the basin during the month, but enhanced easterlies were becoming more persistent west of the International Date Line (Fig. T20). Upper-level winds were anomalously westerly near and just east of the International

Date Line (Fig. T21). Convection was weakly suppressed over the central tropical Pacific and was more enhanced over Indonesia compared to last month (Fig. T25). Overall, the combined ocean and atmosphere system reflects ENSO-Neutral during September, but are more clearly trending toward La Niña conditions.

The multi-model averages favor borderline Neutral-La Niña conditions (3-month average Niño-3.4 index less than or equal to  $-0.5^{\circ}\text{C}$ ) persisting during the Northern Hemisphere fall and continuing into the winter (Figs. F1-F13). Because of the recent cooling in the Niño-3.4 region and signs of renewed atmospheric coupling, the forecaster consensus now favors the formation of a weak La Niña in the near term, becoming less confident that La Niña will persist through the winter. In summary, La Niña is favored to develop (~70% chance) during the Northern Hemisphere fall 2016 and slightly favored to persist (~55% chance) during winter 2016-17.

Weekly updates of oceanic and atmospheric conditions are available on the Climate Prediction Center homepage ([El Niño/La Niña Current Conditions and Expert Discussions](#)).



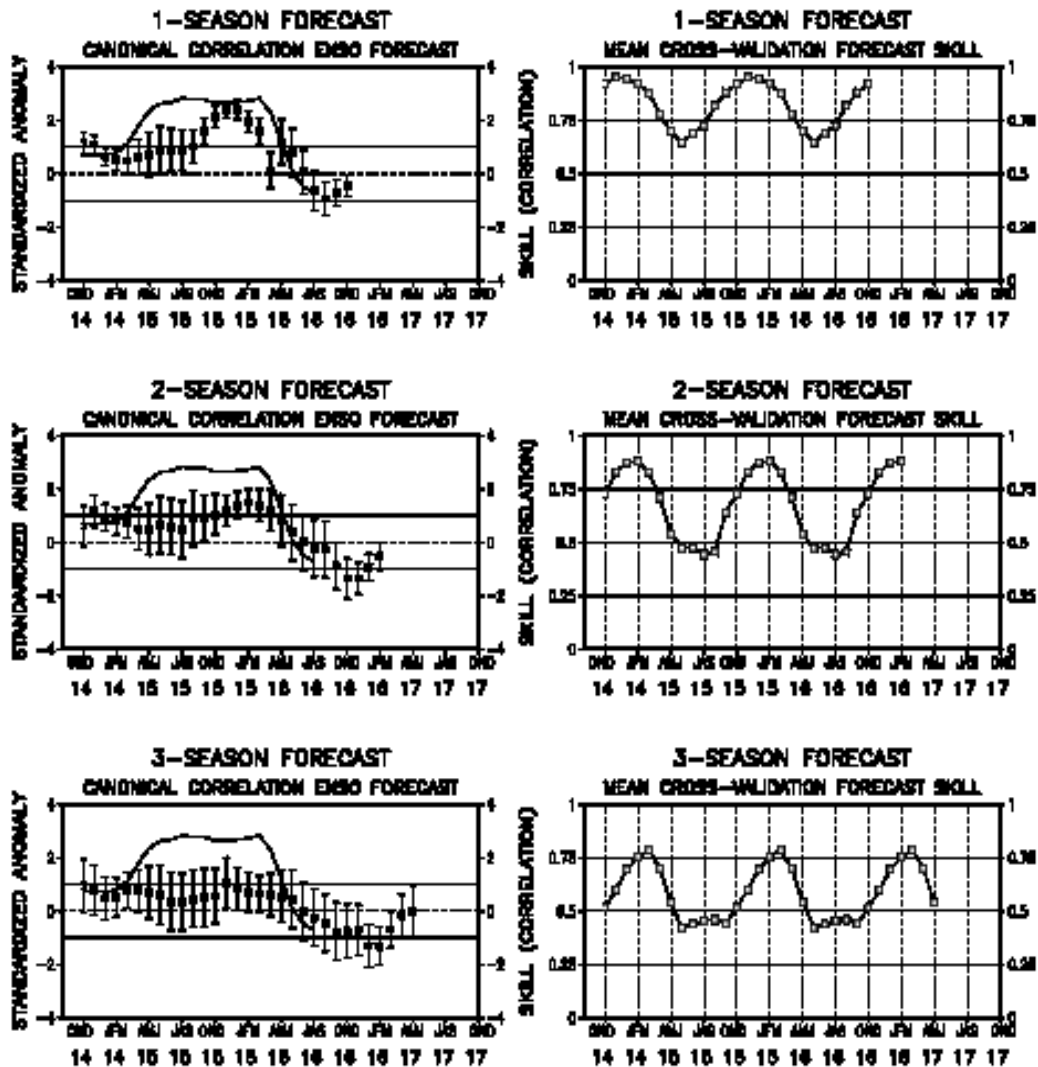


FIGURE F1. Canonical correlation analysis (CCA) sea surface temperature (SST) anomaly prediction for the central Pacific ( $5^{\circ}\text{N}$  to  $5^{\circ}\text{S}$ ,  $120^{\circ}\text{W}$  to  $170^{\circ}\text{W}$  (Barnston and Ropelewski, 1992, *J. Climate*, 5, 1316-1345). The three plots on the left hand side are, from top to bottom, the 1-season, 2-season, and 3-season lead forecasts. The solid line in each forecast represents the observed SST standardized anomaly through the latest month. The small squares at the mid-points of the forecast bars represent the real-time CCA predictions based on the anomalies of quasi-global sea level pressure and on the anomalies of tropical Pacific SST, depth of the  $20^{\circ}\text{C}$  isotherm and sea level height over the prior four seasons. The vertical lines represent the one standard deviation error bars for the predictions based on past performance. The three plots on the right side are skills, corresponding to the predicted and observed SST. The skills are derived from cross-correlation tests from 1956 to present. These skills show a clear annual cycle and are inversely proportional to the length of the error bars depicted in the forecast time series.

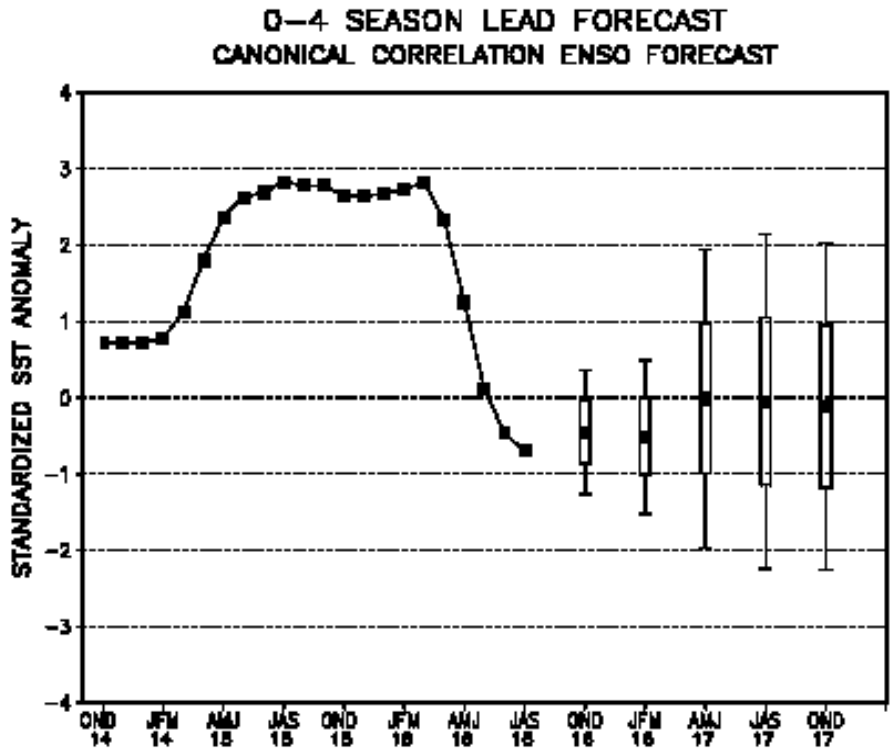


FIGURE F2. Canonical Correlation Analysis (CCA) forecasts of sea-surface temperature anomalies for the Nino 3.4 region (5N-5S, 120W-170W) for the upcoming five consecutive 3-month periods. Forecasts are expressed as standardized SST anomalies. The CCA predictions are based on anomaly patterns of SST, depth of the 20C isotherm, sea level height, and sea level pressure. Small squares at the midpoints of the vertical forecast bars represent the CCA predictions, and the bars show the one (thick) and two (thin) standard deviation errors. The solid continuous line represents the observed standardized three-month mean SST anomaly in the Nino 3.4 region up to the most recently available data.

Last update: Thu Oct 13 2016  
initial conditions: 20Oct2016-11Oct2016

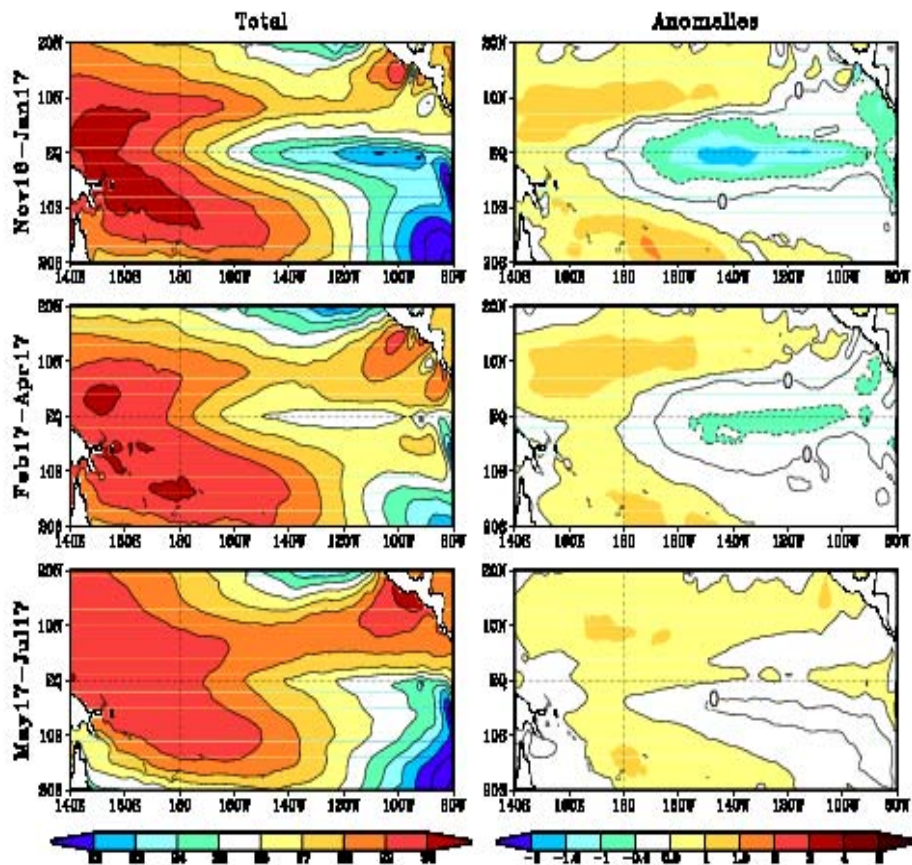


FIGURE F3. Predicted 3-month average sea surface temperature (left) and anomalies (right) from the NCEP Coupled Forecast System Model (CFS03). The forecasts consist of 40 forecast members. Contour interval is 1°C, with additional contours for 0.5°C and -0.5°C. Negative anomalies are indicated by dashed contours.



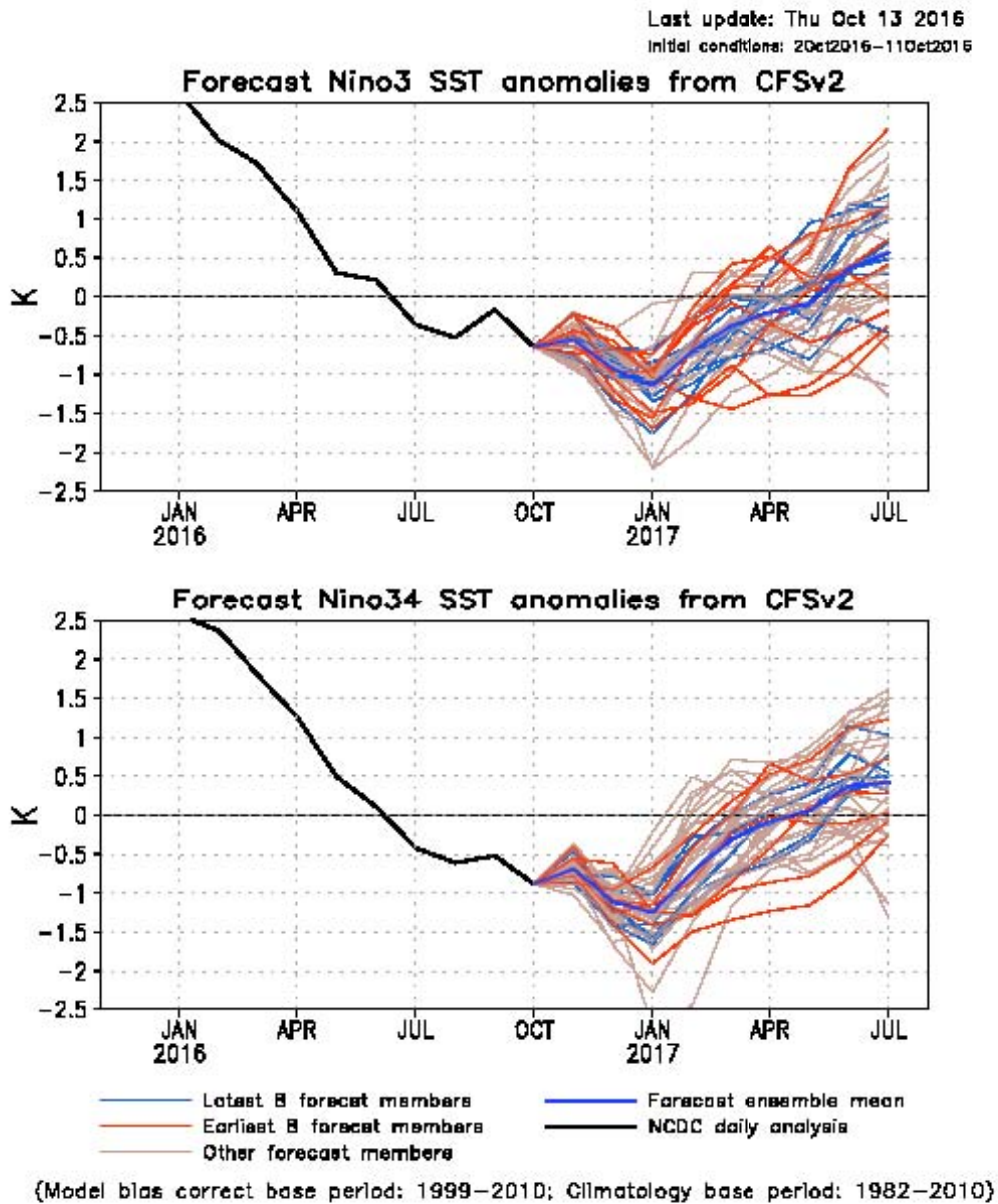


FIGURE F4. Predicted and observed sea surface temperature (SST) anomalies for the Nino 3 (top) and Nino 3.4 (bottom) regions from the NCEP Coupled Forecast System Model (CFSv2). The forecasts consist of 40 forecast members. The ensemble mean of all 40 forecast members is shown by the blue line, individual members are shown by thin lines, and the observation is indicated by the black line. The Nino-3 region spans the eastern equatorial Pacific between 5N-5S, 150W-90W. The Nino 3.4 region spans the east-central equatorial Pacific between 5N-5S, 170W-120W.

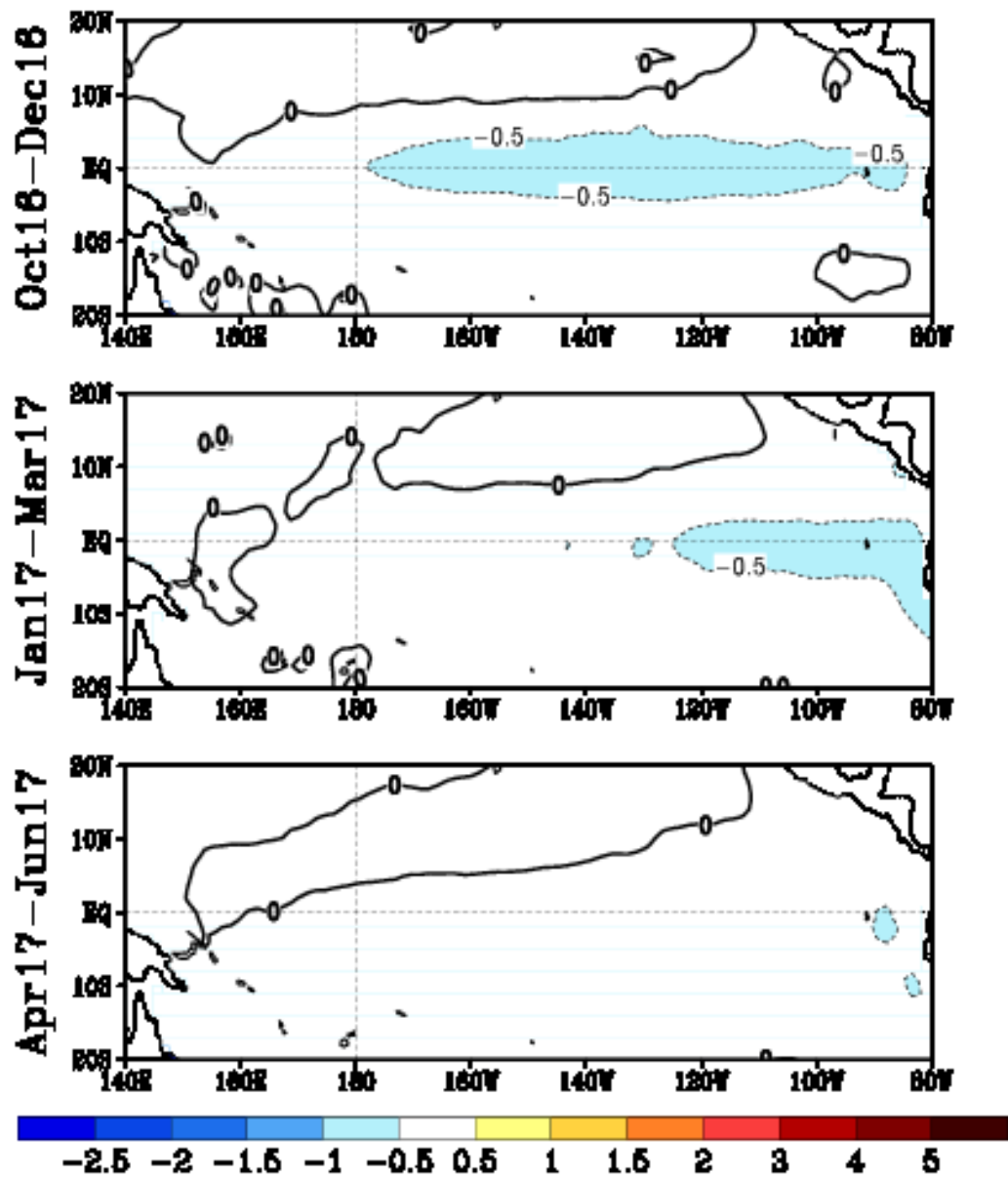


FIGURE F5. Predicted 3-month average sea surface temperature anomalies from the NCEP/CPC Markov model (Xue et al. 2000, *J. Climate*, **13**, 849-871). The forecast is initiated in SEP 2016 . Contour interval is 0.3C and negative anomalies are indicated by dashed contours. Anomalies are calculated relative to the 1971-2000 climatology.

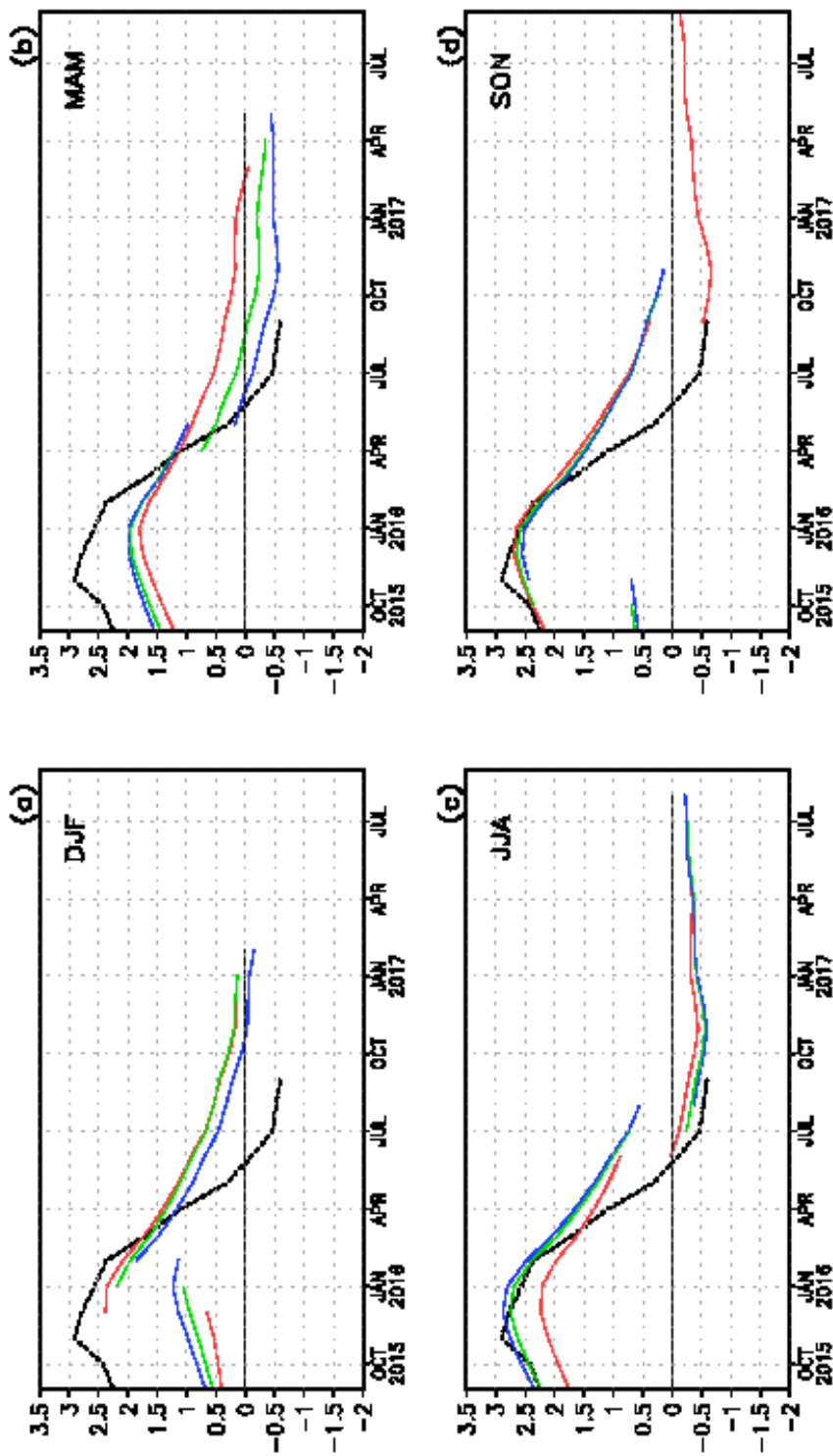
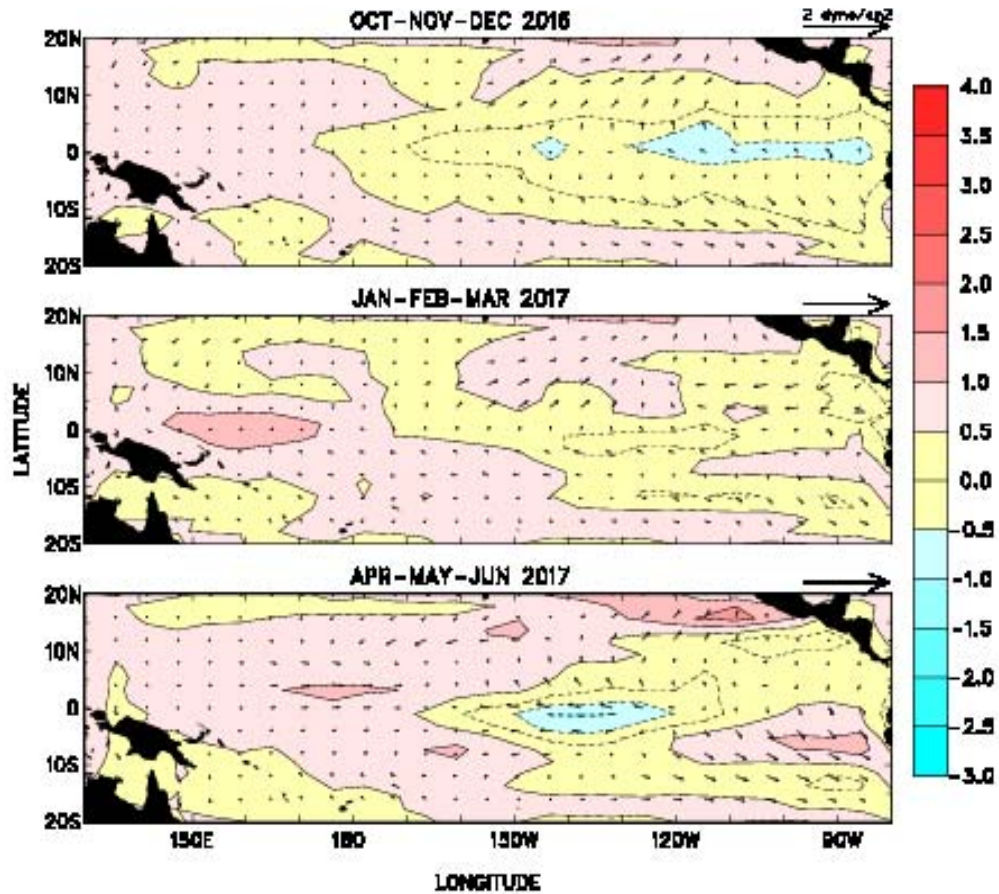


FIGURE F6. Time evolution of observed and predicted SST anomalies in the Niño 3.4 region (up to 12 lead months) by the NCEP/CPC Markov model (Xue et al. 2000, *J. Climate*, **13**, 849-871). Anomalies are calculated relative to the 1971-2000 climatology. Shown in each panel are the forecasts grouped by three consecutive starting months: (a) is for December, January, and February, (b) is for March, April, and May, (c) is for June, July, and August, and (d) is for September, October, and November. The observed Niño 3.4 SST anomalies are indicated by the black dashed lines. The Niño 3.4 region spans the east-central equatorial Pacific between 5N-5S, 170W-120W.



### LDEO FORECASTS OF SST AND WIND STRESS ANOMALIES



**FIGURE F7.** Forecasts of the tropical Pacific Predicted SST (shading) and vector wind anomalies for the next 3 seasons based on the LDEO model. Each forecast represents an ensemble average of 3 sets of predictions initialized during the last three consecutive months (see Figure F8).

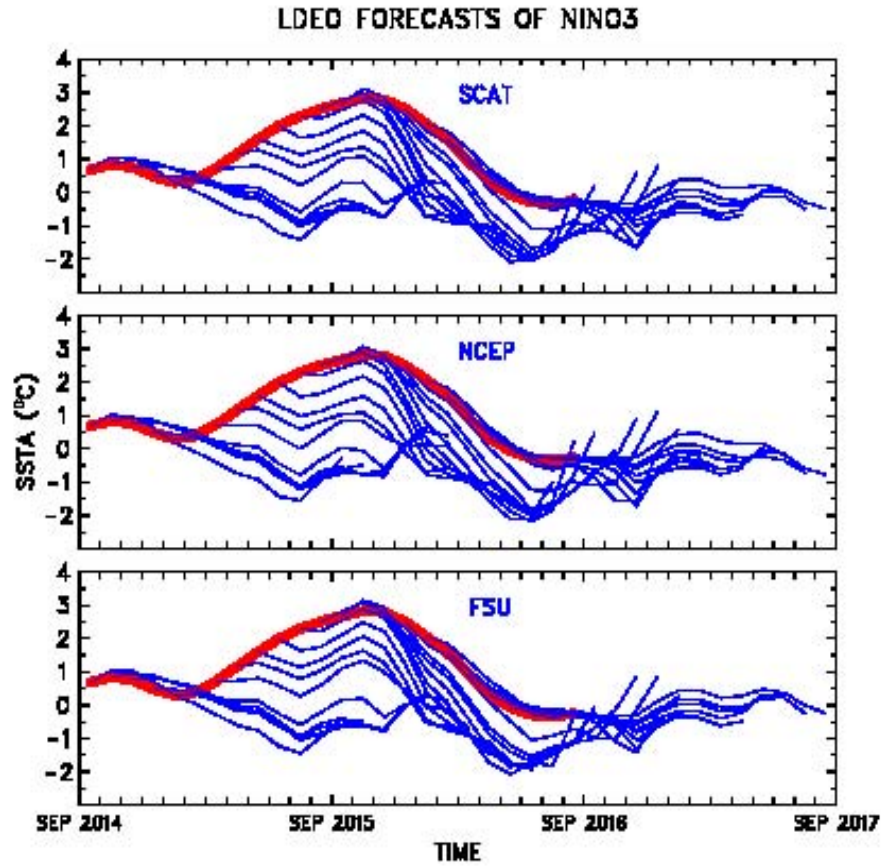


**FIGURE F8.** LDEO forecasts of SST anomalies for the Nino 3 region using wind stresses obtained from (top) QuikSCAT, (middle) NCEP, and (bottom) Florida State Univ. (FSU), along with SSTs (obtained from NCEP), and sea surface height data (obtained from TOPEX/POSEIDON) data. Each thin blue line represents a 12-month forecast, initialized one month apart for the past 24 months. Observed SST anomalies are indicated by the thick red line. The Nino-3 region spans the eastern equatorial Pacific between 5N-5S, 150W-90W.

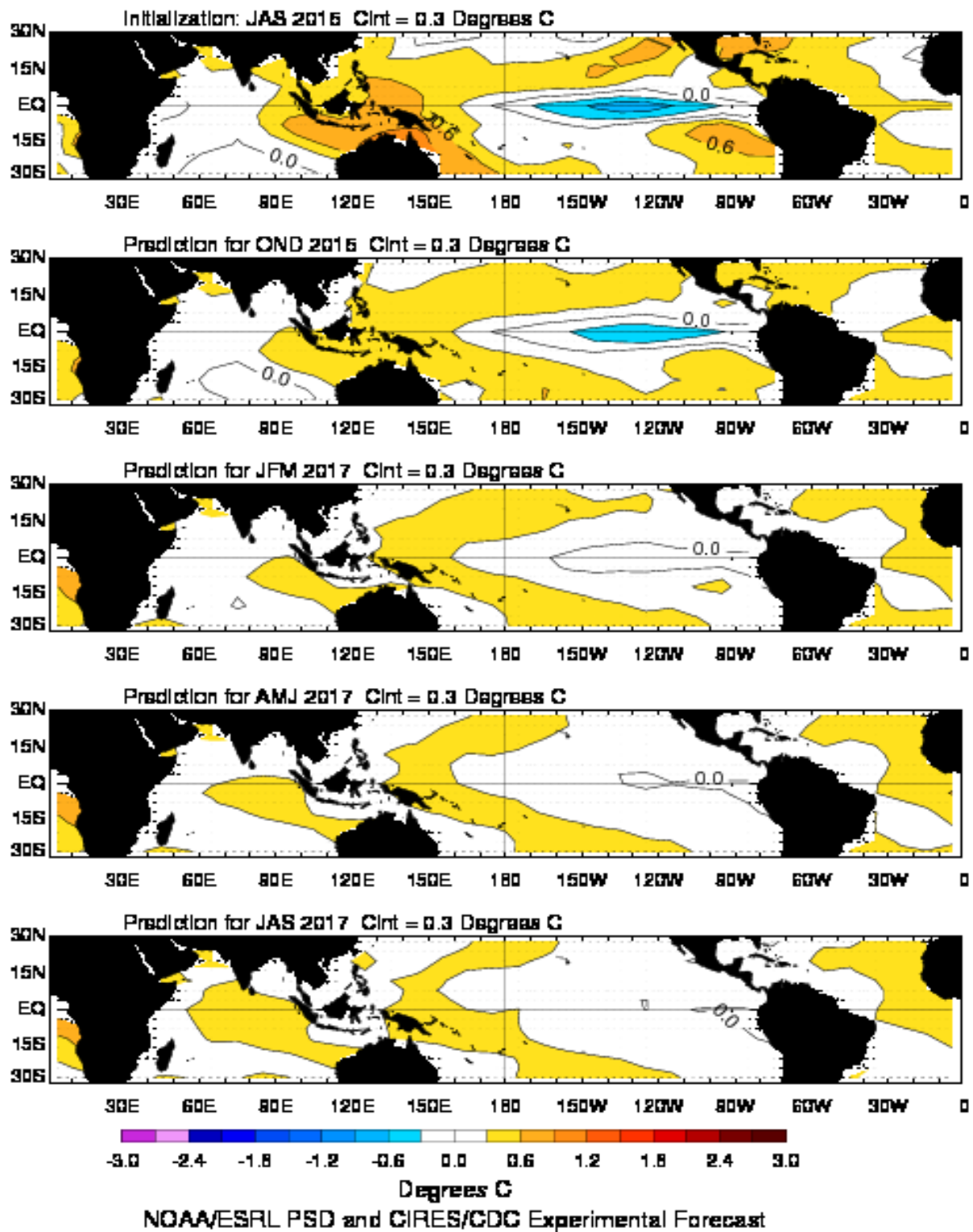


FIGURE F9. Forecast of tropical SST anomalies from the Linear Inverse Modeling technique of Penland and Magorian (1993: *J. Climate*, 6, 1067-1076). The contour interval is 0.3C. Anomalies are calculated relative to the 1981-2010 climatology and are projected onto 20 leading EOFs.



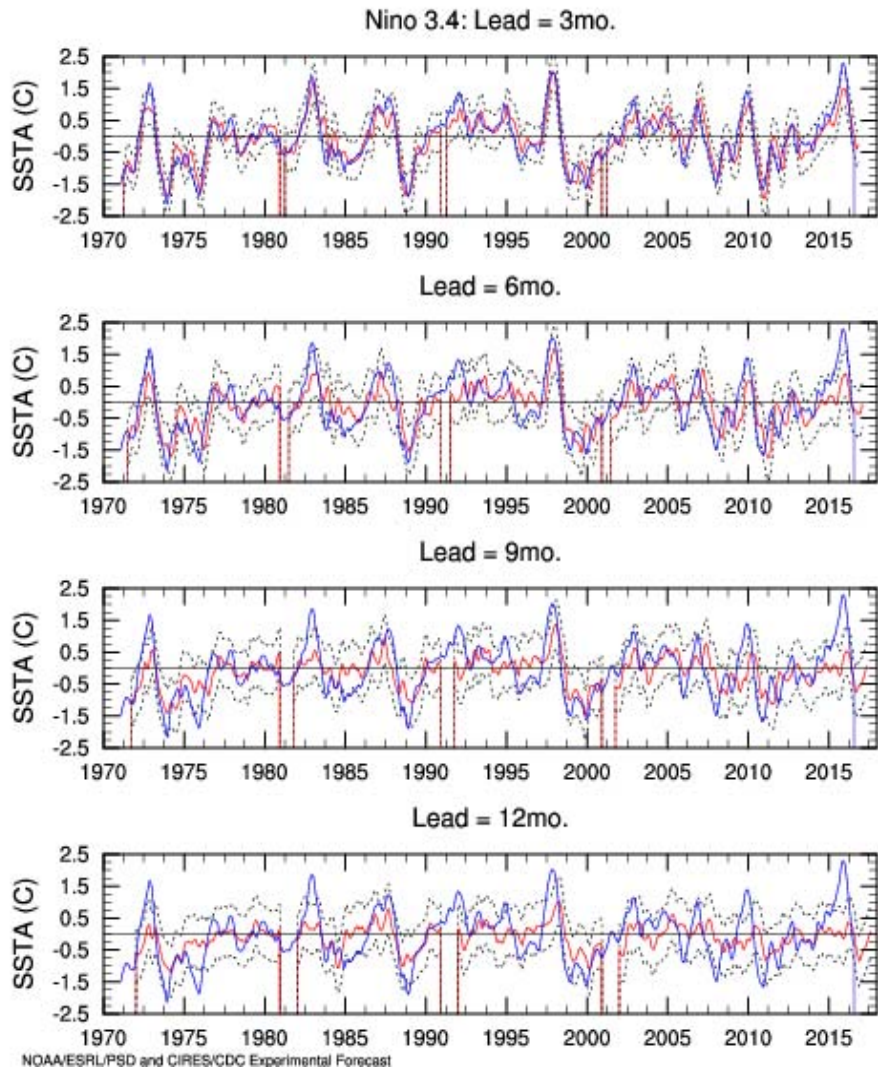


FIGURE F10. Predictions of Niño 3.4 SSTA (blue solid line) and verification (solid red line). The Niño3.4 Index was calculated in the area 6N-6S, 170W-120W. The 1980-2010 climatology was subtracted from ERSST data between 1950 and 2010, after which they were projected onto 20 EOFs containing 90% of the variance. Significant 1950-2010 trends were subtracted from the corresponding PCs, the forecast was made on the detrended anomalies, after which the trend was added to the forecast. The dotted lines indicate the one standard deviation confidence interval for the forecasts based on a perfect adherence to assumption.

### SIO/MPI HCM-T3.0 Tropical SST Anomaly Forecast, 12 Sep 2016

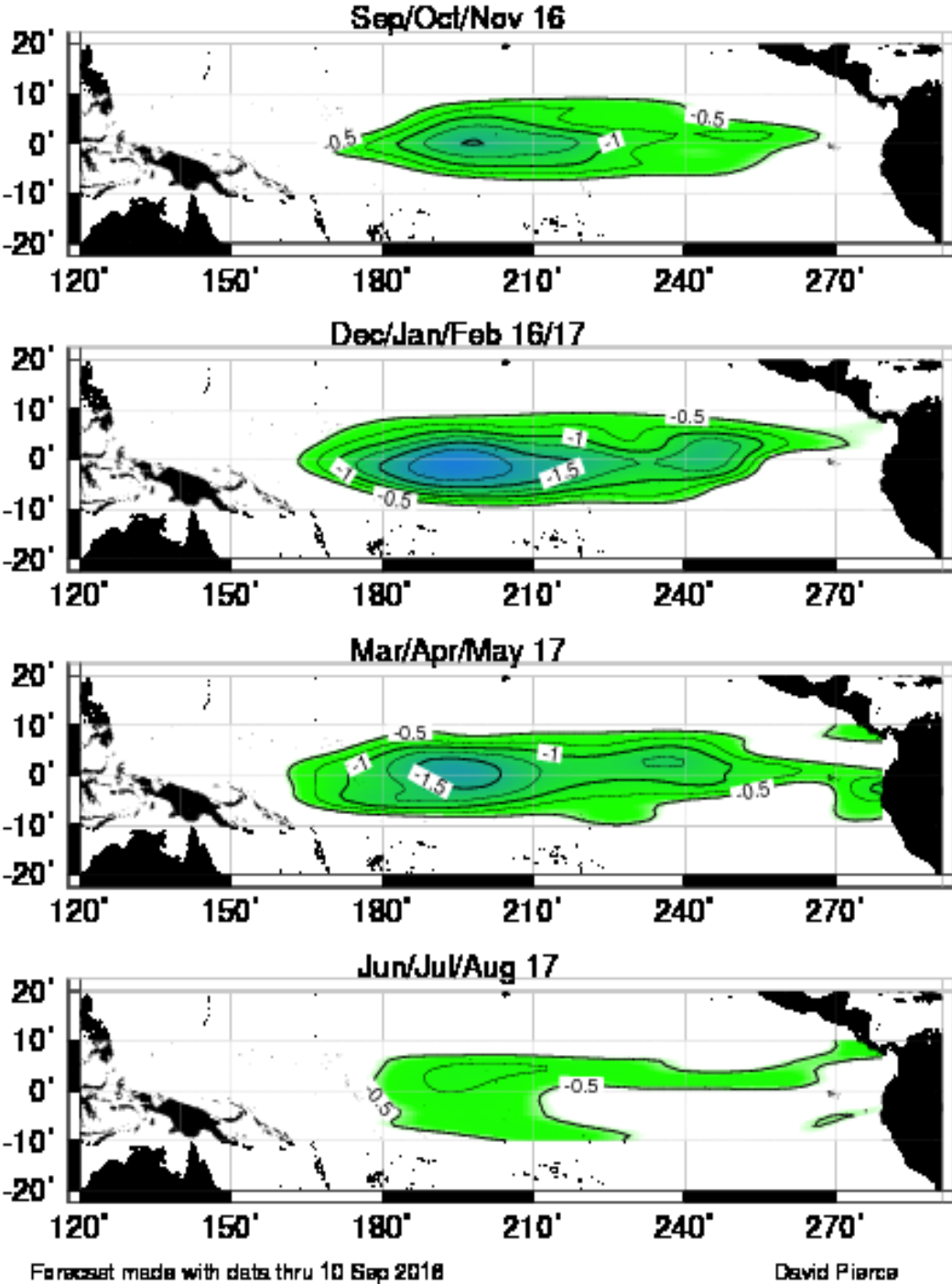


FIGURE F11. SST anomaly forecast for the equatorial Pacific from the Hybrid Coupled Model (HCM) developed by the Scripps Institution of Oceanography and the Max-Planck Institut fuer Meteorologie.

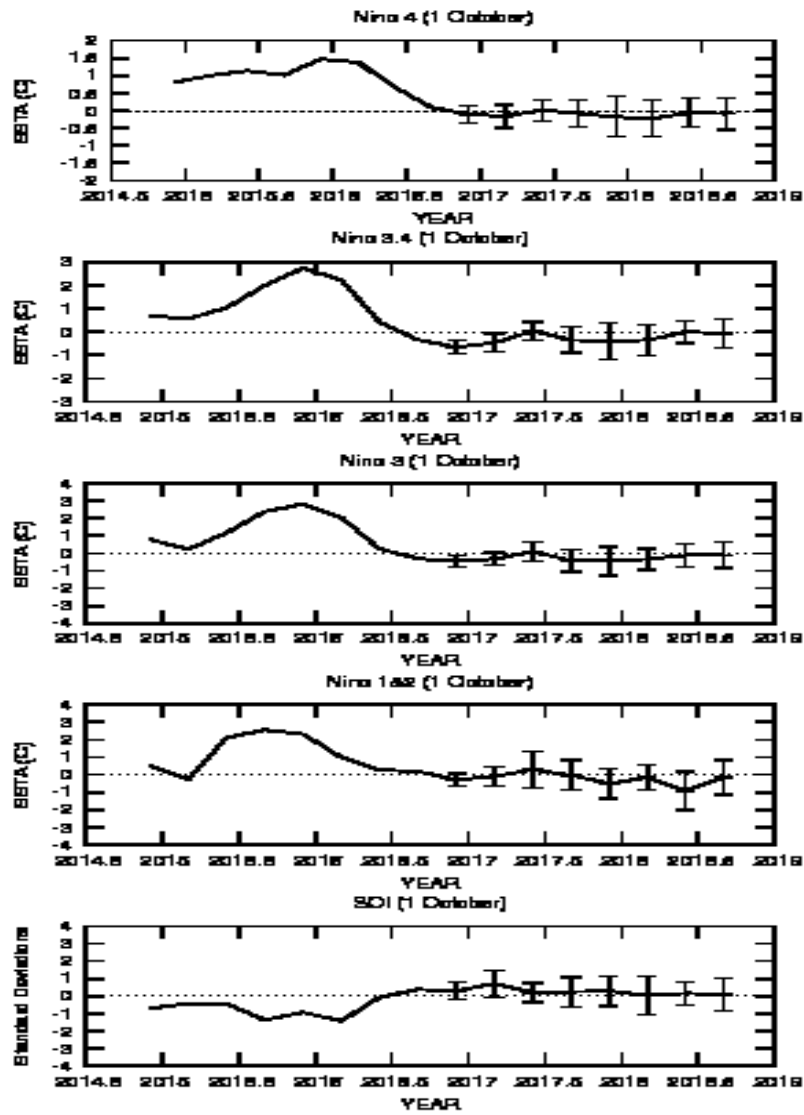


FIGURE F12. ENSO-CLIPER statistical model forecasts of three-month average sea surface temperature anomalies (green lines, deg. C) in (top panel) the Nino 4 region (5N-5S, 160E-150W), (second panel) the Nino 3.4 region (5N-5S, 170W-120W), (third panel) the Nino 3 region (5N-5S, 150W-90W), and (fourth panel) the Nino 1+2 region (0-10S, 90W-80W) (Knaff and Landsea 1997, *Wea. Forecasting*, **12**, 633-652). Bottom panel shows predictions of the three-month standardized Southern Oscillation Index (SOI, green line). Horizontal bars on green line indicate the adjusted root mean square error (RMSE). The Observed three-month average values are indicated by the thick blue line. SST anomalies are departures from the 1981-2010 base period means, and the SOI is calculated from the 1951-1980 base period means.



## Mid-Sep 2016 Plume of Model ENSO Predictions

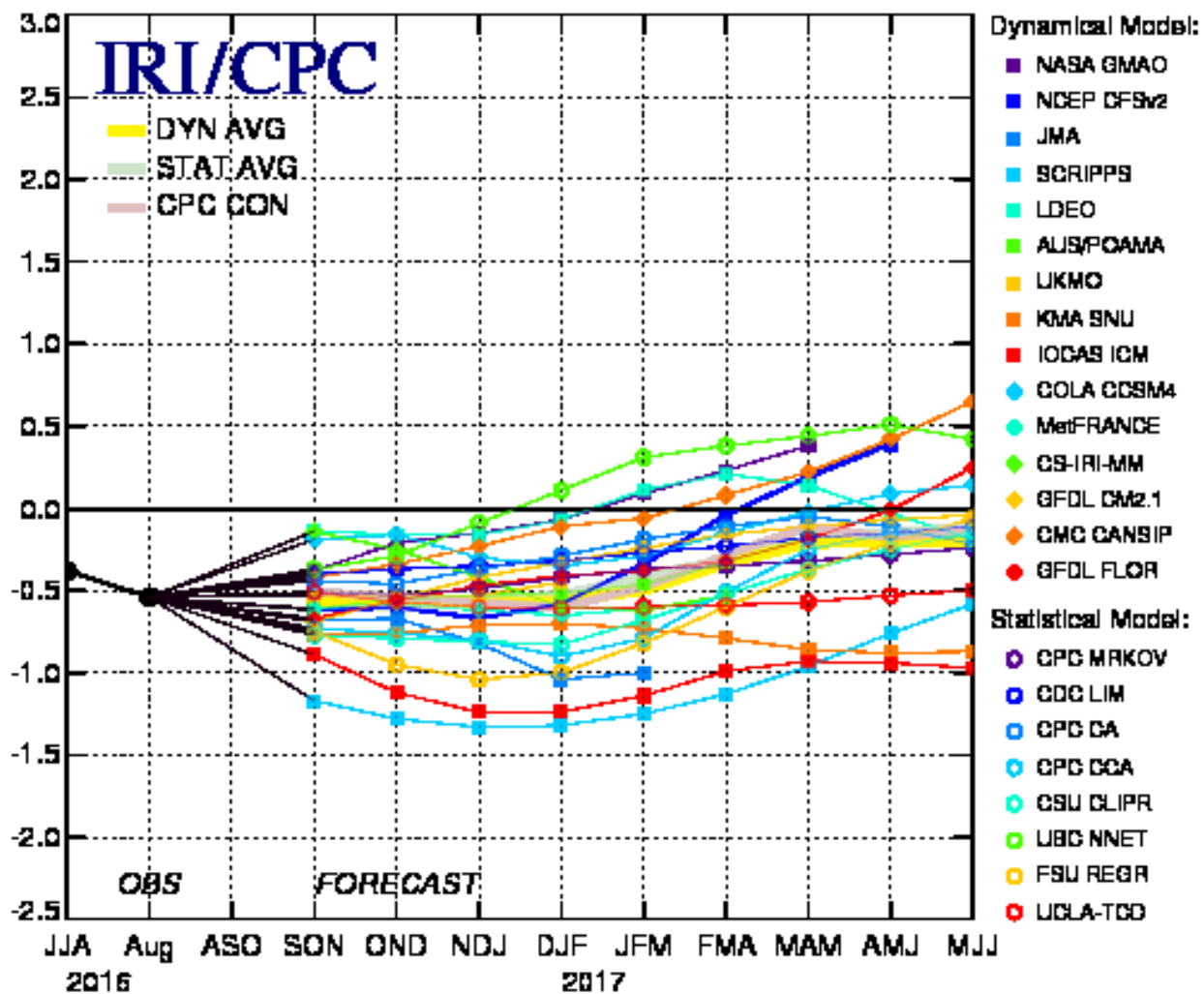


FIGURE F13. Time series of predicted sea surface temperature anomalies for the Nino 3.4 region (deg. C) from various dynamical and statistical models for nine overlapping 3-month periods. The Nino 3.4 region spans the east-central equatorial Pacific between 5N-5S, 170W-120W. Figure provided by the International Research Institute (IRI).

# Extratropical Highlights – September 2016

## 1. Northern Hemisphere

The 500-hPa circulation during September featured above-average heights over eastern North America, northern Europe and central Russia, and below-average heights over the high latitudes of the North Atlantic (Fig. E9).

The main land-surface temperature signals during September included well above-average temperatures in eastern North America, Europe, and central Russia (Fig. E1). The main precipitation signals included above-average totals in the north-central and southeastern U.S., and below-average totals along the U.S. Gulf Coast, the northeastern U.S., and northern Europe (Fig. E3).

### a. North America

The 500-hPa circulation during September featured a broad trough over western North America and above-average heights over eastern North America (Fig. E9). This pattern was associated with well above-average surface temperature across the eastern half of North America, with many areas recording departures exceeding the 90th percentile of occurrences (Fig. E1).

Precipitation during September was above average in both the north-central and southeastern U.S., and below-average along the U.S. Gulf Coast and in the northeastern U.S. (Fig. E3). Area-averaged rainfall totals in the northeastern U.S. have been below-average for the past seven months (Fig. E5).

According to the U.S. Drought Monitor, exceptional or extreme drought continued during September across central and southern California, and was also observed in northern Georgia, northern Alabama, western New York, and large portions of eastern New England. Severe drought was evident in eastern Oregon, western Nevada, and central/ northern Mississippi.

### b. Europe/ western Russia

The 500-hPa circulation during September featured above-average heights over Europe and central Russia, and below-average heights over the high latitudes of the North Atlantic (Fig. E9). This overall pattern was associated with a continuation of above-average surface temperatures across Europe and central Russia, with departures in many areas exceeding the 90th percentile of occurrences (Fig. E1). Northern Europe also recorded below-average precipitation during September, with area-average totals near the lowest 10th percentile of occurrences (Fig. E4).

### c. Northern Africa

The West African monsoon season, which lasts from June-September, was above average this year (Fig. E3). Area-averaged totals were above average during each month from June-September

2016, with the June and July totals nearing the 100th percentile of occurrences and the September totals nearing the 90th percentile of occurrences (Fig. E4).

## 2. Southern Hemisphere

The mean 500-hPa circulation during September featured below-average heights over most of Antarctica. It also featured an anomalous zonal wave-3 pattern in the middle latitudes, with above-average heights over the central ocean basins and below-average heights over the high latitudes of the South Pacific and southern Australia (Fig. E15). The anomalous trough over southern Australia contributed to well below-average surface temperatures in the southwest (Fig. E1) and to above-average precipitation in the east (Fig. E3). Northeastern Australia has recorded well above-average precipitation during the last four months (Fig. E4).

The Antarctic ozone hole typically develops during August and reaches peak size in late September. It then typically decreases in size during October and November, and dissipates in early December (Fig. S8). During September 2016, the size of the ozone hole was below the average of the 2006-2015 period. This decreased size was associated with anomalously low areal extents of both the SH polar vortex and polar stratospheric clouds (Fig. S8).



# TELECONNECTION INDICES

Month	North Atlantic			North Pacific				EURASIA		
	NAO	EA	WP	EP-NP	PNA	TNH	EATL/ WRUS	SCAND	POLEUR	
SEP 16	0.7	3.5	-1.7	-1.4	0.1	---	0.1	-1.0	-1.3	
AUG 16	-2.2	2.1	-0.4	-0.4	-0.9	---	-3.3	-0.4	2.4	
JUL 16	-1.7	1.8	-1.4	-0.4	0.5	---	-1.0	-0.7	-0.2	
JUN 16	-0.1	0.4	-0.6	1.3	-0.6	---	-1.9	-0.9	-1.1	
MAY 16	-0.7	0.2	0.6	0.1	-0.9	---	-2.0	1.0	-0.4	
APR 16	0.3	1.0	-0.3	1.5	0.6	---	-0.5	-0.1	-1.6	
MAR 16	0.4	0.7	-0.2	0.2	0.4	---	0.3	-0.2	-0.2	
FEB 16	1.3	1.9	1.6	0.2	1.7	0.2	-2.4	-0.5	-2.3	
JAN 16	-0.4	1.0	1.0	-0.3	1.9	-0.3	-0.5	-0.7	-2.6	
DEC 15	2.0	3.1	0.6	---	0.5	0.0	1.3	0.1	0.6	
NOV 15	1.7	1.5	0.8	-0.9	-0.2	---	0.6	-0.4	-0.7	
OCT 15	1.0	0.2	-0.7	0.3	2.1	---	0.6	0.6	-0.5	
SEP 15	-0.5	0.1	-1.4	-1.4	-0.8	---	-1.7	1.1	-0.1	

TABLE E1-Standardized amplitudes of selected Northern Hemisphere teleconnection patterns for the most recent thirteen months (computational procedures are described in Fig. E7). Pattern names and abbreviations are North Atlantic Oscillation (NAO); East Atlantic pattern (EA); West Pacific pattern (WP); East Pacific - North Pacific pattern (EP-NP); Pacific/North American pattern (PNA); Tropical/Northern Hemisphere pattern (TNH); East Atlantic/Western Russia pattern (EATL/WRUS)-called Eurasia-2 pattern by Barnston and Livezey, 1987, *Mon. Wea. Rev.*, **115**, 1083-1126); Scandinavia pattern (SCAND-called Eurasia-1 pattern by Barnston and Livezey 1987); and Polar Eurasia pattern (POLEUR). No value is plotted for calendar months in which the pattern does not appear as a leading mode.

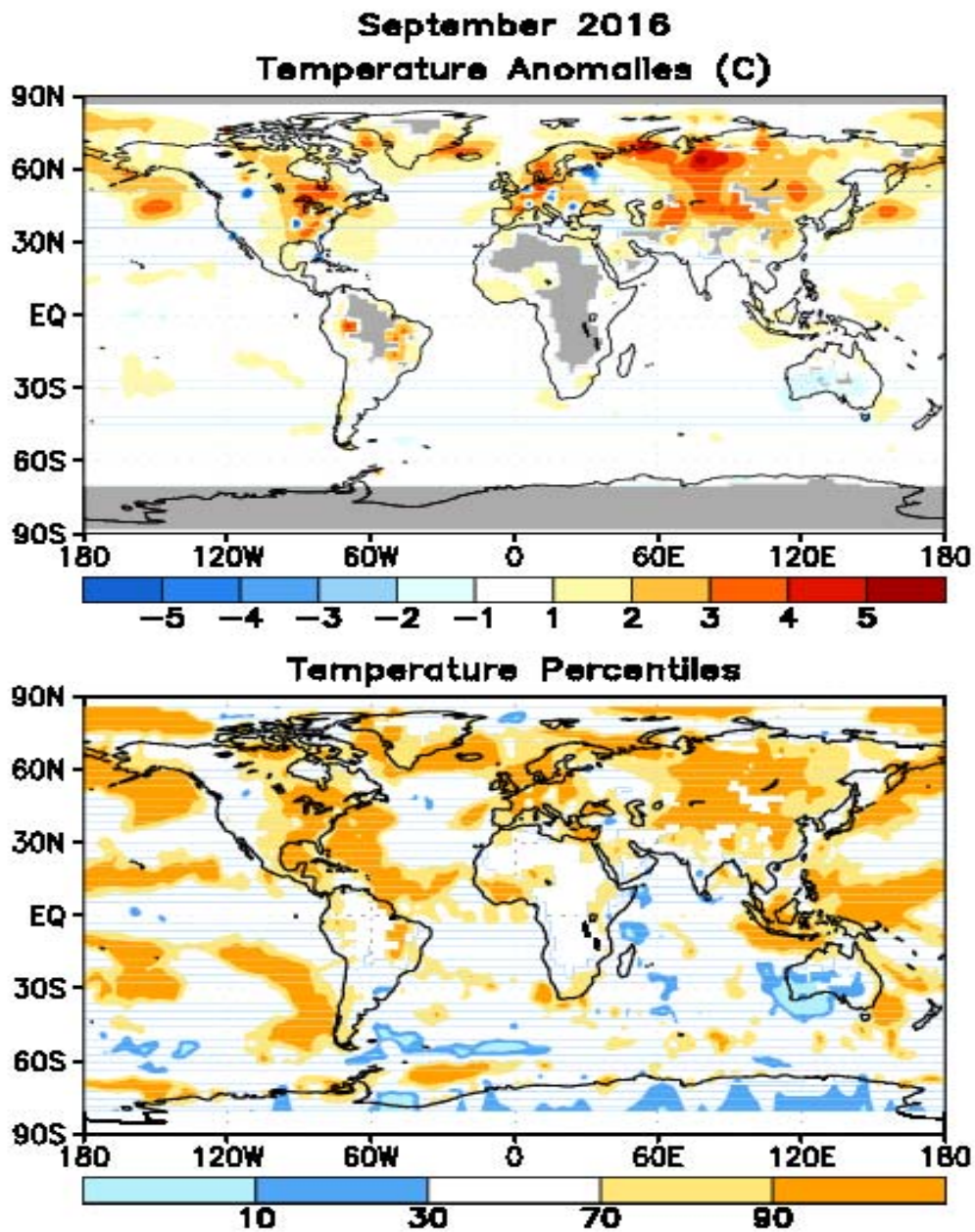


FIGURE E1. Surface temperature anomalies ( $^{\circ}\text{C}$ , top) and surface temperature expressed as percentiles of the normal (Gaussian) distribution fit to the 1981–2010 base period data (bottom) for SEP 2016. Analysis is based on station data over land and on SST data over the oceans (top). Anomalies for station data are departures from the 1981–2010 base period means, while SST anomalies are departures from the 1981–2010 adjusted OI climatology. (Smith and Reynolds 1998, *J. Climate*, **11**, 3320-3323). Regions with insufficient data for analysis in both figures are indicated by shading in the top figure only.

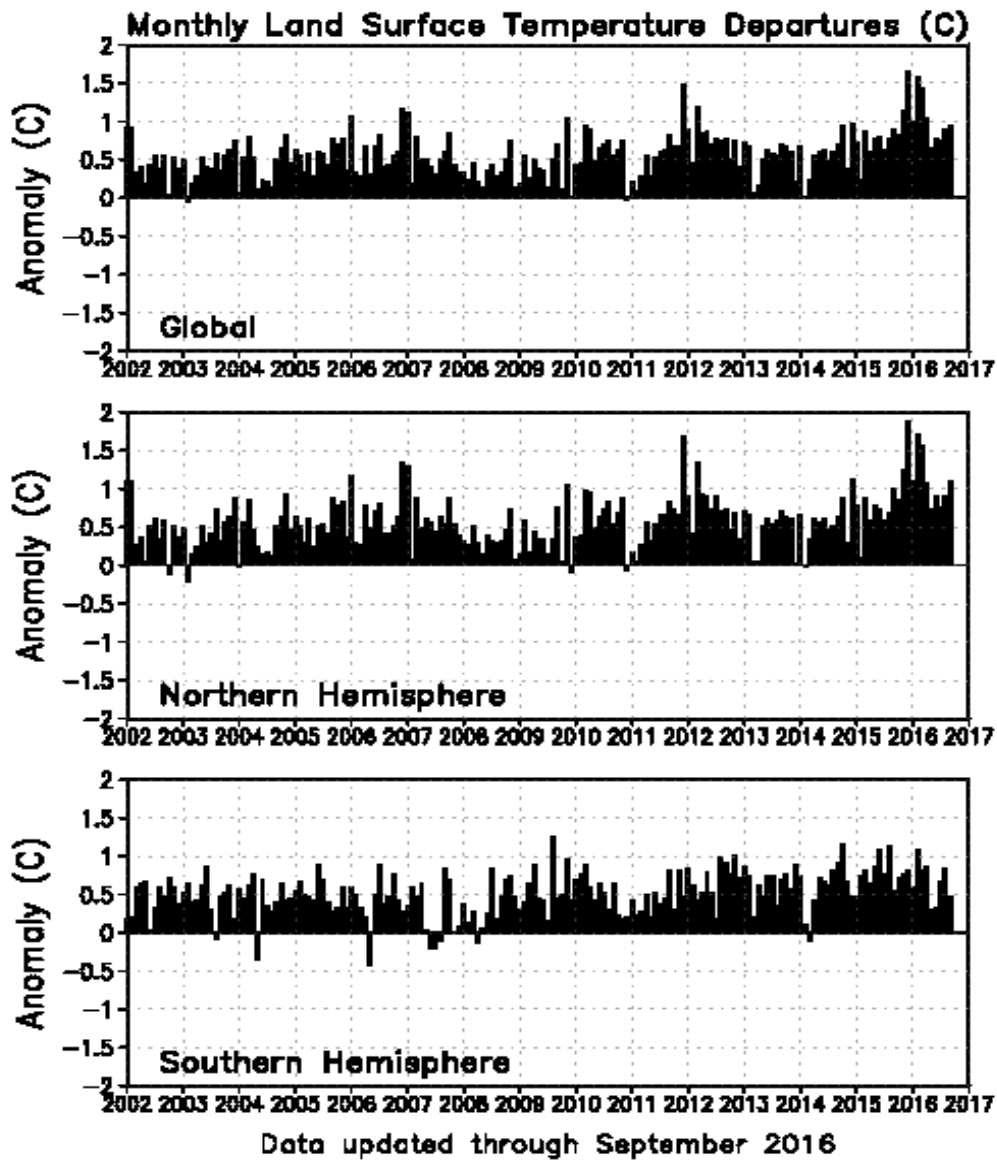


FIGURE E2. Monthly global (top), Northern Hemisphere (middle), and Southern Hemisphere (bottom) surface temperature anomalies (land only, °C) from January 1990 - present, computed as departures from the 1981–2010 base period means.



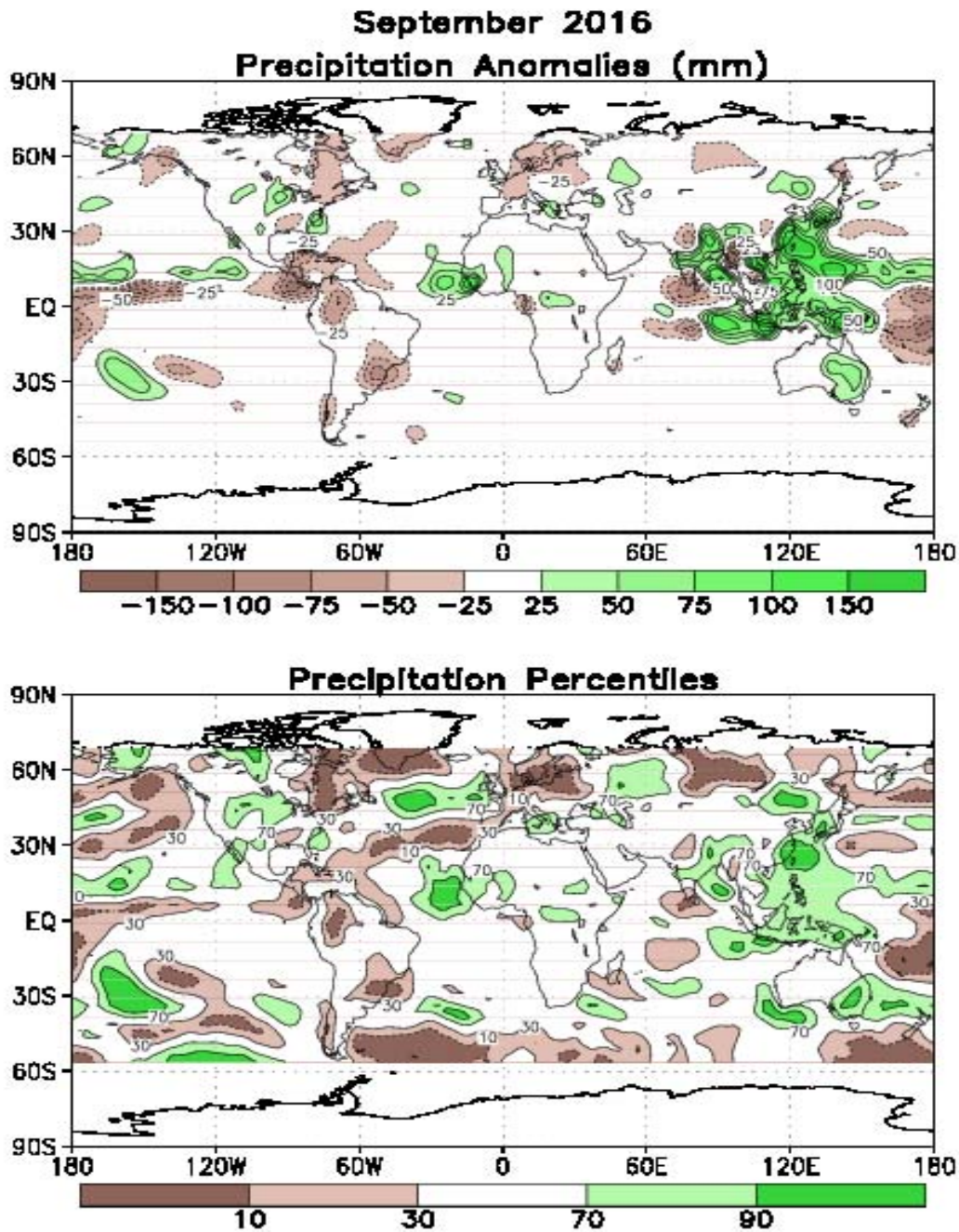


FIGURE E3. Anomalous precipitation (mm, top) and precipitation percentiles based on a Gamma distribution fit to the 1981–2010 base period data (bottom) for SEP 2016. Data are obtained from a merge of raingauge observations and satellite-derived precipitation estimates (Janowiak and Xie 1999, *J. Climate*, **12**, 3335–3342). Contours are drawn at 200, 100, 50, 25, -25, -50, -100, and -200 mm in top panel. Percentiles are not plotted in regions where mean monthly precipitation is <5mm/month.

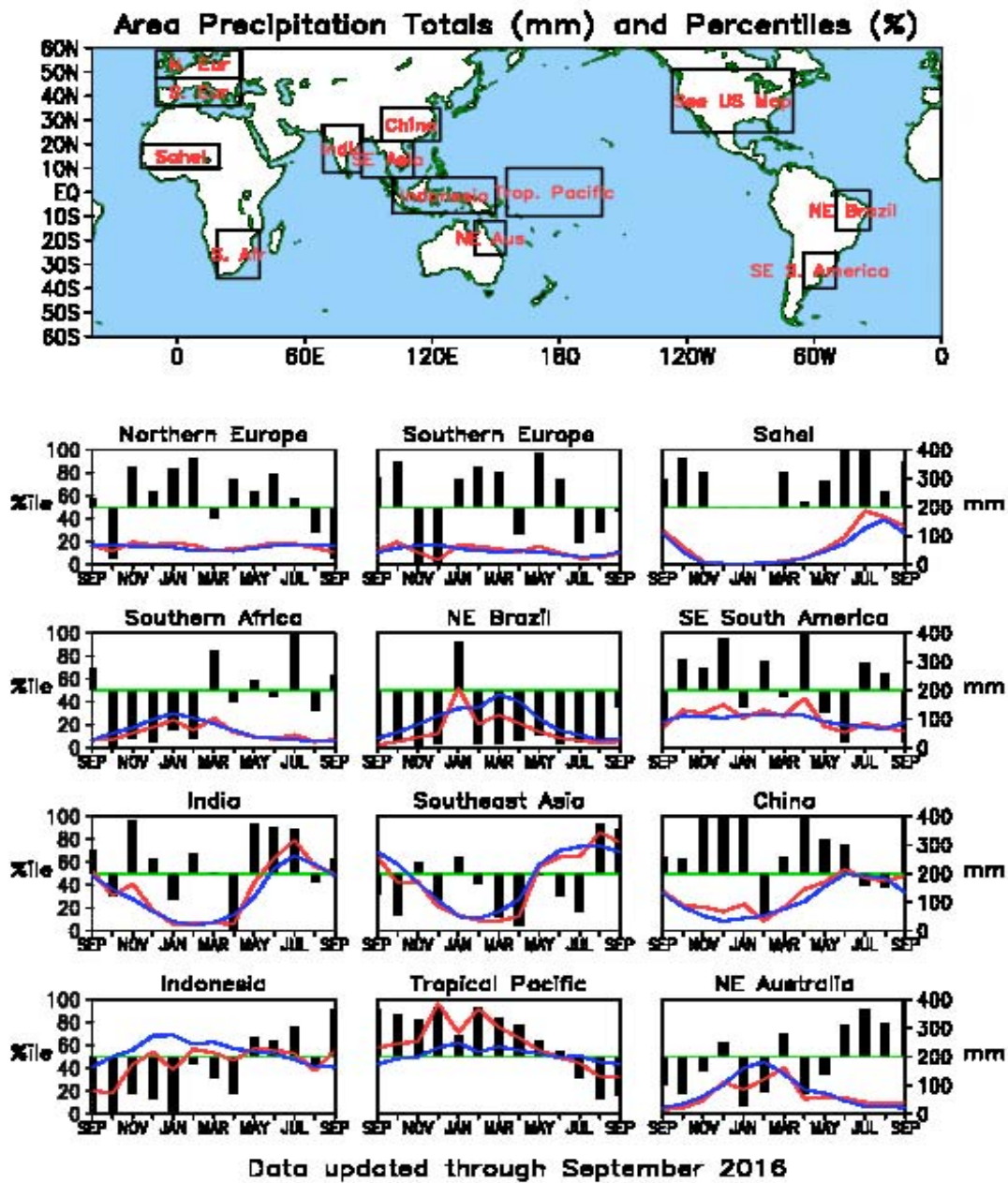


FIGURE E4. Areal estimates of monthly mean precipitation amounts (mm, solid lines) and precipitation percentiles (%), bars) for the most recent 13 months obtained from a merge of raingauge observations and satellite-derived precipitation estimates (Janowiak and Xie 1999, *J. Climate*, 12, 3335–3342). The monthly precipitation climatology (mm, dashed lines) is from the 1981–2010 base period monthly means. Monthly percentiles are not shown if the monthly mean is less than 5 mm.

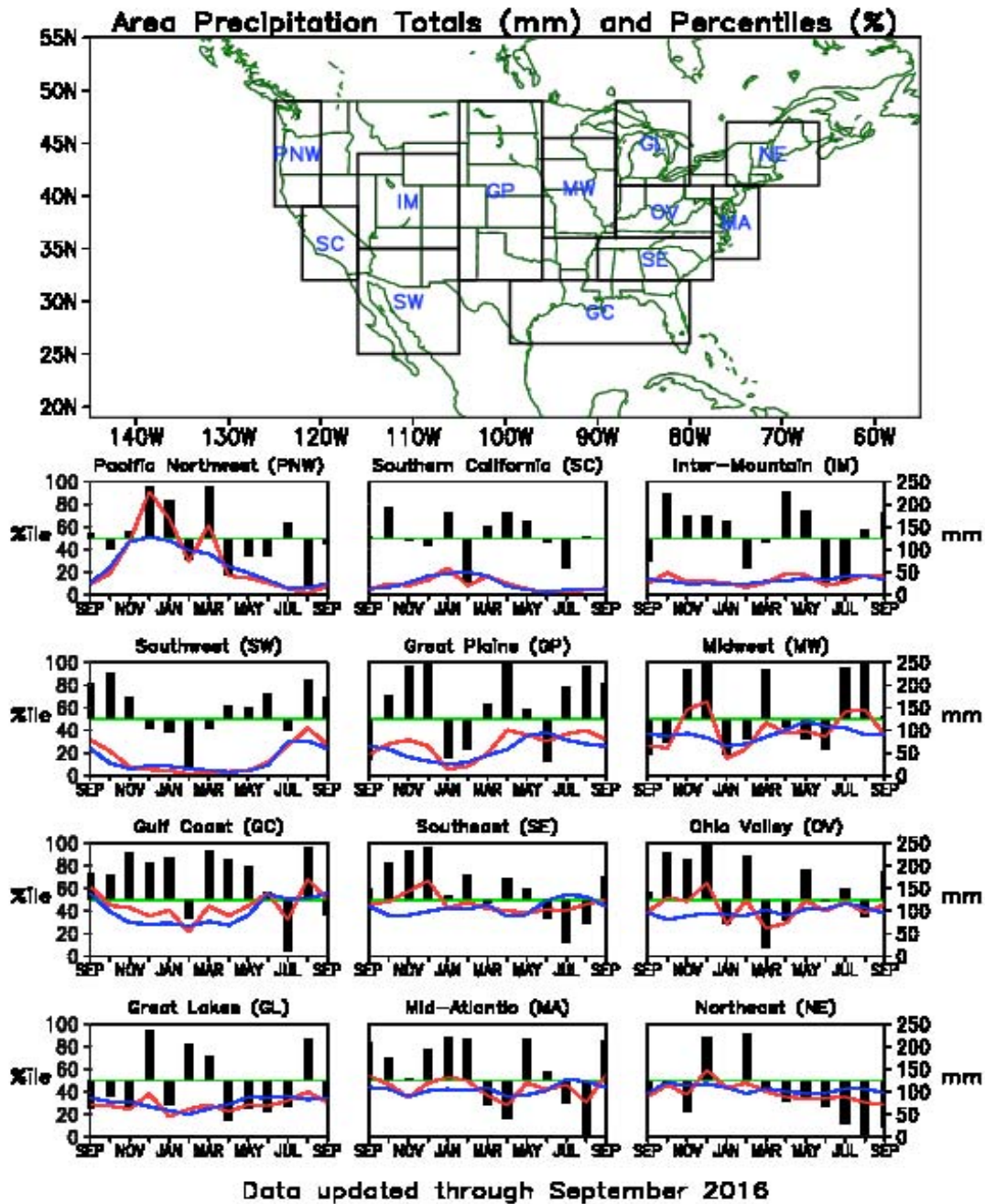


FIGURE E5. Areal estimates of monthly mean precipitation amounts (mm, solid lines) and precipitation percentiles (% , bars) for the most recent 13 months obtained from a merge of raingauge observations and satellite-derived precipitation estimates (Janowiak and Xie 1999, *J. Climate*, 12, 3335–3342). The monthly precipitation climatology (mm, dashed lines) is from the 1981–2010 base period monthly means. Monthly percentiles are not shown if the monthly mean is less than 5 mm.



Monthly Accumulation -- September, 2016

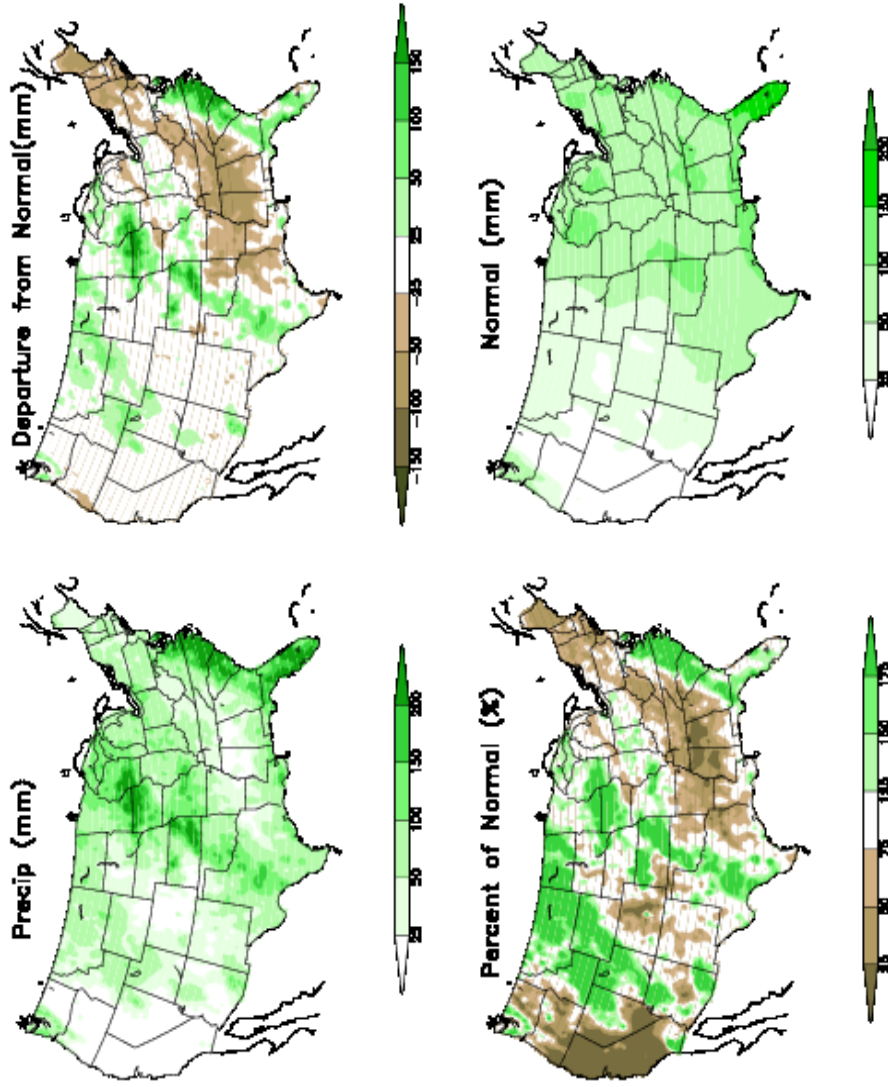
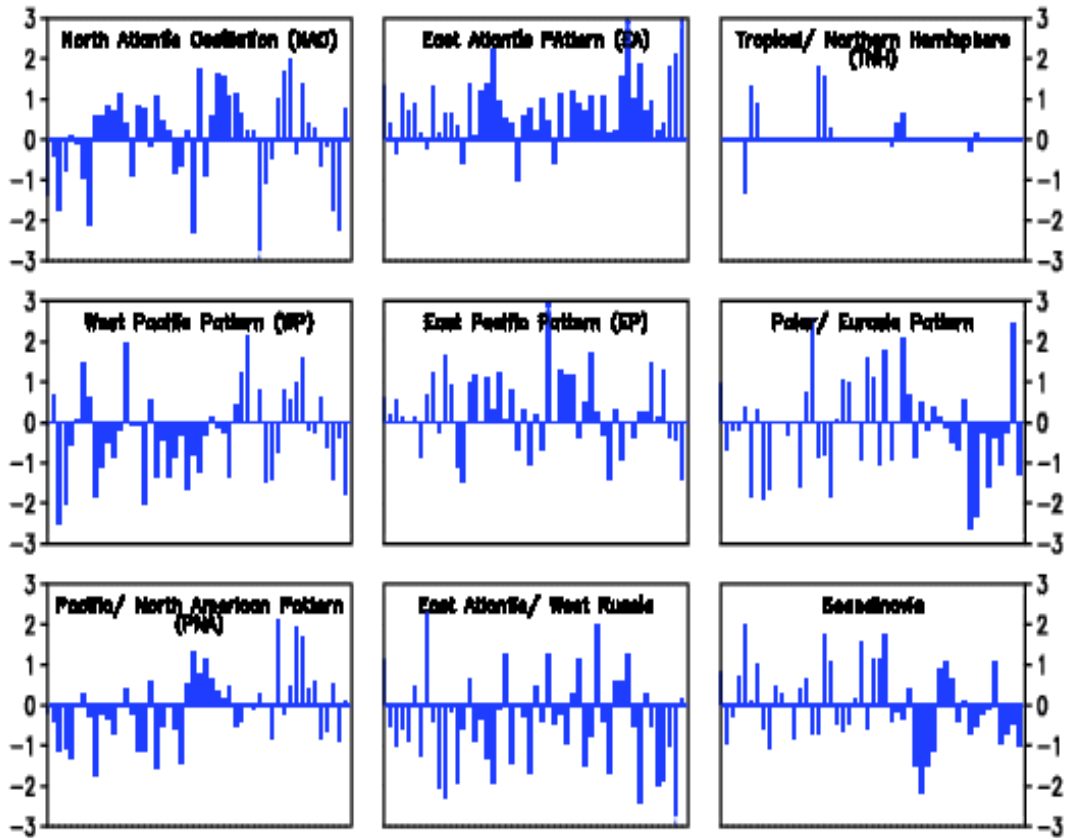


FIGURE E6. Observed precipitation (upper left), departure from average (upper right), percent of average (lower left), and average precipitation (lower right) for SEP 2016. The units are given on each panel. Base period for averages is 1981–2010. Results are based on CPC’s U. S. daily precipitation analysis, which is available at <http://www.cpc.ncep.noaa.gov/products/precip/realtime>.

## Monthly Teleconnection Indices



**Data updated through September 2016**

FIGURE E7. Standardized monthly Northern Hemisphere teleconnection indices. The teleconnection patterns are calculated from a Rotated Principal Component Analysis (RPCA) applied to monthly standardized 500-hPa height anomalies during the 1981-2010 base period. To obtain these patterns, ten leading un-rotated modes are first calculated for each calendar month by using the monthly height anomaly fields for the three-month period centered on that month: [i.e., The July modes are calculated from the June, July, and August standardized monthly anomalies]. A Varimax spatial rotation of the ten leading un-rotated modes for each calendar month results in 120 rotated modes (12 months x 10 modes per month) that yield ten primary teleconnection patterns. The teleconnection indices are calculated by first projecting the standardized monthly anomalies onto the teleconnection patterns corresponding to that month (eight or nine teleconnection patterns are seen in each calendar month). The indices are then solved for simultaneously using a Least-Squares approach. In this approach, the indices are the solution to the Least-Squares system of equations which explains the maximum spatial structure of the observed height anomaly field during the month. The indices are then standardized for each pattern and calendar month independently. No index value exists when the teleconnection pattern does not appear as one of the ten leading rotated EOF's valid for that month.

**September 2016**  
**Sea-Level Pressure and Anomaly**

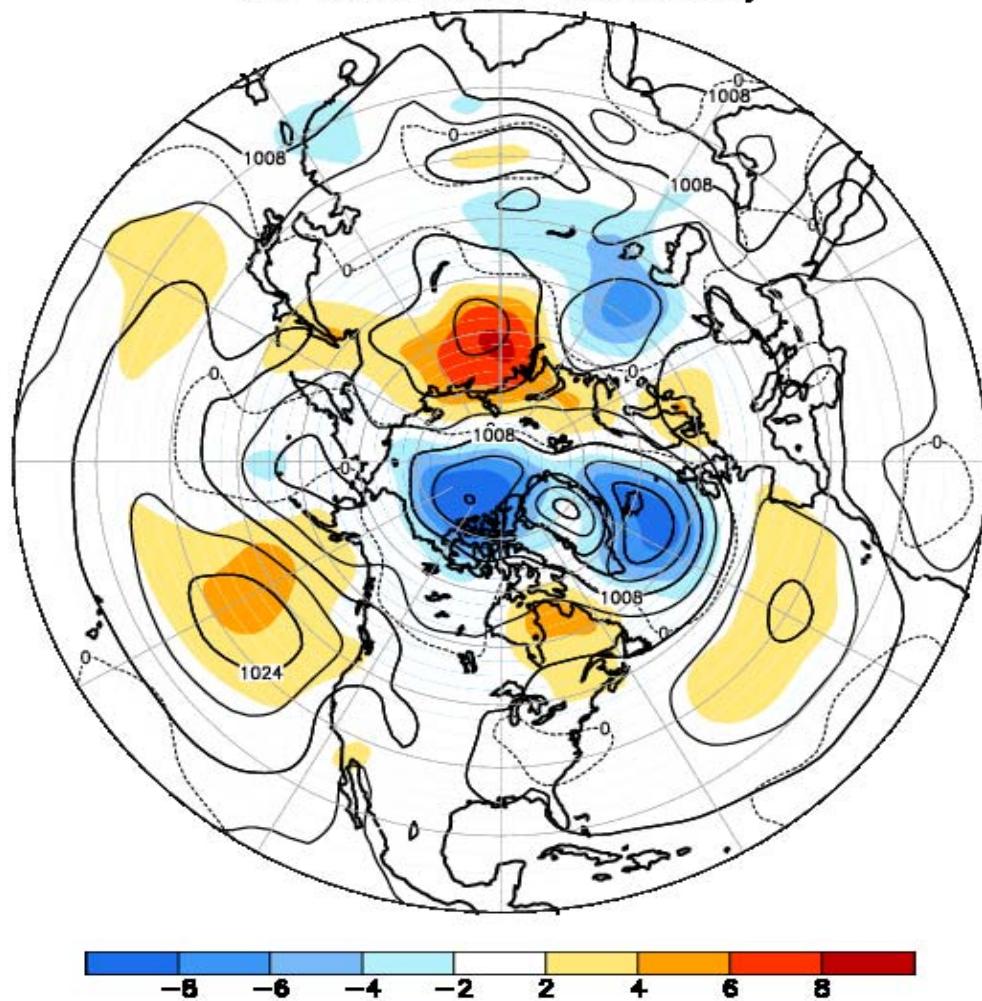


FIGURE E8. Northern Hemisphere mean and anomalous sea level pressure (CDAS/Reanalysis) for SEP 2016. Mean values are denoted by solid contours drawn at an interval of 4 hPa. Anomaly contour interval is 2 hPa with values less (greater) than -2 hPa (2 hPa) indicated by dark (light) shading. Anomalies are calculated as departures from the 1981-2010 base period monthly means.



September 2016  
500-hPa Height and Anomaly

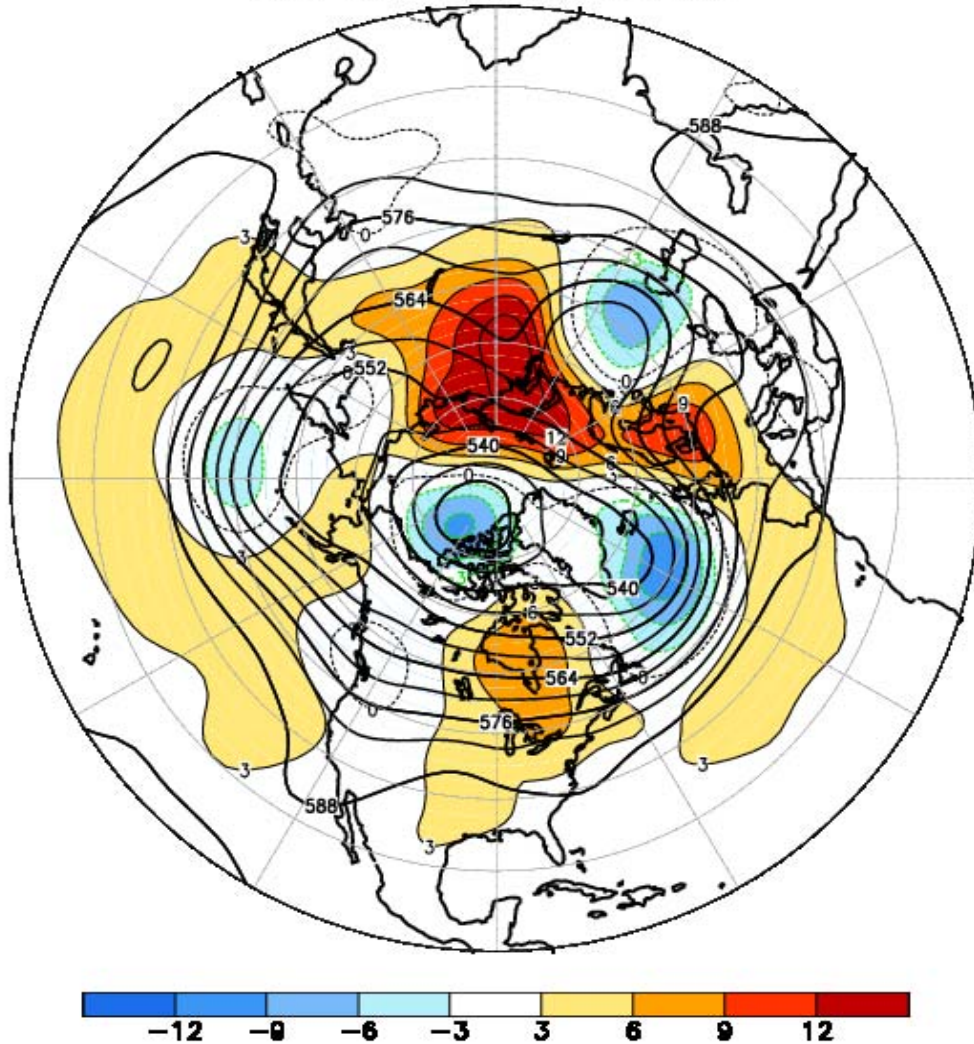


FIGURE E9. Northern Hemisphere mean and anomalous 500-hPa geopotential height (CDAS/Reanalysis) for SEP 2016. Mean heights are denoted by solid contours drawn at an interval of 6 dam. Anomaly contour interval is 3 dam with values less (greater) than -3 dam (3 dam) indicated by dark (light) shading. Anomalies are calculated as departures from the 1981-2010 base period monthly means.

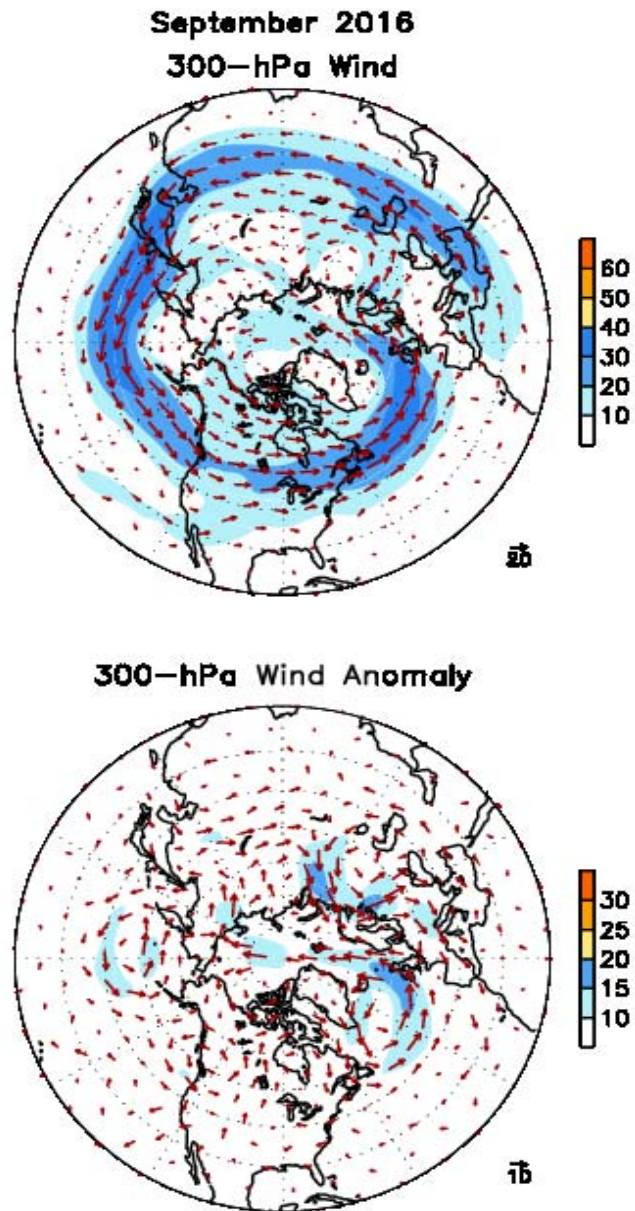


FIGURE E10. Northern Hemisphere mean (left) and anomalous (right) 300-hPa vector wind (CDAS/Reanalysis) for SEP 2016. Mean (anomaly) isotach contour interval is 10 (5)  $\text{ms}^{-1}$ . Values greater than 30  $\text{ms}^{-1}$  (left) and 10  $\text{ms}^{-1}$  (rights) are shaded. Anomalies are departures from the 1981-2010 base period monthly means.

**September 2016**  
**500-hPa: Percentage of Anomaly Days**

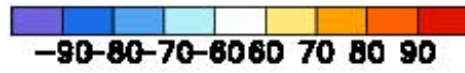
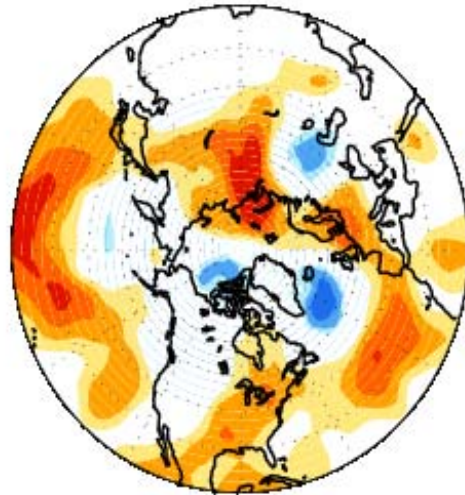


FIGURE E11. Northern Hemisphere percentage of days during SEP 2016 in which 500-hPa height anomalies greater than 15 m (red) and less than -15 m (blue) were observed. Values greater than 70% are shaded and contour in-



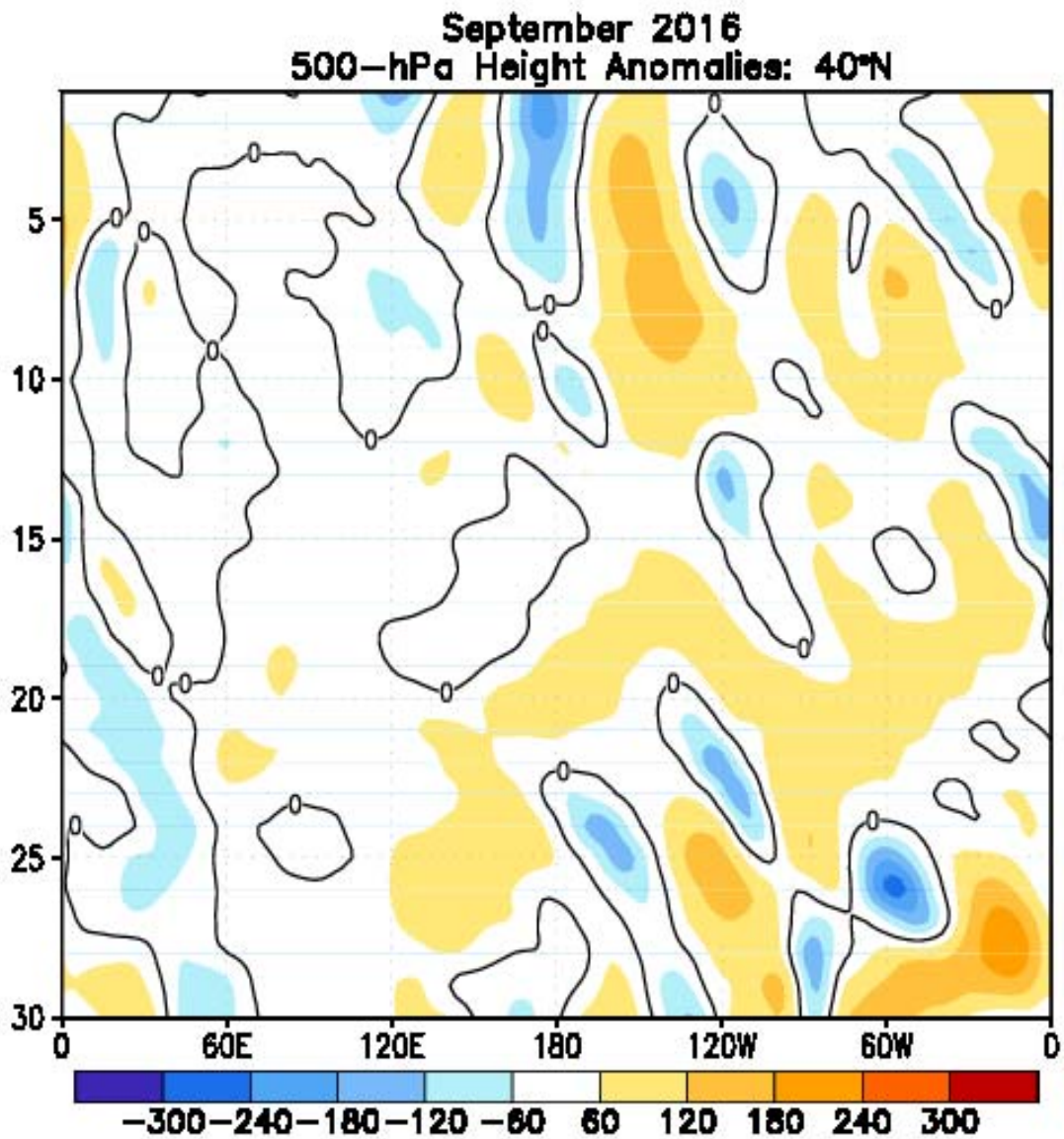
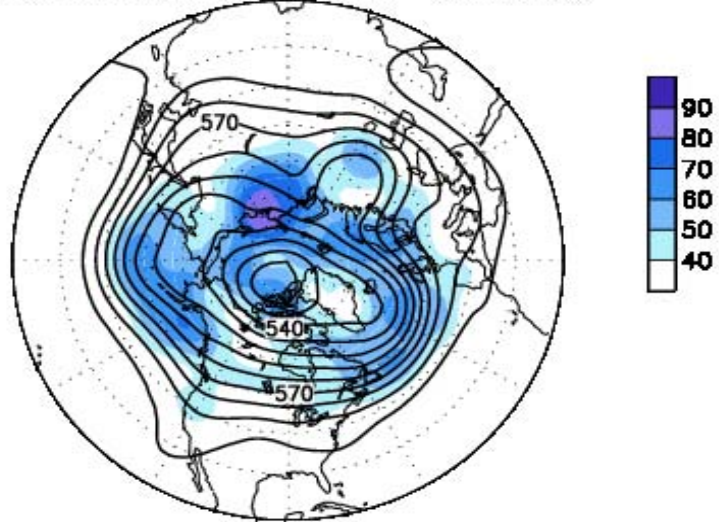


FIGURE E12. Northern Hemisphere: Daily 500-hPa height anomalies for SEP 2016 averaged over the 5° latitude band centered on 40°N. Positive values are indicated by solid contours and dark shading. Negative values are indicated by dashed contours and light shading. Contour interval is 60 m. Anomalies are departures from the 1981-2010 base period daily means.

**September 2016**  
**500-hPa Heights (Contours)**  
**High Frequency Std. Dev. (Shading)**



**500-hPa Heights (Contours)**  
**Normalized High Frequency Variance (Shading)**

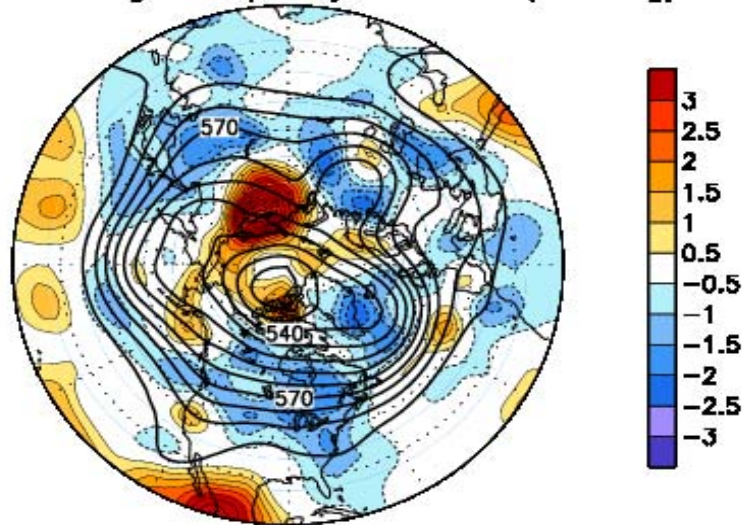


FIGURE E13. Northern Hemisphere 500-hPa heights (thick contours, interval is 6 dam) overlaid with (Top) Standard deviation of 10-day high-pass (HP) filtered height anomalies and (Bottom) Normalized anomalous variance of 10-day HP filtered height anomalies. A Lanczos filter is used to calculate the HP filtered anomalies. Anomalies are departures from the 1981-2010 daily means.

**September 2016**  
**Sea-Level Pressure and Anomaly**

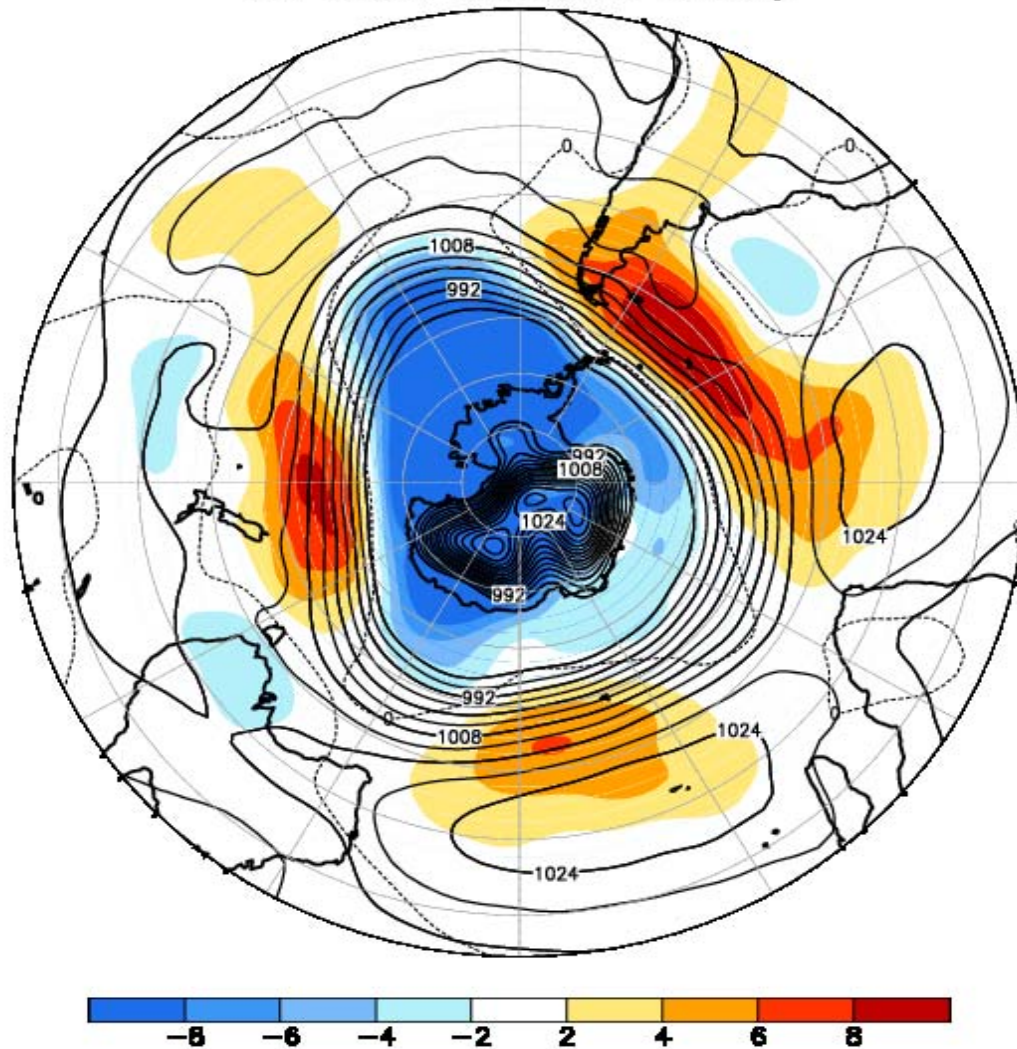


FIGURE E14. Southern Hemisphere mean and anomalous sea level pressure(CDAS/Reanalysis) for SEP 2016. Mean values are denoted by solid contours drawn at an interval of 4 hPa. Anomaly contour interval is 2 hPa with values less (greater) than -2 hPa (2 hPa) indicated by dark (light) shading. Anomalies are calculated as departures from the 1981-2010 base period monthly means.



September 2016  
500-hPa Height and Anomaly

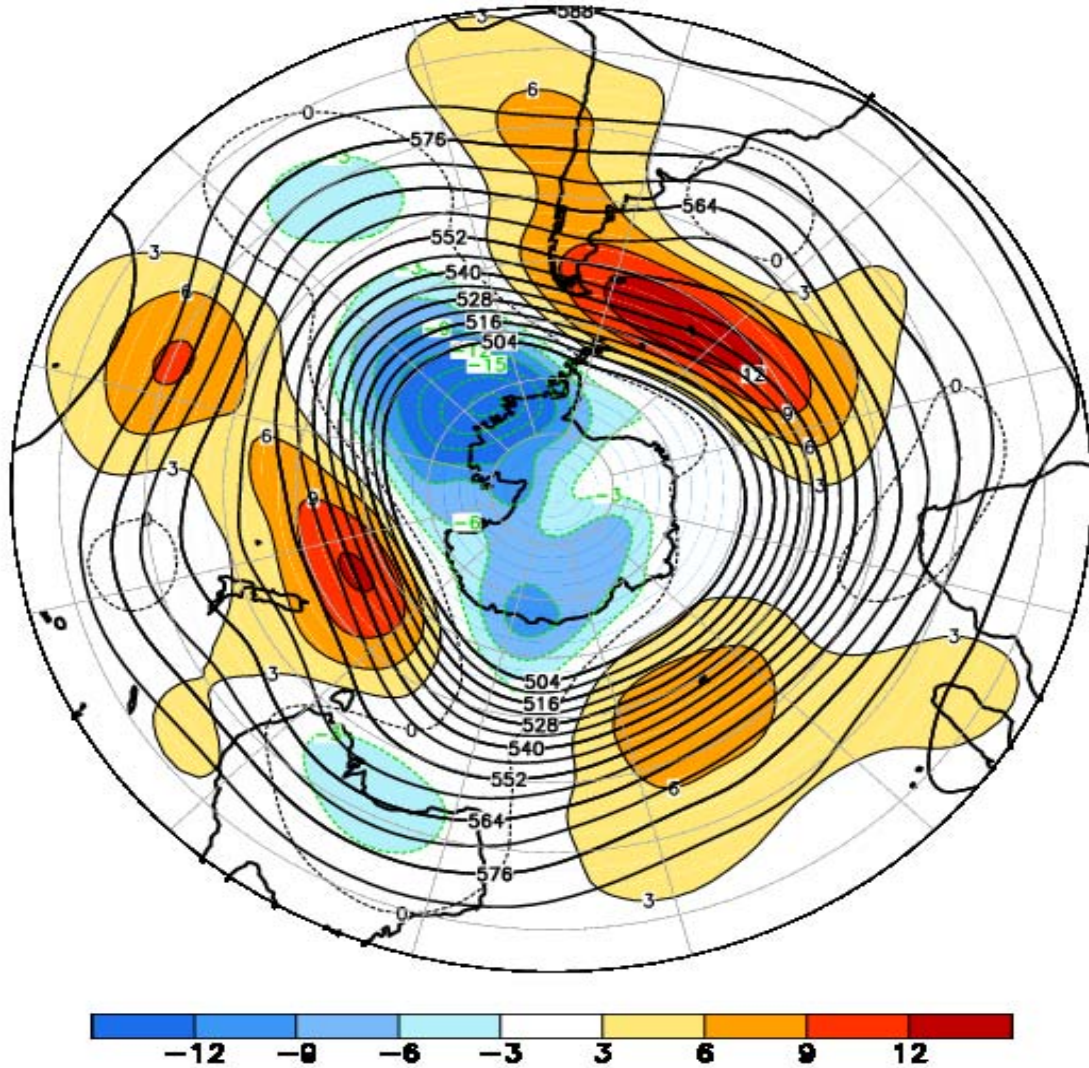
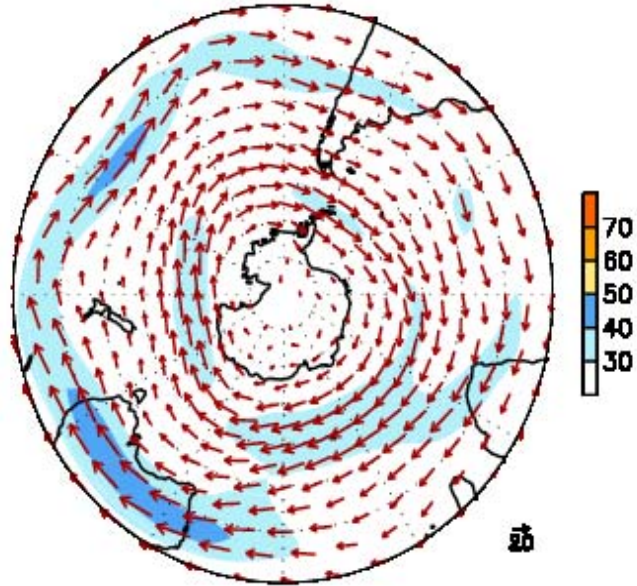


FIGURE E15. Southern Hemisphere mean and anomalous 500-hPa geopotential height (CDAS/Reanalysis) for SEP 2016. Mean heights are denoted by solid contours drawn at an interval of 6 dam. Anomaly contour interval is 3 dam with values less (greater) than -3 dam (3 dam) indicated by dark (light) shading. Anomalies are calculated as departures from the 1981-2010 base period monthly means.

September 2016  
300-hPa Wind



300-hPa Wind Anomaly

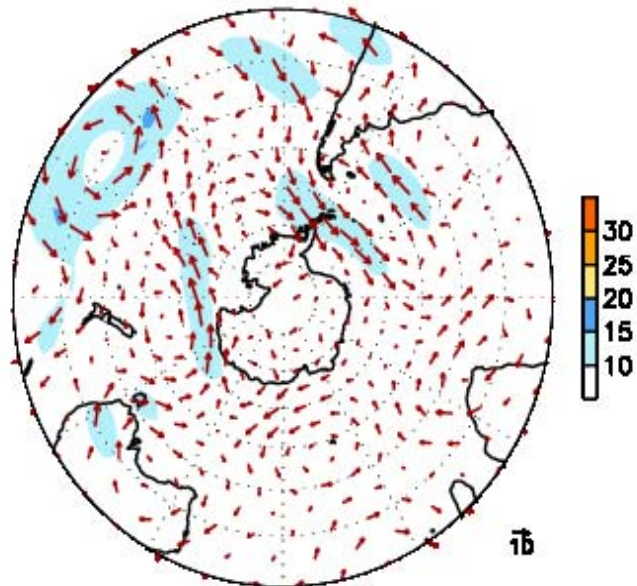


FIGURE E16. Southern Hemisphere mean (left) and anomalous (right) 300-hPa vector wind (CDAS/Reanalysis) for SEP 2016. Mean (anomaly) isotach contour interval is 10 (5)  $\text{ms}^{-1}$ . Values greater than 30  $\text{ms}^{-1}$  (left) and 10  $\text{ms}^{-1}$  (rights) are shaded. Anomalies are departures from the 1981-2010 base period monthly means.

**September 2016**  
**500-hPa: Percentage of Anomaly Days**

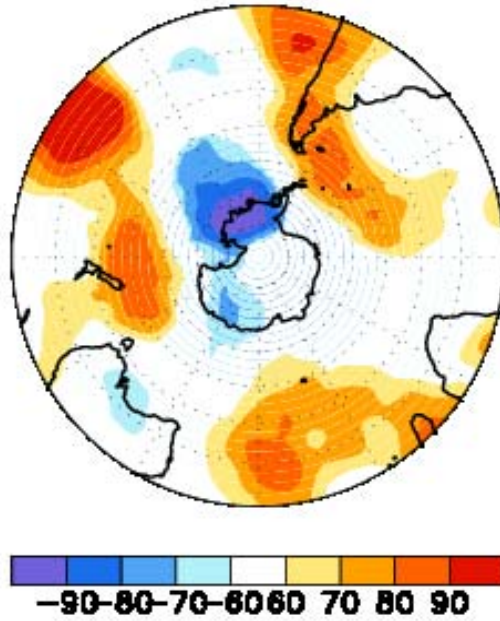


FIGURE E17. Southern Hemisphere percentage of days during SEP 2016 in which 500-hPa height anomalies greater than 15 m (red) and less than -15 m (blue) were observed. Values greater than 70% are shaded and contour in-



**September 2016  
500-hPa Height Anomalies: 40°S**

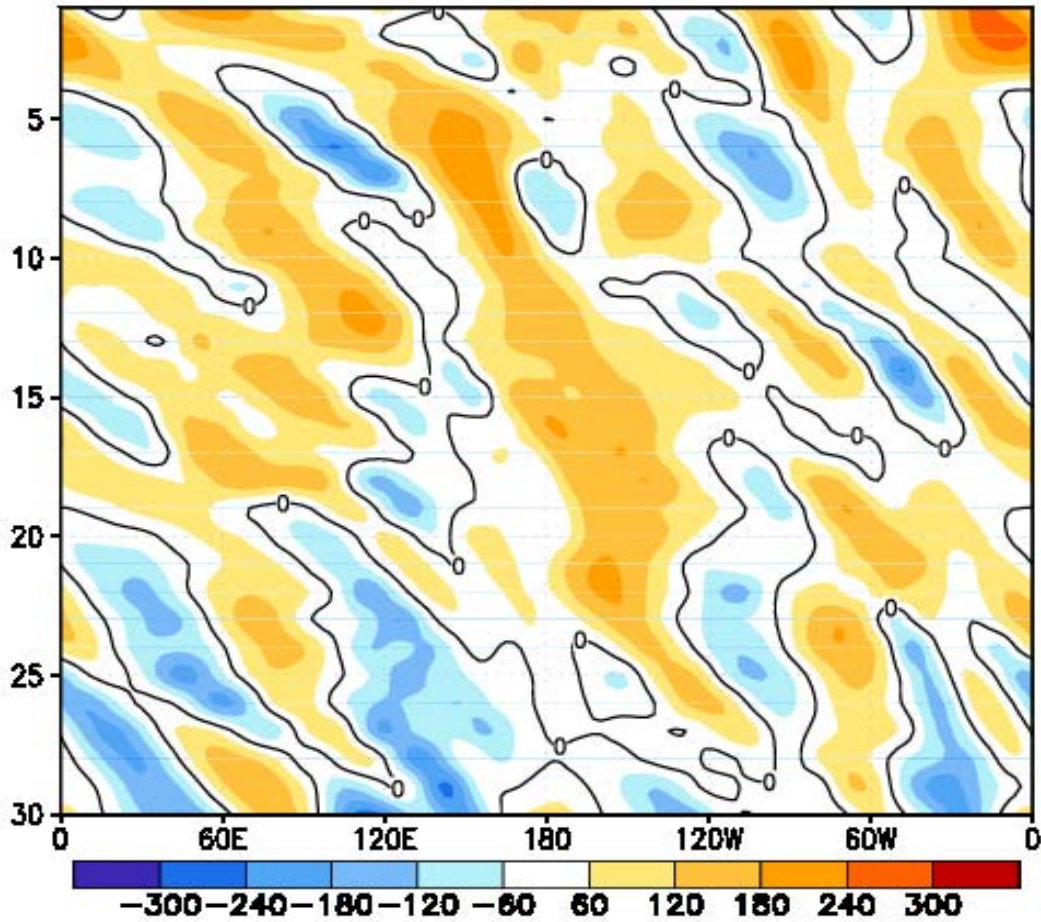


FIGURE E18. Southern Hemisphere: Daily 500-hPa height anomalies for SEP 2016 averaged over the 5° latitude band centered on 40°S. Positive values are indicated by solid contours and dark shading. Negative values are indicated by dashed contours and light shading. Contour interval is 60 m. Anomalies are departures from the 1981-2010 base period daily means.

**September 2016  
Height Anomalies**

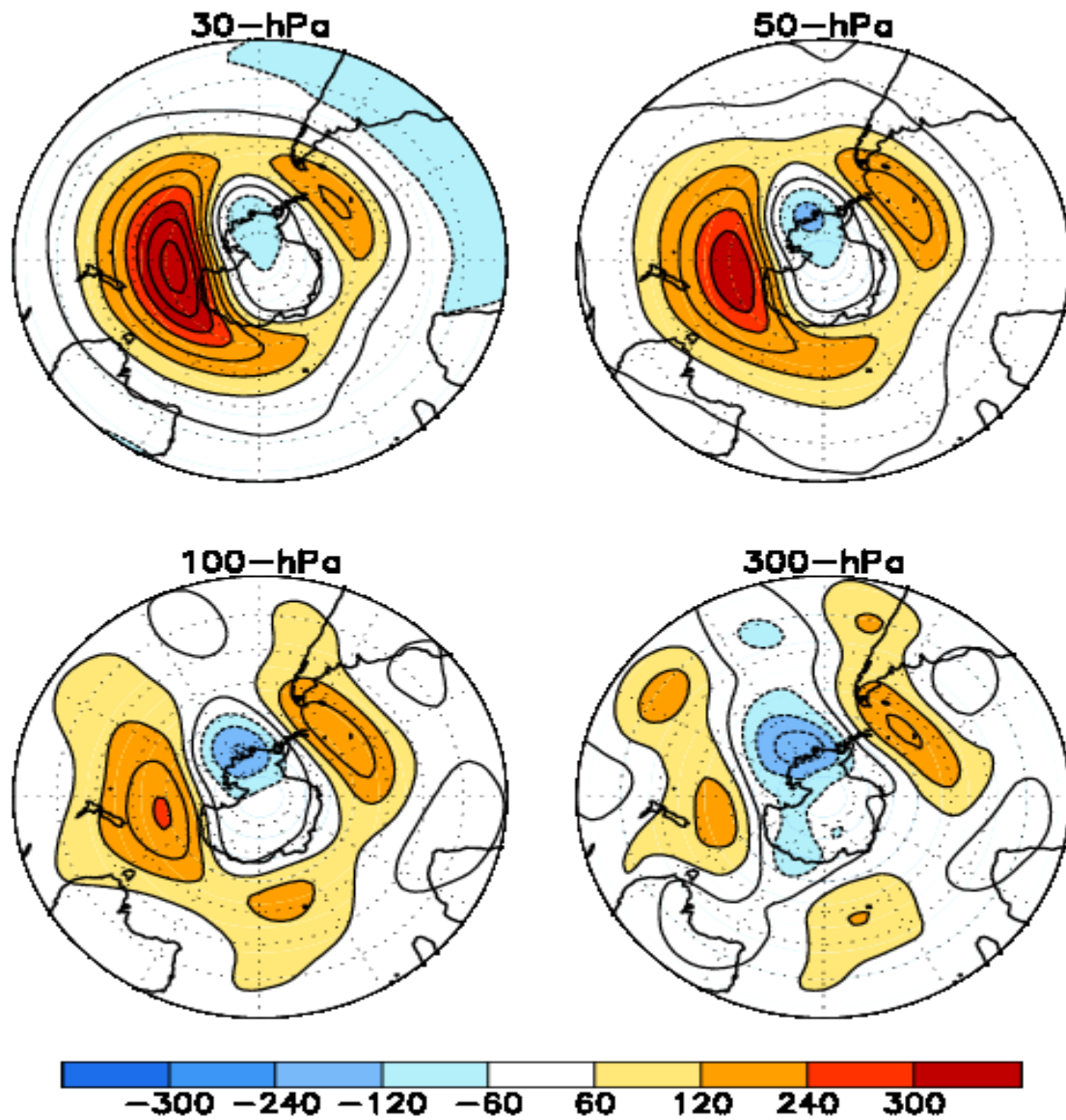


FIGURE S1. Stratospheric height anomalies (m) at selected levels for SEP 2016. Positive values are indicated by solid contours and dark shading. Negative values are indicated by dashed contours and light shading. Contour interval is 60 m. Anomalies are calculated from the 1981-2010 base period means. Winter Hemisphere is shown.

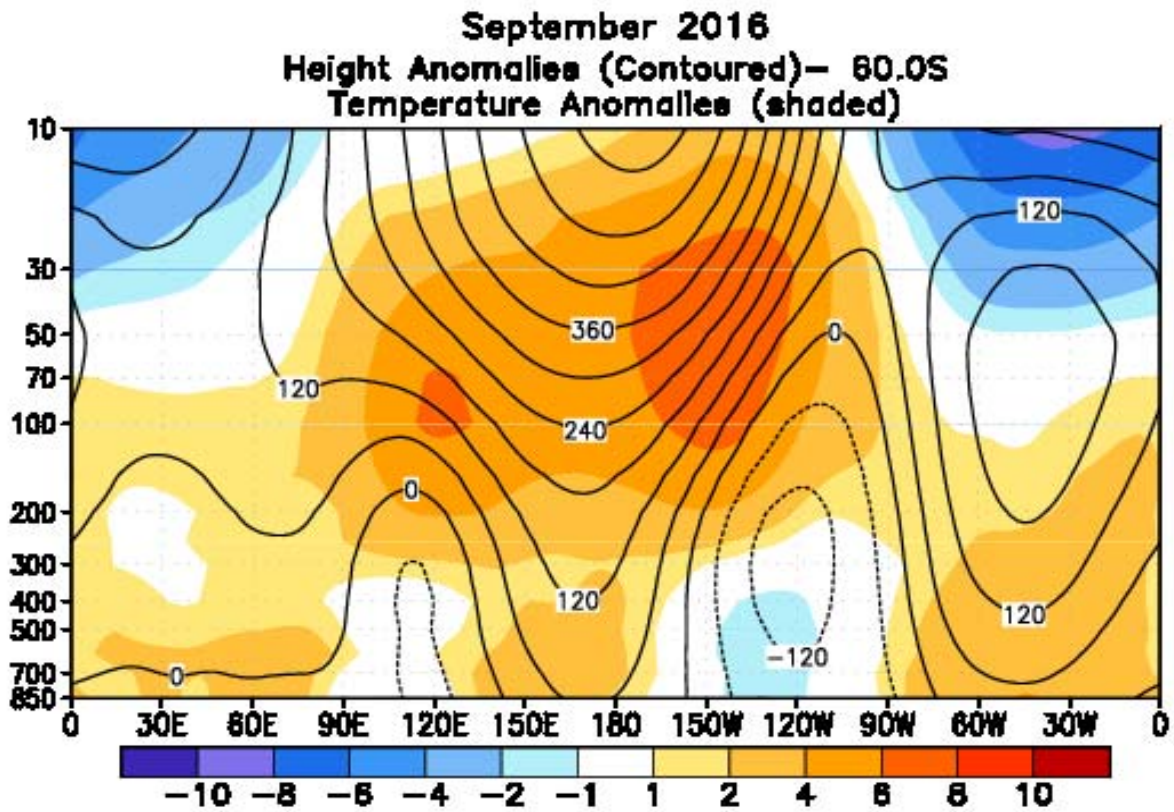


FIGURE S2. Height-longitude sections during SEP 2016 for height anomalies (contour) and temperature anomalies (shaded). In both panels, positive values are indicated by solid contours and dark shading, while negative anomalies are indicated by dashed contours and light shading. Contour interval for height anomalies is 60 m and for temperature anomalies is 2°C. Anomalies are calculated from the 1981-2010 base period monthly means. Winter Hemisphere is shown.



### 50hPa JAS Mean Temperature Anomalies

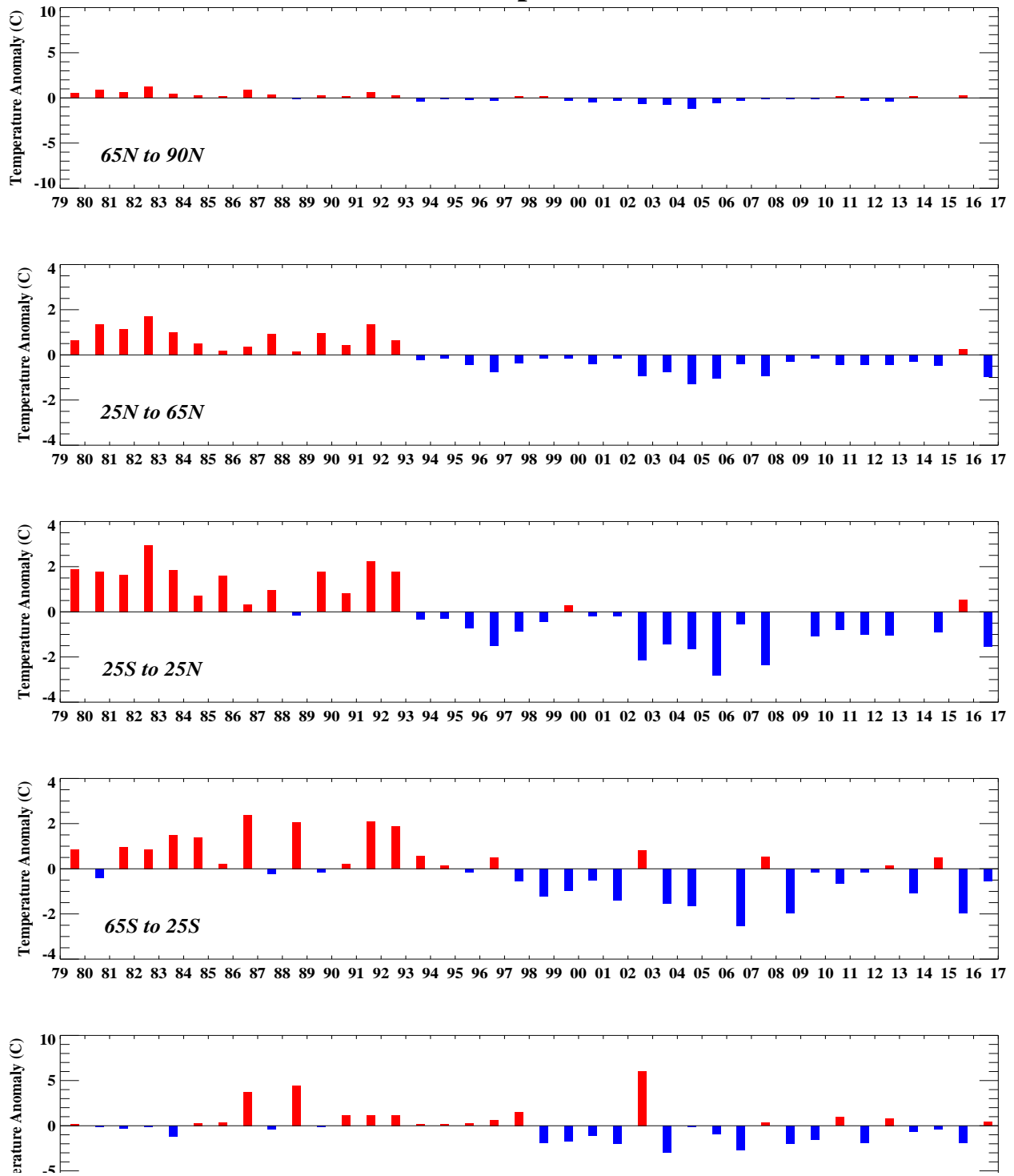


FIGURE S3. Seasonal mean temperature anomalies at 50-hPa for the latitude bands 65°–90°N, 25°–65°N, 25°N–25°S, 25°–65°S, 65°–90°S. The seasonal mean is comprised of the most recent three months. Zonal anomalies are taken from the mean of the entire data set.

### Zonal Mean Temperature for 2015 & 2016

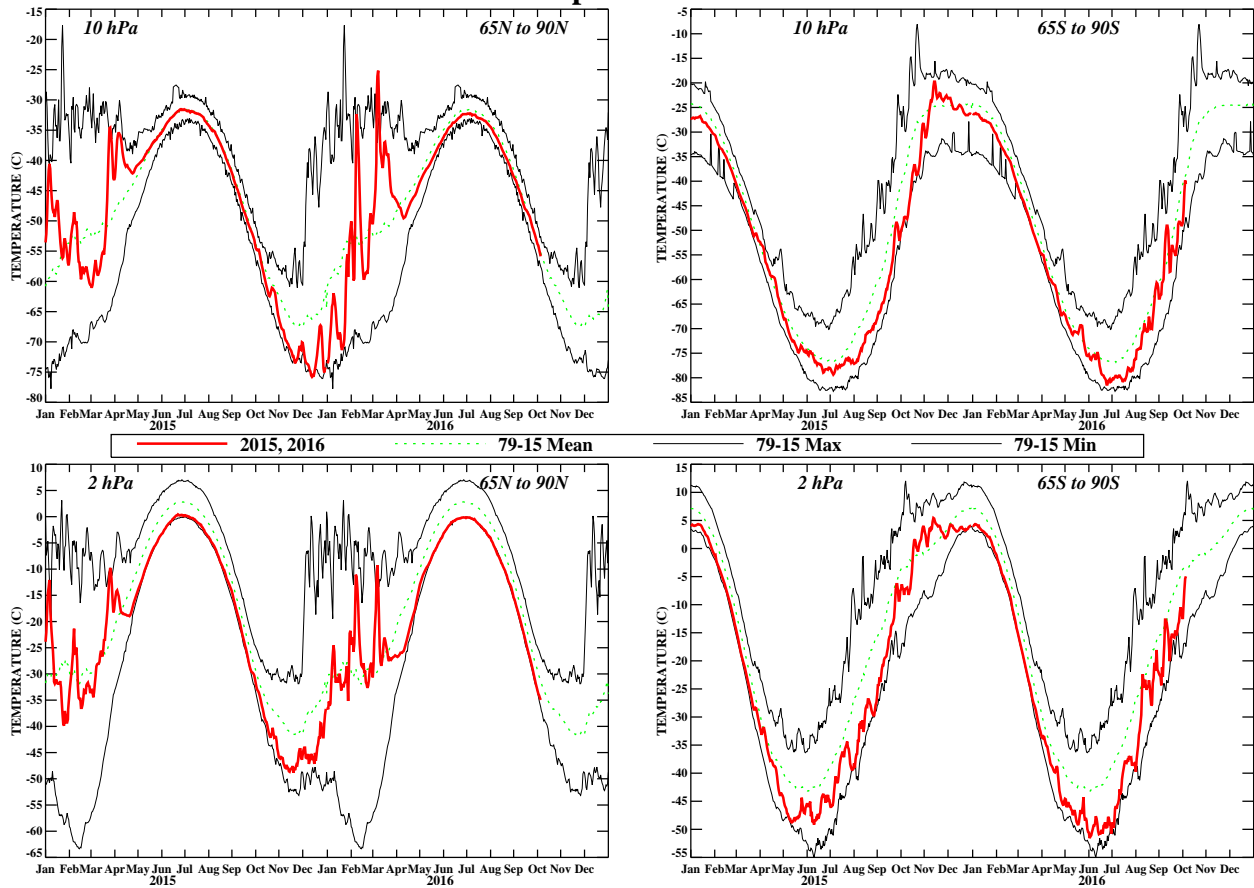


FIGURE S4. Daily mean temperatures at 10-hPa and 2-hPa (thick line) in the region 65°–90°N and 65°–90°S for the past two years. Dashed line depicts the 1981–2010 base period daily mean. Thin solid lines depict the daily extreme maximum and minimum temperatures.

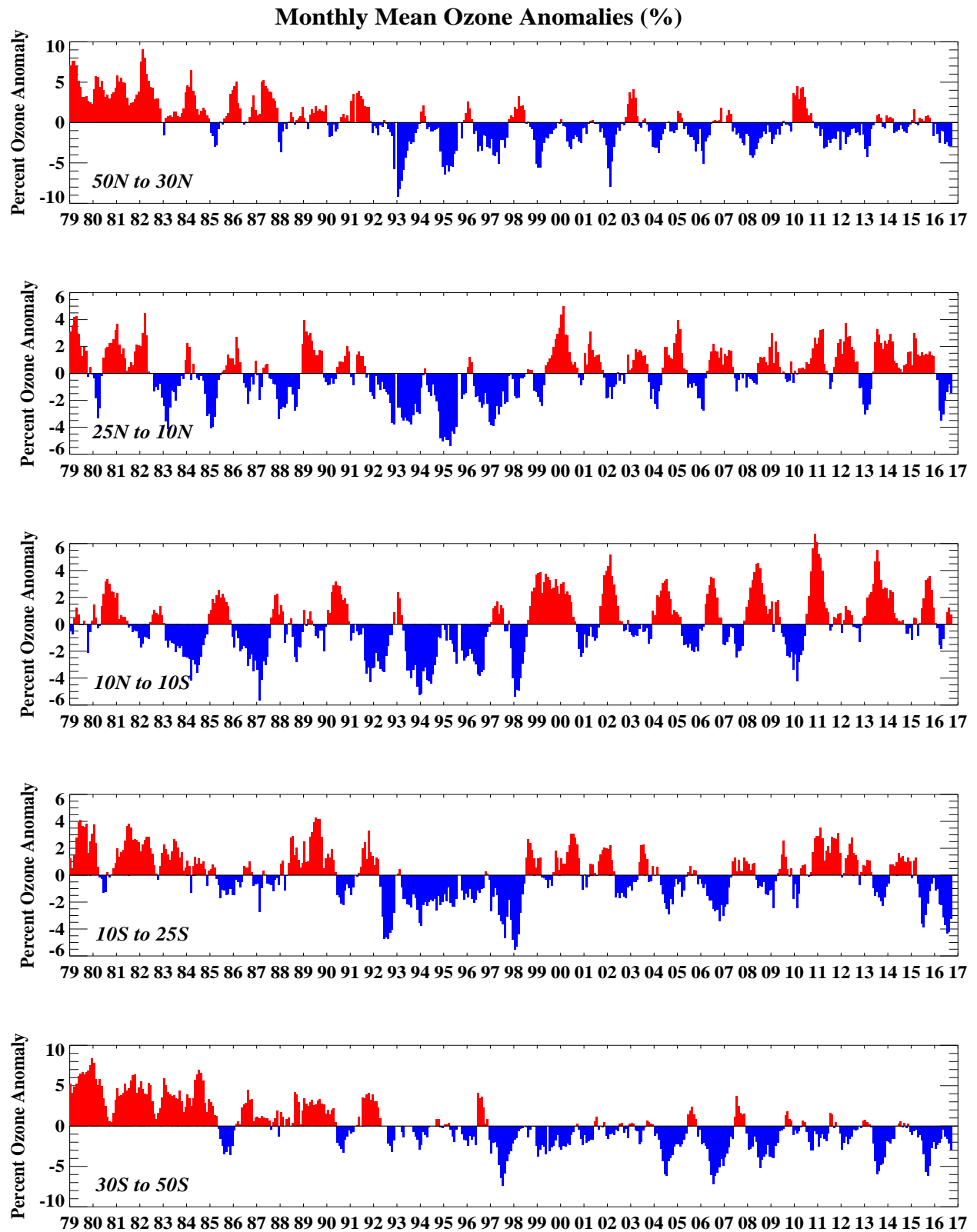


FIGURE S5. Monthly ozone anomalies (percent) from the long term monthly means for five zones: 50N-30N (NH mid-latitudes), 25N-10N (NH tropical surf zone), 10N-10S (Equatorial-QBO zone), 10S-25S (SH tropical surf zone), and 30S-50S (SH mid-latitudes). The long term monthly means are determined from the entire data set



**SEPTEMBER PERCENT DIFF (2016 - AVG[79-86])**

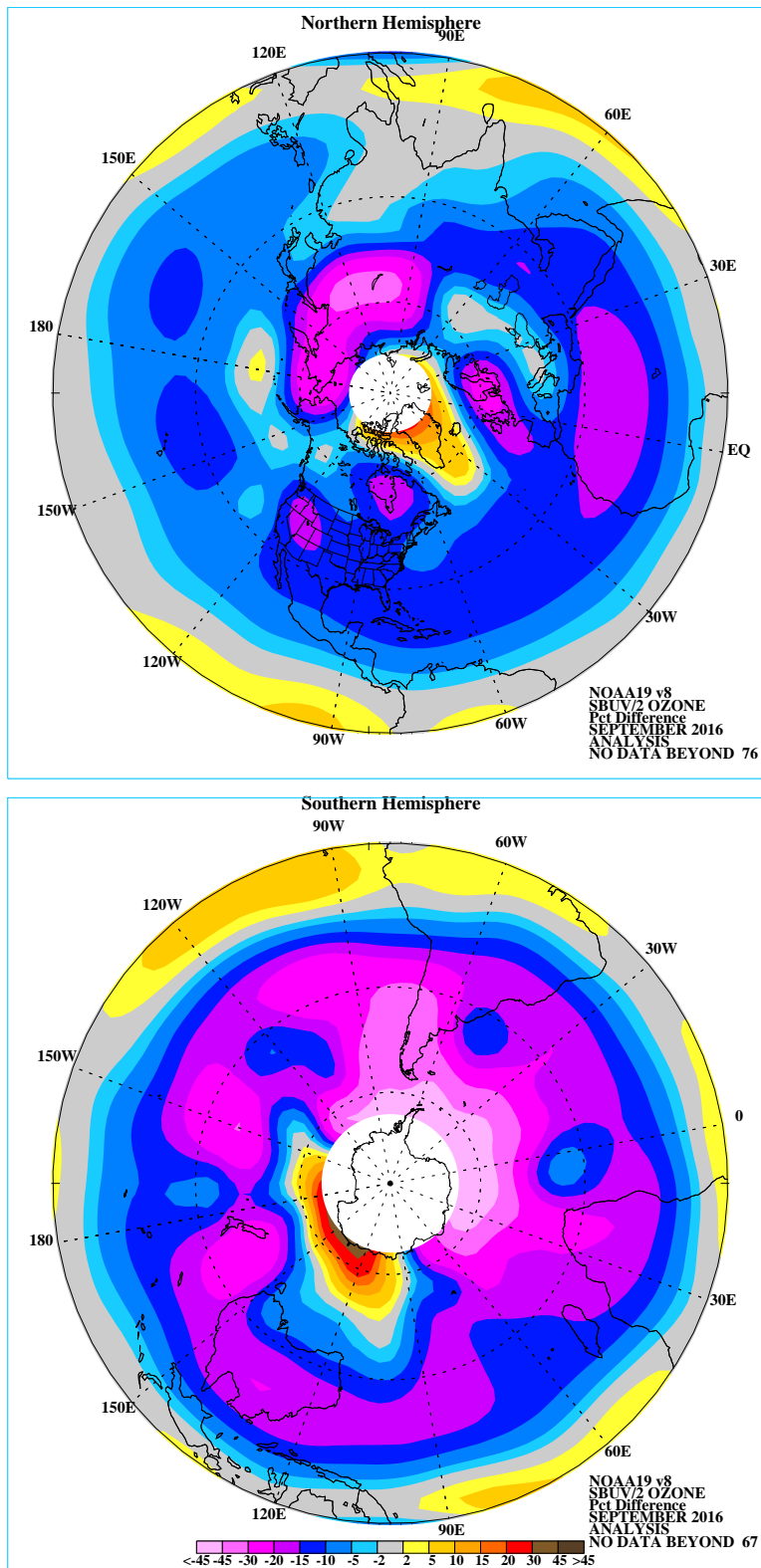


FIGURE S6. Northern (top) and Southern (bottom) Hemisphere total ozone anomaly (percent difference from monthly mean for the period 1979-1986). The region near the winter pole has no SBUV/2 data.

# Fz at 100 hPa (Sep. 2016)

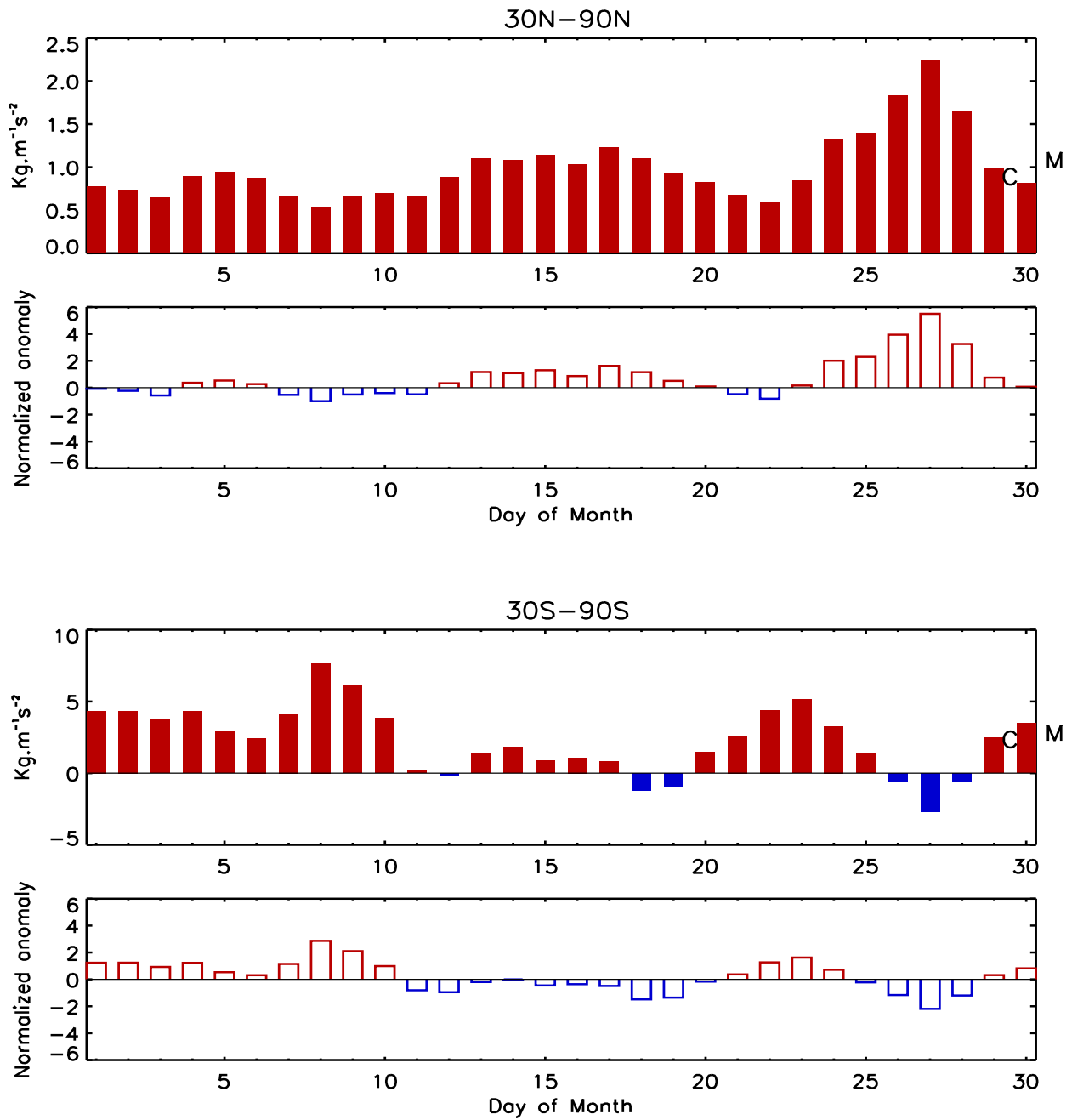


FIGURE S7. Daily vertical component of EP flux (which is proportional to the poleward transport of heat or upward transport of potential energy by planetary wave) at 100 hPa averaged over (top) 30°N–90°N and (bottom) 30°S–90°S for SEP 2016. The EP flux unit ( $\text{kg}\cdot\text{m}^{-1}\cdot\text{s}^{-2}$ ) has been scaled by multiplying a factor of the Brunt Vaisala frequency divided by the Coriolis parameter and the radius of the earth. The letter ‘M’ indicates the current monthly mean value and the letter ‘C’ indicates the climatological mean value. Additionally, the normalized departures from the monthly climatological EP flux values are shown.

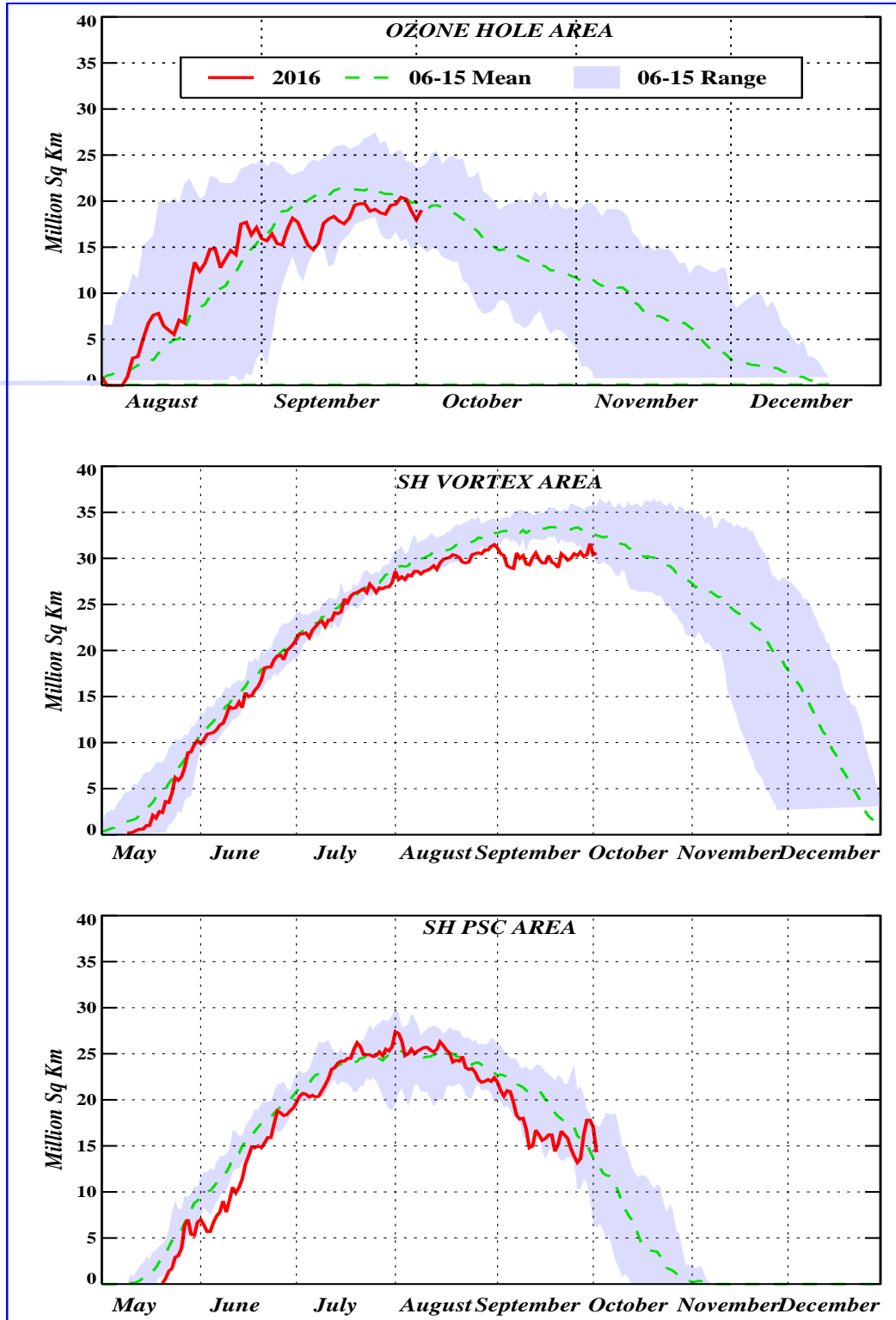


FIGURE S8. Daily time series showing the size of the SH polar vortex (representing the area enclosed by the 32 PVU contour on the 450K isentropic surface), and the areal coverage of temperatures < -78C on the 450K isentropic surface.



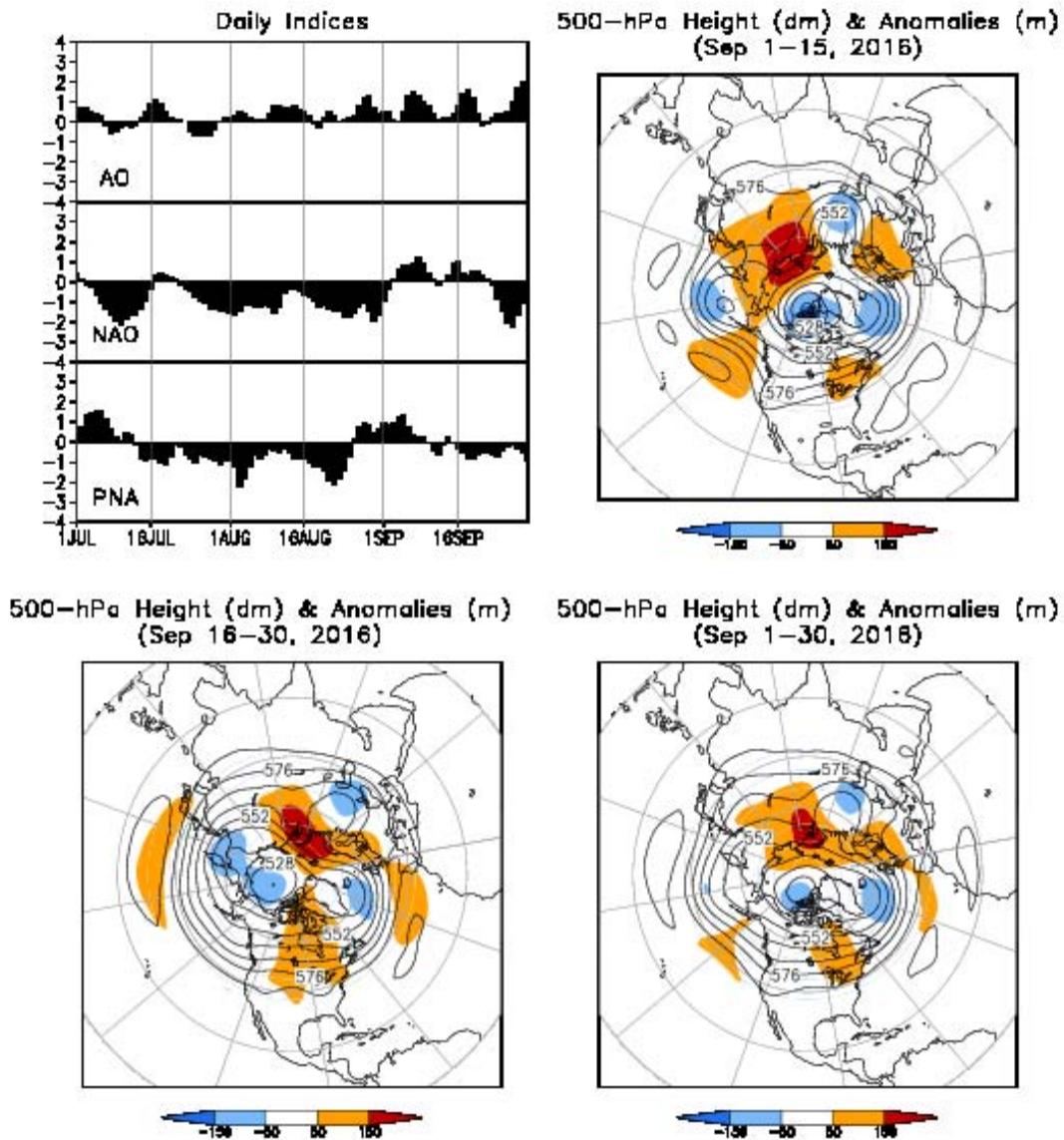


FIGURE A2.1. (a) Daily amplitudes of the Arctic Oscillation (AO) the North Atlantic Oscillation (NAO), and the Pacific-North American (PNA) pattern. The pattern amplitudes for the AO, (NAO, PNA) are calculated by projecting the daily 1000-hPa (500-hPa) height anomaly field onto the leading EOF obtained from standardized time-series of daily 1000-hPa (500-hPa) height for all months of the year. The base period is 1981–2010.

(b-d) Northern Hemisphere mean and anomalous 500-hPa geopotential height (CDAS/Reanalysis) for selected periods during SEP 2016 are shown in the remaining 3 panels. Mean heights are denoted by solid contours drawn at an interval of 8 dam. Dark (light) shading corresponds to anomalies greater than 50 m (less than -50 m). Anomalies are calculated as departures from the 1981-2010 base period daily means.

**SSM/I Snow Cover for Sep 2016  
anomaly based on departure from 1987-2010 baseline**

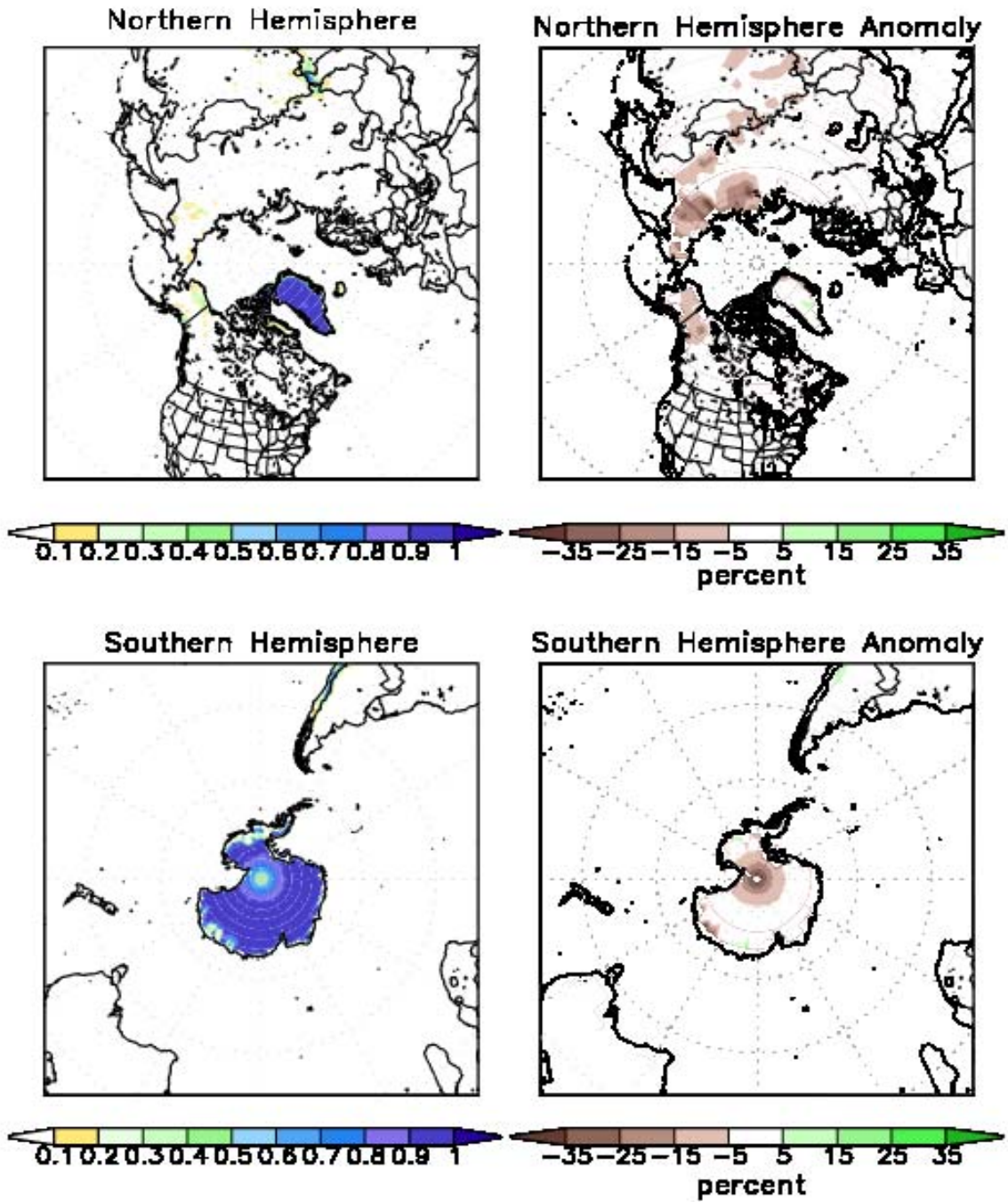


FIGURE A2.2. SSM/I derived snow cover frequency (%) (left) and snow cover anomaly (%) (right) for the month of SEP 2016 based on 1987 - 2010 base period for the Northern Hemisphere (top) and Southern Hemisphere (bottom). It is generated using the algorithm described by Ferraro et. al, 1996, Bull. Amer. Meteor. Soc., vol 77, 891-905.